DRL-532 DISTRIBUTION OF THIS DOCUMENT IS UNLIMITED CR-21

EXPERIMENTAL INVESTIGATION OF THE EFFECTS OF SURFACE ROUGHNESS ON COMPRESSIBLE TURBULENT BOUNDARY LAYER SKIN FRICTION AND HEAT TRANSFER

by

Frank Levi Young

A Technical Report Resulting from Research Under Bureau of Naval Weapons Contract NOrd-16498, Task UTX-2, and Authorized for Publication Under APL/JHU Subcontract 181471, Task E

DISTRIBUTION OF THIS DOCUMENT IS UNLIMITED

May, 1965 Copy No. 19

DEFENSE RESEARCH LABORATORY

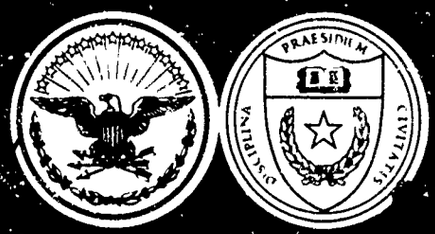

THE UNIVERSITY OF TEXAS · AUSTIN 12, TEXAS

ABSTRACT

An experimental investigation was carried out to determine the effects of surface roughness on the turbulent boundary layer skin friction and heat transfer rates in air at a Mach number of 4.93. Four flat plate model configurations were tested, one with a smooth surface and three with rough surfaces consisting of 90° V-grooves oriented perpendicular to the flow direction. Simultaneous measurements of the local skin friction and heat transfer were made using a floating-element skin friction balance and an insulated-mass calorimeter for Reynolds numbers near 10 million and wall-to-free stream temperature ratios from 2.9 to 5.2. The results of these measurements and of boundary layer pressure surveys are presented in both graphical and tabular form and are compared with theoretical predictions. Agreement of the smooth plate results with accepted theories acts to substantiate the results of measurements using the rough-surfaced models. A method is given to determine the equivalent incompressible sand-grain roughness of a surface based on experimental knowledge of the skin friction in compressible flow. In addition, a method to account for heat transfer effects in the calculation of skin friction coefficients for rough plates is suggested. Using the experimental results, the validity of the Reynolds analogy between heat transfer and skin friction is examined. A method to determine the Reynolds number based on the length of the turbulent boundary layer from measurements of the skin friction and momentum thickness for smooth or rough flat plates is also given.

PREFACE

The development of turbulent boundary layer theory has gone hand-in-hand with the progress of related experimental studies. Today, although more accuracy is demanded of theories and engineering relations than ever before, the flow regimes of interest have become more difficult to deal with both theoretically and experimentally. These difficulties cause attention to be focused on the need for more complete examination of many fundamental aerodynamic problems. An example of such a problem is the one considered here, that of the influence of a roughened surface on the turbulent boundary layer. It is a problem which has received relatively little attention with respect to the compressible boundary layer, particularly where heat transfer conditions are included. Accurate measurements within the boundary layer are, at best, difficult under these flow conditions but are necessary to a further understanding of boundary layer phenomena. To obtain reliable measurements of skin friction and heat transfer without limiting theoretical assumptions, the use of the floating element skin friction balance and insulated mass calorimeter in a wind tunnel model is very attractive. Because the skin friction balance is extremely sensitive to temperature changes, however, its use under heat transfer conditions has been generally unsuccessful. In the present investigation both of these instruments were used and have provided a reasonably high degree of accuracy under the flow conditions examined, thus adding to the experimental knowledge of the turbulent boundary layer.

The success of an exacting experimental program is the result of the effort and cooperation of many people. I would first like to express my appreciation to Dr. M. J. Thompson, Associate Director of the Defense Research Laboratory and Head of the Laboratory's Aeromechanics Division,

for his guidance and for affording me the opportunity to work with the Laboratory during my assignment at The University of Texas. My appreciation and thanks also to Messrs. Westkaemper and Hill of the Aeromechanics Division, whose assistance was invaluable. Gratitude is due also to all members of the Defense Research Laboratory Staff whose cooperation made completion of this work possible, as well as to the United States Air Force for the opportunity to participate in both the academic and research programs of The University of Texas.

This work was done under BuWeps Contract Number 16498 and the support of the United States Navy is gratefully acknowledged.

March 19, 1965 Frank L. Young

TABLE OF CONTENTS

TABLE OF CONTENTS (CONT'D)

NOMENCLATURE

c	- specific heat
c_p	- specific heat of air at a constant pressure
h	- heat transfer coefficient, defined by Eq. (65)
k	- universal mixing length constant
ℓ	- mixing length
m	- mass
p	- pressure
q	- local heat flux/dynamic pressure
r	- temperature recovery factor
t	- time
u	- x-direction velocity
v	- y-direction velocity
x	- distance coordinate along the surface in the streamwise direction and originating at the turbulent origin
y	- distance coordinate normal to the surface and originating at the surface
A, B, C, D, E, G, G	- constants of integration
C_f	- local skin friction coefficient
C_F	- mean skin friction coefficient
C_h	- local heat transfer coefficient (Stanton number)
D	- roughness function
F_c	- function given in Table I
F_{rx}	- function given in Table II
H	- V-groove roughness height

NOMENCLATURE (Cont'd)

K	- sand-grain roughness height
L	- plate length
M	- Mach number
P	- roughness pitch or peak-to-peak roughness spacing
P_r	- Prandtl number
R	- universal gas constant
R_x	- Reynolds number based on the length of the turbulent boundary layer
S	- Reynolds analogy factor $= \frac{C_f}{2C_h}$
T	- temperature
U_τ	- friction velocity $= \sqrt{\tau_w/\rho_w}$
γ	- ratio of specific heats for air, taken to be 1.40
δ	- boundary layer thickness
Δ	- increment/average deviation of experimental data from the arithmetic mean
ϵ	- eddy viscosity
ϵ_k	- eddy conductivity
θ	- boundary layer momentum thickness
λ	- function defined by Eq. (89)
μ	- dynamic viscosity
ν	- kinematic viscosity
ρ	- mass density
τ	- shear stress
ω	- viscosity-temperature power law exponent

SUBSCRIPTS:

aw	- adiabatic wall
c	- calorimeter
cu	- copper
exp	- experimental
i	- incompressible
K	- roughness
o	- isentropic stagnation condition
s	- solder/laminar sublayer
t	- turbulent
w	- wall value
1	- indicates conditions at the edge of the boundary layer
2	- indicates conditions behind a normal shock wave

OTHER SYMBOLS:

'	- indicates a turbulent fluctuating component
—	- denotes a time-mean value

I. INTRODUCTION

One of the most practical problems to be investigated within the framework of Prandtl's boundary layer concept is that of the drag of rough surfaces. Economic considerations prompted early experimental investigations to determine the quantitative effects of roughness on the skin friction of ships and on the pressure losses in fluid distribution systems. Although these applications remain important today, advances in many varied technologies have broadened the scope of interest to include such diverse fields as meteorology, biophysics, nuclear and missile engineering. In fact, wherever the effects of a turbulent boundary layer are important, the influence of surface roughness must be considered. In the field of aerodynamics, which is that of principal concern here, the need for an accurate knowledge of the effects of turbulent boundary layers is often a vital one.

Aerodynamic problems of interest today include not only those of low-speed flight but those of high-speed flight and the associated high temperatures. The effects of both compressibility and heat transfer on boundary layer characteristics are significant in the flight regimes of all high performance flight vehicles and spacecraft even though their entire flight paths may not remain within an atmosphere. Less is known of the behavior of the boundary layer at high flight speeds than at low speeds yet the accurate prediction of its effects is more critical. Skin friction drag, for example, is of increased importance because for modern, streamline aerodynamic shapes it is a large portion of the total drag. The degree of surface roughness which can be tolerated under these circumstances should be known accurately to allow economic manufacturing tolerances. Knowledge and control of heat transfer rates in high-speed flight may also be

critical with regard to structural failure or distortion. Even with the availability of high temperature materials, induced thermal stresses must be considered in vehicle design. Because surface roughness influences heat transfer rates, it becomes an important consideration here as well as for skin friction.

Certain important qualitative effects of roughness on the boundary layers of flat plates have been observed and are now well established for the case of incompressible flow. Moreover, according to the limited information presently available, these effects appear to remain consistent with observations made in the case of compressible flow. Briefly, these can be summarized as follows:

1. No increase in the skin friction drag of a surface occurs if the boundary layer remains laminar.

2. Uniformly distributed roughness on a surface affects the turbulent boundary layer according to the roughness height relative to the boundary layer thickness.

3. No increase in skin friction drag occurs for a surface with a turbulent boundary layer if the roughness height is less than the usual laminar sublayer thickness.

4. Roughness elements of sufficient height encourage the transition from a laminar to a turbulent boundary layer.

5. As the height of a uniformly distributed roughness is increased beyond the laminar sublayer thickness, both the skin friction drag and heat transfer rate increase.

6. For roughness heights greater than a certain value, the drag of a uniformly rough surface demonstrates similarity with that of a bluff body, i.e., it becomes a quadratic function of the flow velocity.

7. The fluid velocity in the vicinity of the plate surface is retarded to a much greater degree than for the case of a smooth plate.

For flight at high Mach numbers, the increased boundary layer thickness tends to increase the height of uniformly distributed roughness which can be permitted without a corresponding increase in drag. Also the increased length of large flight vehicles allows an increase in the absolute size of distributed surface roughness that can be tolerated in regions where the boundary layer has thickened. The relief provided by these circumstances must be regarded cautiously, however, since a large part of any high speed vehicle may be exposed to low Mach number flow as a result of the bow shock wave or of shock waves emanating from surface projections.

The accurate prediction of roughness effects in high-speed flight regimes is complicated by the fact that few experimental data are available for rough surfaces in compressible, nonadiabatic flow. When it is considered that all turbulent boundary layer theories rely heavily on experimental results for even modest accuracy, it is apparent that they must remain severely limited in the flight regime considered here. The purpose of the present investigation was to obtain local skin friction and heat transfer data for both smooth and uniformly rough flat plates in compressible flow in order to extend experimental knowledge into this flow regime. The following chapters present the theoretical considerations applicable to the investigation, a description of the experimental program and data reduction methods, as well as a discussion of the experimental data obtained and the conclusions drawn from them.

II. THEORY

The complete solution to an aerodynamic boundary layer problem provides a detailed knowledge of the distribution of fluid properties, velocities, and their derivatives within the thin boundary layer, as well as knowledge of the fluid interaction with the solid boundary. Although the objective of many boundary layer theories includes such a rational description of the flow itself, the practical goal is often limited to the accurate prediction of boundary layer effects such as skin friction and heat transfer. This latter statement is particularly true regarding the turbulent boundary layer. The success of existing turbulent boundary layer theories is due in large part to their reliance on experimental data. Because of their empirical, or semi-empirical nature, however, extrapolation into uninvestigated flow regimes is often risky. When new measurements become available, as in the present case, it is important to compare them with the predictions of existing theories. The effectiveness of a particular theory is thus evaluated and perhaps proved under new flow conditions. If, on the other hand, consistent deviations exist, the experimental data may lead to a natural extension or modification of the theory. To this end, the results of appropriate turbulent boundary layer theories for smooth and rough flat plates are presented here. First, the general boundary layer equations are given and the surface conditions of interest are described. The particular cases of flow past smooth and rough plates are then treated separately for incompressible and compressible flow. This is followed by a brief discussion of appropriate heat transfer relations. Details available in the literature will not be given, but the limitations and validity of the theories will be discussed. Finally methods for the determination of the equivalent sand-grain roughness of a surface and of

the effective Reynolds number, R_x, are given. An emphasis is placed on those factors necessary to the logical discussion of the results obtained in the present experimental program.

A. Review of Existing Theory

1. The Turbulent Boundary Layer on a Flat Plate

In the study of the constant pressure, laminar boundary layer it is usually sufficient to deal with steady flows for which similarity exists, that is, for which a general description of the boundary layer is possible in terms of nondimensional variables. It is also well established that the turbulent boundary layer of both smooth and uniformly rough, flat plates can be treated with a similar generality if the proper selection of nondimensional variables is made (Ref. 1). Indeed, it is this characteristic which permits general conclusions to be drawn from the limited experimental knowledge of a given boundary layer. By virtue of the existence of turbulence, however, it is no longer meaningful to discuss steady flow in the usual sense. In fact, the concepts of turbulent fluid motions and true steady-state boundary layer flow are contradictory. For very practical reasons, therefore, it is customary to consider each of the dependent variables of the turbulent boundary layer problem as consisting of a steady component and a fluctuating component. That is, for example:

$$\rho = \bar{\rho} + \rho'$$

or

$$\rho u = \overline{\rho u} + (\rho u)' \quad .$$

The steady or time-mean value is defined by:

$$\bar{\rho} = \frac{1}{T} \int_{-T/2}^{+T/2} \rho \, dt \quad . \qquad (1)$$

where the time T is taken to be long compared to the period of the fluctuations. As a result of this definition, the time-mean value of any fluctuating quantity is identically zero, e.g., $\overline{\rho'} = 0$. These two-component variables can be substituted into each of the equations required to describe the compressible, turbulent boundary layer. If this is done and, further, if each resulting expression is averaged over the time T as defined by Eq. (1), the final simplified equations can be considered as steady-state equations in the time-mean quantities. This is practical because the characteristic periods of turbulent fluctuations are usually very short compared to the duration of important boundary layer effects. As an example, nearly all measurements made within a turbulent boundary layer result in time-mean values, since the response of the related instrumentation is seldom adequate to detect the influence of turbulent fluctuations. The obvious exception to this is the hot-wire anemometer which is usually designed to measure the fluctuations themselves; however, here the achievement of a sufficiently short response time is a major task. From another practical viewpoint, time-mean values of boundary layer quantities are generally satisfactory in the application of the integral relationships which have been instrumental in the development of boundary layer theory.

The turbulent boundary layer equations for a variable property fluid have been derived by many authors, e.g., Ref. 2, 3, and 4. Those which are applicable to the steady, high-speed flow of air past a smooth or rough, constant temperature flat plate are given below with remarks and assumptions which pertain to the following sections. The conventional coordinate system for two-dimensional flow past a flat plate is used wherein the x-axis lies in the plate surface and is oriented in the free-stream flow direction. The positive y-axis is an outward normal to the plate surface.

In terms of mean dependent variables, the equation of continuity can be written:

$$\frac{\partial}{\partial x}(\overline{\rho u}) + \frac{\partial}{\partial y}(\overline{\rho v}) = 0 \quad . \tag{2}$$

A further expansion of the terms of this equation is possible but is not necessary here.

As a result of the thin boundary layer assumptions, and of neglecting any fluctuations in the viscosity, the x-direction momentum equation for a constant pressure boundary layer is

$$\overline{\rho u}\,\frac{\partial \bar{u}}{\partial x} + \overline{\rho v}\,\frac{\partial \bar{u}}{\partial y} = \frac{\partial}{\partial y}\left[\mu \frac{\partial \bar{u}}{\partial y} - \overline{(\rho v)'\, u'}\right] \quad . \tag{3}$$

The term with the fluctuating quantities on the right hand side does not disappear as a result of the indicated integration because the quantities $(\rho v)'$ and u' are not independent; that is, they are correlated and the term containing their product must be retained in the equation. From its position in the equation, this term is seen to be equivalent to an additional shear stress term. For this reason, it is called the turbulent, or Reynolds, shear stress. Equation (3) may be reduced to the form of the laminar boundary layer equation if an eddy viscosity, ϵ, is defined by

$$-\overline{(\rho v)'\, u'} = \epsilon \frac{\partial \bar{u}}{\partial y} \quad . \tag{4}$$

Unlike μ, however, ϵ is not a property of the fluid.

Under the assumptions leading to Eq. (3), the y-direction momentum equation reduces to:

$$\frac{d\bar{p}}{dy} \approx 0 \quad . \tag{5}$$

Thus, for the boundary layer under consideration, the pressure is essentially constant throughout the fluid.

Another very useful momentum relation is the von Kármán momentum integral equation which equates the local shear stress with the local rate of change of momentum in the boundary layer. For the constant pressure boundary layer, this can be written:

$$\frac{\tau_w}{\rho_1 u_1^2} = \frac{d\theta}{dx} \tag{6}$$

with

$$\theta \equiv \int_0^\delta \frac{\overline{\rho u}}{\rho_1 u_1}\left(1 - \frac{\bar{u}}{u_1}\right)dy \quad .$$

In principle, this is valid for both smooth and rough surfaces.

The working fluid of interest here is air and is assumed to obey the perfect gas law:

$$\bar{p} = R\,\overline{\rho T} \quad . \tag{7}$$

Using Eqs. (5) and (7) and assuming that $\overline{\rho' T'}$ can be neglected, the following useful relations are obtained

$$\frac{\bar{T}}{\bar{T}_1} = \frac{\rho_1}{\bar{\rho}} \quad , \tag{8}$$

and

$$\frac{T_w}{\bar{T}_1} = \frac{\rho_1}{\rho_w} \quad . \tag{9}$$

For compressible and dissipative flows, the energy equation must be included as an additional boundary layer equation. Assuming that c_p is constant for the temperatures of interest and that fluctuations in the thermal conductivity are negligible, the energy equation is

$$\overline{\rho u}\, c_p \frac{\partial \bar{T}}{\partial x} + \overline{\rho v}\, c_p \frac{\partial \bar{T}}{\partial y} = \frac{\partial}{\partial y}\left[k \frac{\partial \bar{T}}{\partial y} - c_p\, \overline{(\rho v)' T'}\right] + \mu\left(\frac{\partial \bar{u}}{\partial y}\right)^2 - \overline{(\rho v)' u'}\, \frac{\partial \bar{u}}{\partial y} \quad . \tag{10}$$

On the right hand side of this equation there are two terms containing correlated fluctuating quantities which do not appear in the laminar flow energy equation. The first of these is the turbulent counterpart of the molecular heat conduction term and may be used to define an eddy conductivity ϵ_k as follows:

$$-c_p \overline{(\rho v)' T'} \equiv \epsilon_k \frac{\partial \bar{T}}{\partial y} \quad . \tag{11}$$

Just as the fluid viscosity and conductivity are used to form the molecular Prandtl number, the eddy viscosity and eddy conductivity may be used to form the turbulent Prandtl number, P_{rt}. That is,

$$P_{rt} = \frac{\epsilon c_p}{\epsilon_k} \quad . \tag{12}$$

The last term of Eq. (10) is the turbulent counterpart of the molecular shear work term and, when combined with Eq. (4), assumes the more familiar form:

$$\epsilon \left(\frac{\partial \bar{u}}{\partial y} \right)^2 \quad .$$

The above equations give considerable insight into the role of turbulent fluctuations in compressible, boundary layer flow. They apply, in general, to the turbulent boundary layers of flat plates--both smooth and with varying degrees of surface roughness--for which the surface boundary conditions differ. The four regimes of interest can be summarized in terms of these surface conditions or roughness size as follows:

1. The smooth plate. Here the turbulance is damped by viscous forces at the surface and a laminar sublayer exists in which the velocity distribution is essentially linear with y.

2. The aerodynamically smooth plate. In this regime the surface is measurably rough but the skin friction is indistinguishable from that of a

smooth plate. The characteristic Reynolds number based on roughness height remains small for this condition. Alternately it may be considered that the roughness remains submerged in the usual laminar sublayer.

3. The transistionally rough plate. For this surface, both the viscous and turbulent forces are of importance. Their relative importance, however, is a function of the roughness size and type and is not fully understood.

4. The fully rough plate. In this regime the turbulent effects dominate the entire boundary layer and the laminar sublayer, in its usual sense, does not exist. The skin friction drag of this surface is similar to the drag of a bluff body and is essentially a quadratic function of the free-stream velocity.

All three regimes of roughness may exist on a single flat plate since the boundary layer thickness is small near the leading edge. From this, it is seen that the relative roughness, x/K or L/K becomes an important parameter in the description of roughness effects.

Although it is not yet possible to solve the turbulent boundary layer equations in a fundamental manner, many useful engineering results are presently available for two dimensional flow including the effects of compressibility and heat transfer. Historically the methods of solution of the turbulent boundary layer problem have evolved from Prandtl's mixing-length theory and have leaned heavily on experimental investigations. This theory and others are treated in the following sections.

2. Incompressible Flow for the Smooth Flat Plate

Here the term "incompressible flow" will be taken to mean constant property flow. For this case, the turbulent shear stress from Eq. (3) becomes

$$\tau = \rho \overline{u' v'} \quad . \tag{13}$$

This term can be replaced in the momentum equation by the product of the velocity gradient, du/dy, and an eddy viscosity in order to reduce the equation to the same form as for the laminar case. This eddy viscosity, however, is not a fundamental property of the fluid but is a largely unknown function of the flow conditions themselves. In order to avoid the need for a direct solution of the momentum equation, Prandtl introduced his mixing-length theory which has since provided the basis for many analyses of the turbulent boundary layer problem. Prandtl (Ref. 5), in analogy with the molecular transfer of momentum, postulated that the turbulent exchange of momentum would relate the x-direction shear stress and velocity gradient as follows

$$\tau = \ell^2 \rho \frac{d\bar{u}}{dy} \left| \frac{d\bar{u}}{dy} \right| \quad . \tag{14}$$

The "mixing length", ℓ, is a coefficient of proportionality and is a characteristic of both the path length and the size of the turbulent fluctuations. Both Prandtl (Ref. 5) and von Kármán (Ref. 6) have introduced expressions defining the mixing length which have found widespread use. That of Prandtl, which relates the mixing length and the coordinate distance from the wall, is simply

$$\ell = ky \quad , \tag{15}$$

and that of von Kármán, which was determined from considerations of dynamic similarity, is

$$\ell = - \frac{k \frac{d\bar{u}}{dy}}{\frac{d^2\bar{u}}{dy^2}} \tag{16}$$

Integration of Eq. (14) using either Eq. (15) or Eq. (16) and assuming that τ remains constant and equal to τ_w near the wall leads to the well-known logarithmic velocity distribution law:

$$\frac{\bar{u}}{U_\tau} = A \log y + B \tag{17}$$

where $U_\tau = \sqrt{\tau_w/\rho}$. The constants of integration, although independent of y, may be functions of the flow conditions. Thus, to obtain results which are universal in nature requires care in the application of the boundary conditions. It is well known, experimentally, that $\bar{u}/U_\tau$ is not a universal function of y; however, such similarity has been demonstrated to exist between $\bar{u}/U_\tau$ and the variable $U_\tau y/\nu$ (Ref. 1). This is illustrated, for example, by the linear velocity distribution in the laminar sublayer when written

$$\frac{u}{U_\tau} = \frac{U_\tau y}{\nu} \tag{18}$$

which reduces to

$$\tau_w = \mu \frac{u}{y} \quad . \tag{19}$$

Determination of the constants A and B of Eq. (17) can be resolved by changing the variable y to $U_\tau y/\nu$ and applying the boundary conditions at the edge of the laminar sublayer; vis., $U_\tau y/\nu\big|_s$ = const. Accomplishing this and using numerical constants determined from experiment (Ref. 2), the result is

$$\frac{\bar{u}}{U_\tau} = 5.85 \log \frac{U_\tau y}{\nu} + 5.56 \quad . \tag{20}$$

Von Kármán (7) used a form of the logarithmic velocity distribution and the momentum integral equation for a flat plate, Eq. (6), to obtain the following relation for the local skin friction coefficient

$$C_f^{-1/2} = 1.70 + 4.15 \log (R_x C_f) \quad . \tag{21}$$

Using the results of von Kármán's analysis, Schoenherr (Ref. 8) found the mean skin friction to be given by

$$C_F^{-1/2} = 4.13 \log (R_x C_F) \quad . \tag{22}$$

These results both include the assumption that the turbulent origin is coincident with the plate leading edge.

Equations (21) and (22) which constitute the von Kármán-Schoenherr equations are widely accepted but are often difficult to apply because C_f and C_F are not explicit functions of R_x. For this reason the Sivells-Payne approximations to the von Kármán-Schoenherr equations are used in this report where incompressible, smooth plate values are needed. The Sivells-Payne equations are

$$C_f = 0.088 \frac{(\log R_x - 2.3686)}{(\log R_x - 1.5)^3} \tag{23}$$

and

$$C_F = \frac{0.088}{(\log R_x - 1.5)^2} \tag{24}$$

An extensive comparison of these equations with the von Kármán-Schoenherr equations is made in Ref. 9. The agreement is shown to be excellent for Reynolds numbers between 10^5 and 10^9.

Apart from mixing length theory, dimensional reasoning and accumulated experimental evidence have been used to show that the velocity boundary layer of a flat plate can be described by two apparently universal, but empirical, laws. The first of these, the law of the wall (Ref. 10), is applicable only in the vicinity of the surface, while the second, the velocity defect law (Ref. 11), is valid only in the outer region of the boundary layer.

If it is assumed that, near the wall, the fluid velocity is governed by the molecular viscosity, fluid density, the wall shear stress, and, of course, the normal distance from the surface, then

$$\bar{u} = f_1(\mu, \rho, \tau_w, y) \quad . \tag{25}$$

The correct nondimensional form of this relation has been found to be

$$\frac{\bar{u}}{U_\tau} = f\left(\frac{U_\tau y}{\nu}\right) \tag{26}$$

In the outer region of the boundary layer, it is best to consider the velocity distribution relative to a coordinate system which is moving with free-stream velocity at the edge of the boundary layer, that is, at a distance δ from the surface. If it is assumed that the effects of the fluid viscosity can be neglected in this region, the functional velocity distribution may be written as

$$u_1 - \bar{u} = g_1(\rho, \tau_w, \delta, y) \quad . \tag{27}$$

The correct nondimensional form for this expression has been shown to be

$$\frac{\bar{u} - u_1}{U_\tau} = g\left(\frac{y}{\delta}\right) \quad . \tag{28}$$

It is remarkable that if a region of concurrent validity of Eqs. (26) and (28) is assumed, the logarithmic velocity distribution law is again obtained. Such a procedure thus gives directly the nature of the functions f and g (Ref. 1). This may be seen by solving Eq. (28) for $\bar{u}/U_\tau$ and setting the result equal to the right-hand side of Eq. (26), i.e.,

$$g\left(\frac{y}{\delta}\right) + \frac{u_1}{U_\tau} = f\left(\frac{y}{\delta} \cdot \frac{U_\tau \delta}{\nu}\right) \quad . \tag{29}$$

From this it is clear that the factor multiplying (y/δ) in f must be equivalent to the term added to g. The function which satisfies this requirement for f and g is the logarithm. Therefore, it follows that

$$\frac{\bar{u}}{U_\tau} = A \log \frac{U_\tau y}{\nu} + B \quad , \tag{30}$$

and

$$\frac{\bar{u} - u_1}{U_\tau} = A \log \frac{y}{\delta} + C \quad . \tag{31}$$

The good agreement of experimental data with both of these laws in their overlapping domains is shown in Ref. 1.

3. Incompressible Flow for the Rough Flat Plate

Prandtl's mixing length theory may be applied to the turbulent boundary layer of a uniformly rough surface as well as that of a smooth surface. Integration of Eq. (14) using either expression for mixing length again leads to Eq. (17), but the constants of integration must be considered anew. Turning again to experiment, it is known that the nondimensional velocity distribution is dependent only on y/K when the roughness elements are large and protrude far through the laminar sublayer. For this experimental fact to be compatible with Eq. (17), the constant of integration must include the term -A log K explicitly. That is, Eq. (17) must become

$$\frac{\bar{u}}{U_\tau} = A \log y - A \log K + D \quad , \tag{32}$$

or simplifying and including A = 5.85,

$$\frac{\bar{u}}{U_\tau} = 5.85 \log \frac{y}{K} + D \quad . \tag{33}$$

The constant of integration, D, is usually called the roughness function. For the fully rough case under consideration, it has a constant value of

approximately 8.5. For the transitionally rough regime between the smooth and fully rough conditions, D has been determined experimentally for sand grain roughness by Nikuradse whose results are shown in Fig. 1. Although these data were determined from pipe-flow experiments, they appear to remain valid for channel and flat-plate flow (Ref. 2). If the roughness function is equal to $5.56 + 5.85 \log U_\tau K/\nu$, then Eq. (33) reduces to that for the smooth plate, Eq. (20).

It is also useful to rewrite Eq. (33) to include the smooth plate relation, Eq. (20), as follows

$$\frac{\bar{u}}{U_\tau} = A \log \frac{U_\tau y}{\nu} + B - A \log \frac{U_\tau K}{\nu} + (D - B) \quad . \tag{34}$$

With the proper constants, this can be written

$$\frac{\bar{u}}{U_\tau} = 5.85 \log \frac{U_\tau y}{\nu} + 5.56 - \frac{\Delta \bar{u}}{U_\tau} \tag{35}$$

where

$$\frac{\Delta \bar{u}}{U_\tau} \equiv 5.85 \log \frac{U_\tau K}{\nu} - 2.94 \quad . \tag{36}$$

The equation written in this form emphasizes the fact that the effect of surface roughness on the velocity distribution may be regarded as a vertical shift in the associated smooth plate velocity profile. Because the magnitude of this shift is strictly a function of the nondimensional roughness height $U_\tau K/\nu$, it makes it possible to compare the observed effects of an arbitrary surface roughness with the known effects of a sand-grain surface roughness for which the constants of Eq. (36) were determined.

Calculations to determine rough-plate skin friction coefficients based on the logarithmic velocity distribution and the experimental roughness function have been carried out by Prandtl and Schlichting (Ref. 12) and more

recently by Clutter (Ref. 13). Their results are complex and are presented in graphical form only. For the fully rough regime, wherein the coefficients are independent of the Reynolds number, the following interpolation formulae are given by Prandtl and Schlichting (Ref. 2).

$$C_f = \left(2.87 + 1.58 \log \frac{x}{K}\right)^{-2.5} \tag{37}$$

$$C_F = \left(1.89 + 1.62 \log \frac{L}{K}\right)^{-2.5} \tag{38}$$

Here, the turbulent origin is again assumed to be coincident with the plate leading edge.

As for the smooth surface, it is again possible, with the confidence of experimental knowledge, to arrive at the above velocity distribution by a functional analysis. For the fully rough regime, it must first be assumed that the molecular viscosity is no longer of importance even near the wall. Then, if the roughness height is included as an important variable, the functional expression for the velocity becomes

$$\bar{u} = h_1(\rho, \tau_w, K, y) \quad . \tag{39}$$

The proper nondimensional form of this is

$$\frac{\bar{u}}{U_\tau} = h\left(\frac{y}{K}\right) \quad . \tag{40}$$

The velocity defect law remains a valid description of the velocity distribution in the outer portion of the boundary layer (Ref. 1); thus, for the overlapping region of validity of Eqs. (28) and (40):

$$g\left(\frac{y}{\delta}\right) + \frac{u_1}{U_\tau} = h\left(\frac{y}{\delta} \cdot \frac{\delta}{K}\right) \quad . \tag{41}$$

As before, the indicated relationship between the variables implies that the functions g and h are logarithms. Since the numerical constants must be determined from experiment, the velocity defect law and the law of the

wall for rough surfaces as determined here must be identical to those previously obtained, viz. Eqs. (31) and (33) respectively.

The skin friction coefficients for a fully rough surface as given by Eqs. (37) and (38) are not convenient for certain practical calculations. For that reason, it is desirable to include here the results of an analysis by Droblenkov (Ref. 14). Under the assumption of constant property flow over a fully rough flat surface, he demonstrated that the relationship between C_f and θ/K as derived from the logarithmic velocity distribution, Eq. (33), could be replaced satisfactorily by a one-sixth power relationship for $10^{1.5} < \frac{\theta}{K} < 10^{5.5}$. Subsequent application of the momentum integral equation resulted in the following equations for local and mean skin friction coefficients for a sand-roughened flat plate.

$$C_f = 0.0139\left(\frac{x}{K}\right)^{-1/7} \tag{42}$$

$$C_F = 0.0162\left(\frac{L}{K}\right)^{-1/7} \tag{43}$$

The results of these equations are compared with those of Eqs. (37) and (38) in Fig. 2. For $10^4 < \frac{x}{K} < 10^{6.2}$ the agreement is seen to be good; for smaller values of $\frac{x}{K}$, the exponent in Eqs. (42) and (43) should be changed slightly. In both cases the turbulent boundary layer was assumed to begin at the plate leading edge.

4. Compressible Flow for the Smooth Flat Plate

From an examination of Eqs. (2) through (10), it is evident that the problem of compressible, boundary layer flow is even less amenable to direct attack than is that of constant property flow. As an alternative to the direct solution of these differential equations, various generalizations or extensions of the incompressible theory have been presented by many

investigators. As before, however, experimental results have played a fundamental role in the development of each theory. Of the several methods used to arrive at practical results, three will be discussed briefly. The first of these involves a generalization of the mixing-length theory while the remaining two use the incompressible theory in a more direct manner; one by introducing the concept of a reference temperature, the other by invoking a semiempirical coordinate transformation.

For compressible flow, the turbulent shear stress from Eq. (3) is

$$\tau = -\overline{(\rho v)' u'} \tag{44}$$

This can be expanded leaving only

$$\tau = -\bar{\rho}\overline{(u' v')} \tag{45}$$

if the terms $\bar{v}\ \overline{\rho' u'}$ and $\overline{\rho' u' v'}$ are assumed to be negligible (Ref. 3). Equation (45) suggests that the proper from of the mixing-length theory for compressible flow is

$$\tau = \bar{\rho}\, \ell^2 \frac{d\bar{u}}{dy} \left| \frac{d\bar{u}}{dy} \right| \quad . \tag{46}$$

If the mean temperature is now assumed to be a function of the mean x-direction velocity only, Eqs. (3) and (10) can be used to derive the following relation:

$$\frac{\bar{T}}{T_1} = \frac{T_w}{T_1} - \left(\frac{T_w}{T_1} - 1\right)\frac{\bar{u}}{u_1} + \frac{\gamma-1}{2} M_1^2 \frac{\bar{u}}{u_1}\left(1 - \frac{\bar{u}}{u_1}\right) \quad . \tag{47}$$

This is the Crocco form of the energy equation and is valid through the entire boundary layer only if both the molecular and turbulent Prandtl numbers are unity (Ref. 15). For constant pressure through the boundary layer, Eqs. (8) and (47) may be used to eliminate the density in Eq. (46). Assuming either Prandtl's or von Kármán's expression for mixing length and a constant shear stress near the wall, Eq. (46) may then be integrated to

determine the velocity distribution. Since both the density and velocity distributions are then known functions of y, the momentum integral equation can be applied, from which approximate skin friction relations can be derived. Unlike the incompressible case, however, each mixing length expression leads to a somewhat different result for the skin friction coefficients. Wilson (Ref. 16) used von Kármán's expression for the compressible, adiabatic case while Van Driest (Ref. 3) used Prandtl's expression and later (Ref. 17) von Kármán's expression for the compressible nonadiabatic case. In a recent comparison of the predictions of these and 18 other turbulent boundary layer theories with available experimental data, Spalding and Chi (Ref. 18) concluded that the method of Van Driest (using von Kármán's mixing length) gave the best results. In this method, Van Driest assumed the Prandtl numbers to be unity and arrived at the following formula for the local skin friction coefficient:

$$\frac{0.242}{A_1 C_f^{1/2} \left(T_w/T_1\right)^{1/2}} \left(\sin^{-1}\alpha + \sin^{-1}\beta\right) = 0.41 + \log\left(R_x C_f\right) - \omega \log \frac{T_w}{T_1} \tag{48}$$

where

$$A_1^2 = \frac{\frac{\gamma-1}{2} M_1^2}{T_w/T_1} \quad ; \quad B_1 = \frac{1 + \frac{\gamma-1}{2} M_1^2}{T_w/T_1} - 1$$

$$\alpha = \frac{2A_1^2 - B_1}{\left(B_1^2 + 4A_1^2\right)^{1/2}} \quad ; \quad \beta = \frac{B_1}{\left(B_1^2 + 4A_1^2\right)^{1/2}} \quad .$$

In the form given, Eq. (48) includes the assumption that the viscosity-temperature relationship is

$$\frac{\mu}{\mu_w} = \left(\frac{\bar{T}}{T_w}\right)^{\omega} \quad . \tag{49}$$

Also, according to Van Driest, the universal velocity distribution for compressible boundary layer flow is given by

$$\frac{\sin^{-1}\left[\frac{2A_1^2\left(\bar{u}/u_1\right) - B_1}{\left(B_1^2 + 4A_1^2\right)^{1/2}}\right] + \sin^{-1}\left[\frac{B_1}{\left(B_1^2 + 4A_1^2\right)^{1/2}}\right]}{A_1\, U_\tau/u_1} = E + F \log \frac{U_\tau y}{\nu_w} \tag{50}$$

rather than by Eq. (20). In this case it is necessary that the friction velocity be determined using the wall value of the fluid density, that is, $U_\tau = \sqrt{\tau_w/\rho_w}$.

The reference temperature or T-prime method to determine compressible, turbulent flow skin friction utilizes the incompressible equations directly by evaluating them at some reference temperature which is intermediate between the wall and free-stream values. This reference temperature is, in general, a function of both the free-stream Mach number, M_1, and the wall-to-free-stream temperature ratio, T_w/T_1. The method was originally proposed by Johnson and Rubesin (Ref. 19) for the compressible, laminar boundary layer and was extended to the compressible, turbulent boundary layer with heat transfer first by Fischer and Norris (Ref. 20) and later by several others (Refs. 21, 22, 23).

Peterson (Ref. 24) recently compared the skin friction results of seven compressible, turbulent boundary layer theories (including that of Van Driest) with data from 21 sources. In his evaluation, the von Kármán-Schoenherr equations were used as the incompressible reference theory.

Peterson concluded that the results of the Sommer-Short T-prime method (Ref. 21) most accurately matched the experimental data. The reference temperature, T', for this method was determined empirically and is

$$\frac{T'}{T_1} = 1 + 0.035\, M_1^2 + 0.45\left(\frac{T_w}{T_1} - 1\right) \quad . \tag{51}$$

The disagreement between authors as to which compressible boundary-layer theory is the most accurate is indicative not only of the different methods of comparison of theory and experiment but of the general accuracy of existing theories and available experimental data.

In many theories the compressible-flow skin friction coefficient is a function of the flow Reynolds number and may be regarded as the familiar incompressible function transformed to new coordinates which are dependent on both the Mach number, M_1, and temperature ratio, T_w/T_1. Spalding and Chi (Ref. 18) combined both theoretical and experimental results to deduce such coordinates, $F_c C_f$ and $F_{rx} R_x$, which minimize the root-mean-square error between predicted skin-friction coefficients and existing experimental data. Their new method is simple to apply and, using the incompressible-flow relations of Spalding (Ref. 25), predicts skin friction coefficients over a wide range of flow conditions with an rms error of 9.9% as compared to 11% for Van Driest's method. The functions F_c and F_{rx} are given in Tables I and II for a wide range of Mach numbers and temperature ratios. They may be used in conjunction with any valid, incompressible-flow skin friction formula for smooth flat plates to find the compressible-flow skin friction coefficients corresponding to a given M_1 and T_w/T_1.

5. Compressible Flow for the Rough Flat Plate

As for the incompressible case, the mixing length theory differential equation (here Eq. 46) can be integrated for the rough plate as well as for

the smooth plate, but again the boundary conditions must be reconsidered. Following a method similar to the one which led to Eq. (48) for the smooth plate, but assuming $\ell = ky$, Van Driest (Ref. 15) obtained the following formula for the local skin friction coefficient of a fully rough flat plate.

$$\frac{0.242}{A_1 C_f^{1/2} \left(T_w/T_1\right)^{1/2}} \left(\sin^{-1} \alpha + \sin^{-1} \beta\right) = 1.40 + \log\left(\frac{x}{K} C_f^{1/2}\right) \quad . \quad (52)$$

Fenter (Ref. 26), using mixing length theory and von Kármán's mixing length, Eq. (16), derived a similar but more complex expression for the skin friction coefficient which in addition considers the transitionally rough regime.

For the incompressible, turbulent boundary layer, the nondimensional velocity distribution was found to be logarithmic, Eq. (33). According to both of the above analyses, however, the corresponding velocity distribution in the compressible turbulent boundary layer should have the form:

$$\frac{\sin^{-1}\left[\frac{2A_1^2\left(\bar{u}/u_1\right) - B_1}{\left(B_1^2 + 4A_1^2\right)^{1/2}}\right] + \sin^{-1}\left[\frac{B_1}{\left(B_1^2 + 4A_1^2\right)^{1/2}}\right]}{A_1 \, U_\tau/u_1} = G + F \log \frac{y}{K} \quad (53)$$

where $U_\tau = \sqrt{\tau_w/\rho_w}$. Insufficient data exist to determine the dependence of G on heat transfer; but from the experimental results of Goddard (Ref. 27), it appears that for the compressible, adiabatic case, at least, G has the same value as for the incompressible case.

On the basis of a physical argument, Liepmann and Goddard (Ref. 28) arrived at a very simple relationship between the compressible- and incompressible-flow skin friction coefficients for a fully rough surface. They assumed, as suggested by Schiller (Ref. 29), that the skin friction drag of a fully rough surface is wholly the summation of the form drag of the individual roughness elements. Since, at reasonably high Reynolds

numbers, the drag coefficient, C_d, of a bluff body shows little dependence on Reynolds number or Mach number, the skin friction drag coefficient of a fully-rough surface can be written:

$$C_f = \frac{C_d (n \cdot S) \frac{1}{2} \bar{\rho}_K \bar{u}_K^2}{\frac{1}{2} \rho_1 u_1^2} \quad . \tag{54}$$

Here n is the number of roughness elements per unit surface area, and S is a characteristic area of the element. The local dynamic pressure acting on an element is defined by $1/2\ \bar{\rho}_K \bar{u}_K^2$, and the flow around the elements is assumed to be subsonic. If the identical surface in a similar incompressible flow is used as a reference, then it follows that

$$\frac{C_f}{C_{fi}} = \frac{\bar{\rho}_K \bar{u}_K^2}{\rho_1 \bar{u}_{Ki}^2} \quad . \tag{55}$$

To first order, the velocities $\bar{u}_K$ and $\bar{u}_{Ki}$ were taken by Liepmann and Goddard to be equal and the density $\bar{\rho}_K$ was taken to be the wall value, ρ_w. Equation (55) thus simplifies to

$$\frac{C_f}{C_{fi}} = \frac{\rho_w}{\rho_1} \quad . \tag{56}$$

Alternatively, using Eq. (9), this can be written:

$$\frac{C_f}{C_{fi}} = \frac{T_1}{T_w} \quad . \tag{57}$$

Goddard (Ref. 27) substantiates this remarkably simple result experimentally for the adiabatic case over a range of Mach numbers from 0.70 to 4.54 at Reynolds numbers near 5×10^6.

The above results can be obtained in another manner from the boundary-layer momentum equation, Eq. (3). If, for a fully rough surface, only the turbulent shear stress is important, and these stresses are transmitted to the surface, then

$$\tau_w = -\bar{\rho}_K \overline{u' v'} \quad , \tag{58}$$

and

$$\tau_{wi} = -\rho_l \overline{u' v'} \tag{59}$$

where $\bar{\rho}_K$ is the time-mean value of the fluid density in the vicinity of the roughness elements. For two identical rough surfaces, one in a compressible flow and the other in a hypothetical, constant property flow, each with identical free-stream conditions, it is reasonable to assume that $\overline{u' v'}$ is the same for each. Under these assumptions, then:

$$\frac{\tau_w}{\tau_{wi}} = \frac{C_f}{C_{fi}} = \frac{\bar{\rho}_K}{\rho_l} \quad . \tag{60}$$

If, as an approximation, the density $\bar{\rho}_K$ is taken to be the wall value then the result is the same as previously given, i.e., Eq. (56) or Eq. (57). That this may not be a good approximation under heat transfer conditions is considered further in Discussion of Results.

Clutter (Ref. 13) presents comprehensive engineering charts to determine skin-friction and heat-transfer coefficients for both smooth and rough flat plates over a range of Mach numbers from zero to five. For the smooth plate he used Van Driest's results given above; while for the rough plate, he used Liepmann and Goddard's results, assuming them to remain valid under heat-transfer conditions. To include the transitionally rough plate, he further assumed that the roughness regimes defined by the experimental roughness function (Fig. 1) as determined by Nikuradse for incompressible, pipe flow remain valid for compressible flow as long as wall density values are used to calculate U_τ. The latter assumption seems fairly well substantiated for the compressible, adiabatic case (Ref. 27), but, as yet, too few data are available to substantiate it for the compressible, heat-transfer case. To determine heat-transfer coefficients, Clutter proposed the use of Reynolds analogy between skin friction and heat transfer in the form:

$$C_h = \frac{1}{S}\frac{C_f}{2}$$

with the Reynolds analogy factor, S, equal to 0.825 as suggested by Van Driest (Ref. 15) for smooth plates. Clutter remarks, however, that this value may no not be accurate for rough plates. The methods used in Reference 13 provide a good indication of the present state of the art regarding the practical application of compressible, turbulent boundary-layer theory.

6. Heat Transfer

In turbulent flow, the exchange process usually envisioned requires that macroscopic particles of fluid fluctuate from one location to another nearby while maintaining, briefly, their original characteristics. The concept of this idealized process applies equally well to the transport of heat as to the transport of momentum and led Reynolds in 1874 to suggest the analogy between skin friction and heat transfer. For the low-speed, turbulent boundary layer, Reynolds analogy is now often expressed as

$$C_h = \frac{C_f}{2} \tag{61}$$

where

$$C_h \equiv \frac{h}{c_p \rho_1 u_1} \quad ,$$

and the coefficient h is defined by the relation

$$q = h\left(T_w - T_1\right) \quad .$$

Regardless of the turbulent process, however, the transfer of heat to or from any surface in a continuum flow must ultimately be by transport through a very thin, nonturbulent layer of fluid at the surface. As a consequence of this, molecular diffusion processes play a fundamental role in the transport of heat to surfaces with turbulent boundary layers as well as to those with laminar boundary layers. This fact may be taken into account by modifying Eq. (6) as follows:

$$C_h = \frac{1}{S} \frac{C_f}{2} \tag{62}$$

where S is defined as the Reynolds analogy factor and is a strong function of the molecular Prandtl number of the fluid. The Prandtl number may be regarded as the ratio of the momentum and thermal diffusivities. Colburn (Ref. 30) has shown that, for low-speed, turbulent flow over smooth surfaces, the relation

$$C_h = \frac{1}{P_r^{2/3}} \frac{C_f}{2} \tag{63}$$

predicts the proper variation of S and P_r. In particular, Eq. (63) has been found to give good results for air at Reynolds numbers less than one million. (Ref. 31).

To account for the effects of compressibility and dissipation in high-speed flow, several modifications to Reynolds analogy have been devised (Refs. 4, 15, 31). The simplest of these may be determined by assuming the validity of the Crocco energy equation, Eq. (47), throughout the entire boundary layer. If the y-derivative of this equation is evaluated at the surface where $\bar{u} = 0$, the following relation is obtained:

$$\frac{q_w}{\tau_w} = \frac{c_p \left(T_{aw} - T_w\right)}{u_1} \quad . \tag{64}$$

Then, if the heat transfer coefficient, h, is defined by

$$q_w = h \left(T_{aw} - T_w\right) \tag{65}$$

it again follows that

$$C_h = \frac{C_f}{2} \quad .$$

Note that Eq. (65) arbitrarily designates heat flux <u>to</u> the surface as positive.

More complete analyses than those mentioned above are available in the literature for both compressible and incompressible boundary layers

(Ref. 2). These take into account both the molecular and turbulent Prandtl numbers and require some detailed knowledge of the laminar sublayer. In general, when both the molecular and turbulent Prandtl numbers are equal to unity, the simple Reynolds analogy, Eq. (61), is obtained. Neither the accuracy of the assumptions used in various theories nor the accuracy of available heat transfer data warrants the use of a very refined theory at this time. For this reason Eckert (Ref. 32) suggests that Eq. (62) be used for the compressible, turbulent boundary layer of a smooth plate taking for S a value between 0.80 and 0.85 which is in good agreement with experimental measurements made in air.

Heat transfer between rough surfaces and a compressible, turbulent boundary layer cannot be predicted reliably in any general manner at present. It would appear that because the turbulent mixing extends essentially to the surface in this case, the simple Reynolds analogy, Eq. (61), should apply; or, in other words, that the Reynolds analogy factor should approach unity. This, however, has not been found to be true for low-speed flow (Ref. 33), probably because the actual transfer of heat to the rough surface is not a turbulent process. The modified Reynolds analogy, Eq. (62), may nevertheless remain a useful relationship for engineering purposes if the analogy factor, S, can be specified as some function of a roughness parameter such as $U_\tau K/\nu_w$ for example. Any general relationship for rough surfaces would have to be determined or at least verified experimentally; considering only the variety of possible surface conditions, this would be a monumental undertaking.

B. Determination of Equivalent Roughness Size

The most complete skin friction results presently available for rough surfaces are those for incompressible flow based on Nikuradse's experiments with tubes having various degrees of sand-grain roughness (Ref. 34). These

include the extension of Nikuradse's results to the case of a sand-roughened, flat plate in incompressible flow by Prandtl and Schlichting (Ref. 2). If the characteristic roughness dimension of another type of uniformly rough surface can be expressed in terms of an equivalent sand-grain diameter, then these extensive results can be used to predict skin friction coefficients for that type of surface. For this reason, methods to determine the equivalent roughness of a given surface will be covered briefly here including, in particular, a method to relate experimental measurements in compressible flow to corresponding incompressible-flow results.

For boundary layer experiments in incompressible flow, a knowledge of the nondimensional velocity profile for any type of fully rough surface can be used with Eqs. (35) and (36) to determine from the measured values of $\Delta u/U_\tau$, an equivalent sand-grain diameter K. For experiments in compressible flow with zero heat transfer, it may be possible to follow a similar procedure based on the good agreement of the measured variation of $\Delta u/U_\tau$ with $U_\tau K/\nu_w$ in compressible flow with the incompressible-flow variation given by Eq. (36) (Ref. 27). On the other hand, if for incompressible flow only the skin friction coefficient C_{fi} or C_{Fi} for a fully rough surface is known, Eqs. (37) or (38) may be solved to find the relative roughness x/K or L/K. If the appropriate length of the turbulent boundary layer, x or L, is also known, the equivalent sand-grain diameter, K, may then be determined. Where the turbulent origin of the boundary layer is not known accurately--as, for example, when measurements are made on wind tunnel walls--the latter method may not be feasible. Further, if a relationship between the compressible- and incompressible-flow skin friction coefficients for fully-rough surfaces is known, a similar method could also be used to find the equivalent sand-grain diameter for rough surfaces in compressible-flow experiments. Again,

however, an accurate knowledge of the turbulent origin is necessary. A method to determine the turbulent origin, or, equivalently, the effective Reynolds number for a rough surface in a compressible flow is presented in the next section.

To determine an equivalent roughness from local measurements on a test surface in a compressible flow, it is convenient to work with the quantity $(C_f/C_{fi})_{exp}$, where C_f is determined experimentally and C_{fi} is taken from incompressible thoery, using as the grain diameter the actual height, H, of the test surface roughness. This is particularly advantageous when measurements are made in the transitionally rough regime for which Eqs. (35) and (36) do not apply, since as H is increased from zero, the ratio $(C_f/C_{fi})_{exp}$ approaches a constant value. According to Eq. (57) this constant value should be equal to T_l/T_w for a sand-roughened test surface in a compressible flow with zero heat transfer. That is, for the stated conditions:

$$\frac{C_f}{C_{fi}} = \frac{T_l}{T_w} \quad . \tag{57}$$

From Eq. (42), then

$$C_f = \frac{T_l}{T_w}\left[0.0139\left(\frac{x}{K}\right)^{-1/7}\right] \tag{66}$$

where K is the unknown equivalent sand-grain diameter for the test surface roughness. Dividing both sides of Eq. (66) by C_{fi} based on the measured roughness height, H, gives

$$\left(\frac{C_f}{C_{fi}}\right)_{exp} = \frac{T_l}{T_w}\left(\frac{K}{H}\right)^{1/7} \quad . \tag{67}$$

or

$$K = H\left[\frac{T_w}{T_l}\left(\frac{C_f}{C_{fi}}\right)_{exp}\right]^7 \quad . \tag{68}$$

Thus, from measurements of the quantities C_f/C_{fi} and T_w/T_l, an approximate value for K can easily be obtained.

It is evident from Eq. (67) that a power-law variation of C_f with x/K is necessary in the determination of K from $(C_f/C_{fi})_{exp}$. From Fig. 2 it can be seen that the exponent of the appropriate power law actually varies between -1/6 and -1/7 depending on the relative roughness. Consequently, C_{fi} may be found from the more general results of Prandtl and Schlichting (Ref. 2) if Eq. (67) is modified by selecting the exponent from Fig. 2 corresponding approximately to the effective roughness of the surface.

An identical procedure to that given above can be used if experimental values of the mean skin friction coefficients are available. The one-seventh power law remains valid as a good first approximations.

C. Determination of the Effective Reynolds Number

In most theoretical analyses of the turbulent boundary layer on a flat plate, the origin of the turbulent boundary layer is assumed to be coincident with the leading edge of the plate. In practice, the turbulent origin may not be known accurately even if the surface under consideration is actually a flat plate because the effect of tripping devices and the extent of the transition region may not be known. It is apparent, at least for the extreme cases where a test surface is short or has no leading edge, that a characteristic length of the turbulent boundary layer itself and not of the model must be used to relate experimental data to theory. For this reason, local skin friction and heat transfer measurements are often related to a Reynolds number based on a local boundary layer dimension, usually the momentum thickness, which can be calculated from measurements. Such a choice, though meaningful, lacks the direct physical significance of the Reynolds number based on a geometrical dimension of the model or on the length of the turbulent boundary

layer. Consequently, it is desirable to have a general relationship between R_θ and R_x, where R_x is based on the length of the completely turbulent boundary layer. Many methods to determine the turbulent origin, or equivalently the effective Reynolds number, from boundary layer measurements on smooth surfaces have been published (Ref. 16, 24, 35). Most of these are complex to apply or require an inconvenient number of measurements. The following paragraphs present a method to determine the effective Reynolds number for either smooth or rough surfaces if R_θ, C_f, M_1, and T_w/T_1 are known.

The effective length of the turbulent boundary layer can be defined using the turbulent origin implied by the relation:

$$C_F = \frac{1}{x}\int_o^x C_f dx \tag{69}$$

where the skin friction coefficient C_f and C_F are those for turbulent flow. The momentum integral equation for either a smooth or rough, flat plate is

$$\frac{C_f}{2} = \frac{d\theta}{dx} = \frac{dR_\theta}{dR_x} \quad . \tag{70}$$

Using this, Eq. (69) can be integrated to give

$$\frac{C_F}{2} = \frac{\theta}{x} = \frac{R_\theta}{R_x}$$

or

$$R_x = \frac{R_\theta}{C_F/2} \quad . \tag{71}$$

Equation (71) will provide a means to calculate the value of the effective Reynolds number, if the mean skin friction coefficient, C_F, can be expressed in terms of the local skin friction coefficient, the effective Reynolds number, and known flow parameters. Such expressions are derived below first

for the smooth plate, then for the fully rough plate. The final relations are given in graphical form.

According to Spalding and Chi (Ref. 18), the following functional relationships exist for both compressible and incompressible flow over smooth, flat plates:

$$C_f F_c = \chi(R_x F_{rx})$$

$$C_F F_c = \bar{\chi}(R_x F_{rx}) \quad .$$

Here F_c and F_{rx} are empirical functions of both M_1 and T_w/T_1 and were determined to minimize the error between the theory and all available experimental data. For $M_1 = 0$ and $T_w/T_1 = 1$, that is, for incompressible flow,

$$F_{ci} = F_{rxi} = 1 \quad .$$

From this it follows that

$$\frac{C_f F_c}{C_{fi}} = \frac{\chi(R_x F_{rx})}{\chi(R_{xi})} \quad ,$$

and further, for $R_{xi} = R_x F_{rx}$,

$$\frac{C_f}{C_{fi}} F_c = 1 \quad . \tag{72}$$

Also,

$$\frac{C_F F_c}{C_{Fi}} = \frac{\bar{\chi}(R_x R_{rx})}{\bar{\chi}(R_{xi})} \quad ,$$

and again for $R_{xi} = R_x F_{rx}$,

$$\frac{C_F F_c}{C_{Fi}} = 1 \quad , \tag{73}$$

Thus, from Eqs. (72) and (73), for the condition that $R_x F_{rx} = R_{xi}$,

$$\frac{C_f}{C_{fi}} = \frac{C_F}{C_{Fi}} = \frac{1}{F_c}$$

or

$$\frac{C_f}{C_F} = \frac{C_{fi}}{C_{Fi}} \quad . \tag{74}$$

Using the Sivells-Payne approximations to the von Karman-Schoenherr equations,

$$\frac{C_{fi}}{C_{Fi}} = \frac{\log R_{xi} - 2.3686}{\log R_{xi} - 1.5} \quad ,$$

or

$$\frac{C_{fi}}{C_{Fi}} = 1 - \frac{0.8686}{\log R_{xi} - 1.5}$$

Replacing R_{xi} with $R_x F_{rx}$ and using Eq. (74)

$$\frac{C_f}{C_F} = 1 - \frac{0.8686}{\log R_x F_{rx} - 1.5} \quad .$$

Combining this with Eq. (71) gives

$$\frac{R_\theta}{C_f} = \frac{R_x}{2}\left(1 - \frac{0.8686}{\log R_x - 1.5 + \log F_{rx}}\right)^{-1} \quad . \tag{75}$$

In Fig. 3, $\log R_x$ is plotted against $\log R_\theta/C_f$ with F_{rx} as a parameter. Knowing R_θ, C_f, M_1, and T_w/T_1, the Reynolds number R_x, can be found quickly using this figure and Table II.

For the fully rough surface, the skin friction coefficients are independent of the Reynolds number, R_x. From the discussion resulting in Eq. (60) and according to Goddard (Ref. 27):

$$\frac{C_f}{C_{fi}} = \frac{C_F}{C_{Fi}} \approx \frac{T_1}{T_w} \quad .$$

Under the condition that C_f and C_F are considered at the same value of T_w/T_1,

$$\frac{C_f}{C_F} = \frac{C_{fi}}{C_{Fi}} \quad . \tag{76}$$

Substituting this into Eq. (71) gives

$$\frac{R_\theta}{C_f} = \frac{R_x}{2\left(C_{fi}/C_{Fi}\right)} \tag{77}$$

The ratio C_{fi}/C_{Fi} can be determined from Eq. (37) and (38) taking L = x, or

$$\frac{R_L}{R_K} = \frac{R_x}{R_K} \quad .$$

The resulting relationship is plotted in Fig. 4 using R_K as a parameter. Knowing R_θ, C_f, and R_K, the appropriate value of R_x can be readily determined from this figure. The curve for a smooth plate for $F_{rx} = 1$ is also included in Fig. 4.

There is seen to be little variation between the smooth plate curves and those for small roughness Reynolds numbers, R_K. For this reason, if R_θ and C_f are known for a transitionally rough surface, it is felt that a reasonably accurate value of R_x can be obtained by interpolation between the applicable smooth and rough plate curves.

III. EXPERIMENTAL PROGRAM

The need for extensive experimental work in the development of turbulent boundary layer theory has long been recognized and is due, primarily, to the lack of detailed knowledge of turbulent flow processes. The complicating factors of compressibility and dissipation in high speed flow, as well as surface roughness, add to the need for experimental verification of proposed theories. Indeed, in the absence of any rational or unified theory it may be hoped that cumulative experimental evidence will lead the way to a complete analysis or, at least, to adequate engineering relations. Surprisingly few experimental investigations of the effects of uniformly distributed surface roughness on the compressible turbulent boundary layer have been conducted (Refs. 26, 27, 36, 37, 38). Very limited experimental results are available concerning the effects of both compressibility and heat transfer on the drag of rough surfaces. In particular, the only direct measurements of the local drag of rough surfaces in a compressible flow reported are those of Ref. 38. These measurements were made on an adiabatic surface which had a sand grain roughness. No such local measurements in compressible flow with heat transfer, and none using a skin friction balance--even for smooth surfaces--appear in the literature.

The direct purpose of the present experimental investigation was to determine, by simultaneous measurement, the local heat transfer rates and the local skin friction drag of a flat but uniformly rough, isothermal surface in a high velocity flow. From an aerodynamic point of view, two aspects of the interrelationship of surface roughness, heat transfer, and compressibility were of immediate interest. One was the examination of the combined effects of surface roughness and heat transfer on the local skin friction drag and

the boundary layer characteristics. The other was the observation of the concurrent effects of surface roughness on both the heat transfer rate and skin friction drag as it relates to the analogy between them. From an experimental point of view, the development of a model and adequate instrumentation was necessarily of immediate concern. Of particular importance here was the need for development of a means to make reliable measurements of local skin friction during heat transfer conditions and the development of a surface roughness which would permit the combination of measurements desired.

The use of surface probe techniques or the extrapolation of boundary layer velocity and temperature profiles to determine wall shear stresses and heat transfer requires a theoretical knowledge of boundary layer processes near the wall. For a non-smooth surface no proven method exists for making such measurements at this time. On the other hand, techniques using the relatively direct-measuring skin friction balance and insulated-mass calorimeter require no limiting theoretical assumptions even for rough surfaces; and, in particular, for transitionally rough surfaces. This section describes the experimental program followed to obtain skin friction and heat transfer data for a smooth surface and three rough surfaces under zero heat transfer conditions and for nominal wall to free stream temperature ratios of 3.8, 3.5, 3.2, and 2.9. All tests were conducted at a nominal Mach number of 5 and at Reynolds numbers from 5×10^6 to 1.5×10^7. The experimental apparatus is described below, including details of the transverse, V-groove surface roughness employed, and the procedures used to implement the tests.

A. Experimental Apparatus

The investigation was directed toward use of the DRL Mach 5, heat-transfer wind tunnel and its associated instrumentation, including a recently installed schlieren flow visualization system. To determine both local heat transfer

and local skin friction, a small insulated-mass calorimeter and a displacement-type skin friction balance were mounted side by side in the surface of a flat plate model; the plate spanned the test section of the wind tunnel with the test surface facing downward. To determine the boundary layer pressure distribution and to calculate such boundary layer quantities as displacement thickness and momentum thickness, a total pressure survey system was used at the test station. Similar test series were conducted with four model configurations, one smooth, and three with different sizes of V-groove surface roughness A detailed discussion of the experimental apparatus is given in the following paragraphs.

1. Wind Tunnel

The DRL heat-transfer wind tunnel is an intermittent flow facility having a fixed nozzle block designed to provide air flow at a nominal Mach number of 5 in the test section. The 6 × 7-in. cross section at the test section will accommodate a flat plate model 20 inches long and 6 inches wide. The air supply pressure is regulated pneumatically to approximately 255 psia, while the flow is diffused and exhausted to the atmosphere. The air supply temperature is raised by passing the flow through an iron-zirconia pebble-bed storage heater and is controlled during a run to a preselected value by an electric resistance heater. The storage heaters are initially heated using natural gas. The steady-state operating time of the tunnel is limited by the air storage capacity and varies from 45 seconds with unheated air to 90 seconds with preheated air at the highest total temperatures. Figure 5 shows the tunnel control console and instrumentation. A complete description of this tunnel and associated equipment can be found in References 39, 40, and 41.

For a constant model temperature, a variation in air supply temperature allowed a variation of heat transfer rate from the air to the model.

Because ' the fixed Mach number and total pressure, however, the Reynolds number per foot in the test section necessarily varied with the air supply temperature--decreasing with increasing temperature. Nominal flow conditions for these tests utilized the practical range of the tunnel and were as follows:

Mach Number	4.93
Total Pressure	255 psia
Static Pressure	0.52 psia
Total Temperature	620-1100°R
Static Temperature	108-190°R
Reynolds Number per ft.	$1.5\text{-}0.5 \times 10^7$
T_w/T_1 (for T_w = 555°R)	5.2-2.9

The total pressure for each run was determined from a standard Bourdon gage connected directly to the tunnel settling chamber. Test-section static pressure was determined using conventional mercury manometers connected to static taps in the model. All pressures were recorded by photograph during each test run. The total temperature was determined from a calibrated thermocouple rake located in the settling chamber, and was recorded on a Brown recording potentiometer.

2. Schlieren System

A single-pass schlieren flow visualization system was employed during most test runs. The light source, collimating and focusing lenses, knife edge, and camera were all mounted securely along a four-inch diameter steel tube which was suspended from the ceiling. The entire apparatus was approximately 20 feet long and could be raised out of the way when not needed. When in use, the system was held by fixed supports with the tunnel test section in line with the optical system. Four-inch diameter, optical quartz windows in

the test section side doors permitted the passage of light across the model surface.

The light source was a projector lamp, shielded except for a small slit in the optical path. Source brightness was controlled by adjusting the lamp voltage with a Variac control unit.

The camera consisted of a common iris and shutter movement located neat the knife edge and a 5 × 7-in. photographic plate holder mounted about two feet behind the shutter. The shutter movement and plate holder were connected by a light shield. Focus of the system was accomplished by moving the camera.

3. Flat Plate Model

The basic flat plate model used for this study was outwardly similar to others used earlier in the DRL Mach 5 wind tunnel (Refs. 42 and 43). Both the model and instrumentation, however, were designed specifically for roughness studies and the simultaneous measurement of local heat transfer and skin friction. The plate body was machined from 1 × 6-in. flat copper stock resulting in the basic dimensions of 0.95 × 5.98 × 14.6 inches with a 15° leading-edge wedge angle and a square trailing edge. A wedge-shaped aluminum tailpiece and 0.15-in. thick aluminum cover plates for the back surface and forward wedge completed the final over-all dimensions of 1.10 × 5.98 × 19.2-in. See Fig. 6. A channel 5/16-in. wide and 3/16-in. deep was milled lengthwise into the back of the copper body to allow for instrumentation lead-in wires and static pressure tubing. A groove 3/32-in. wide and 0.050-in. deep was milled into each edge of the copper body for side gaskets to prevent flow around the edges of the model. Two holes, 7/16-in. in diameter and 1-in. deep, were drilled into each edge to allow for pin support of the model through the tunnel wall.

Two cooling passages were cut into the basic copper plate. One of these crossed the plate six times over the length of the main body; the other, a shorter passage, crossed the leading-edge wedge and returned. This was to allow a lower temperature coolant or a higher coolant flow rate to be used near the leading edge to remove the excessive heat from this region in an attempt to maintain an isothermal surface. Access to the cooling passages was through two inlet tubes and two outlet tubes each 5/16-in. in diameter which entered the side of the plate near one of the forward support-pin holes. These tubes along with a 7/16-in. diameter lead-in tube for the instrumentation connections were designed to protrude through a cut-out in a side door of the test section.

At the designated local test station of the plate, 12 1/2-in. aft of the leading edge, cut-outs were made for both a plug-type calorimeter and a floating-element skin friction balance (See Fig. 7.). These cut-outs were centered 1-in. on opposite sides of the model fore-and-aft center line. For the calorimeter, a hole 1 1/16-in. in diameter was drilled through the copper plate. This was designed to accommodate a 1-in. diameter calorimeter 0.15-in. thick. A brass plug 1 1/16-in. diameter and 5/8-in. high was made to fit into the bottom of this hole leaving only a shallow cylindrical recess 0.210-in. deep. Extension of the calorimeter recess through the plate was necessary to permit application of the surface roughness as described below. The plug was necessary to prevent forced convection across the back of the calorimeter and to present a constant temperature environment to the calorimeter.

The cut-out for the skin friction balance was a hole 1 3/8-in. in diameter through the plate. This was designed to accept the skin-friction balance case which held the separately adjustable and removable skin-friction

balance. The balance had a 1-in. diameter surface element, see Fig. 8. The balance case was installed in the plate and remained there as an integral part of the plate.

Five holes 0.035-in. in diameter were drilled through the back of the plate to within 0.050-in. of the surface at approximately 2-in. intervals along the plate centerline. Iron-constantan thermocouples with teflon-insulated leads were installed in these holes using small copper wedges. Three 0.063-in. diameter static pressure taps were drilled through the plate at stations along the model centerline, one of these being aft of the local test station. Stainless steel tubes, 0.060-in. in diameter, were secured to these taps with epoxy cement. See Fig. 6.

4. Calorimeter

The insulated-mass calorimeter was a copper disc installed in the recess in the model becoming a part of the surface of the model but insulated from the adjacent model surface. It was 1-in. in diameter and 0.150-in. thick with a shallow peripheral groove designed to hold a small teflon spacing ring. See Fig. 9. This copper disc had a nominal weight of 17 gms prior to the application of surface roughness which is described below. An iron-constantan thermocouple with teflon-insulated leads was installed to a depth of about 1/8 inch at the edge of the disc. The calorimeter was installed in the recess using epoxy cement which extended only from the plate surface to the teflon ring, a thickness of about 1/16-in. Thus, the teflon and epoxy rings were the only conduction paths to the plate, the remainder of the calorimeter being isolated by a dead-air space within the recess. Since the calorimeter and its thermocouple were electrically as well as thermally insulated from the plate body, it was a simple matter to check the thermocouple leads for a

short circuit to the model. For the rough-surfaced models, the level of the epoxy extended only from the teflon ring to the bottom of the roughness grooves; no attempt was made to apply roughness to the epoxy itself. Alignment of the calorimeter with the plate surface was accomplished by using three long adjusting screws, threaded through widely spaced holes in the removable brass plug behind the calorimeter, in conjunction with a very sensitive depth gage employing a Schaevitz differential transformer, shown in Fig. 10. By this means it was possible to reduce the maximum misalignment between the calorimeter surface and surrounding plate surface to less than 0.0004-in. After the epoxy had set, the adjusting screws were removed and replaced with short brass screws to prevent heat convection through the holes. The thermocouple leads were brought out through a small hole to the channel in the back of the plate and ultimately to a Brown recording potentiometer. The reference junction for this thermocouple was maintained at 32°F by a distilled water ice bath.

Use of the calorimeter depended upon its being cooled below the plate temperature during a run. For this purpose a manually retractable probe was used through which water could be injected onto the calorimeter disc. This cooling probe was made up of a simple steel shaft and 0.098-in. stainless steel tubing and was installed through an access hole in the test section floor. When extended, the probe outlet was adjusted to be within 1/16 in. of the model surface at a point near the leading edge of the calorimeter. Water, introduced using the pressure differential across the tunnel wall, vaporized and flowed across the calorimeter cooling it very effectively. In the retracted position, the probe could be rotated so that it angled downstream and was well out of the way of the model. A second 0.098-in. diameter tube

was also mounted in the shaft and could be used for simultaneous cooling of the balance disc and calorimeter.

5. Skin Friction Balance

A displacement-type skin friction balance consists of a small segment of a test surface, which is free to move in the streamwise direction against a returning force, and a means to measure the resulting movement. The skin friction balance used in these tests is shown in Fig. 8. Each balance disc was one inch in diameter and had a smooth or rough surface identical to that of the plate and calorimeter. No attempt was made to maintain the same edge thickness for each disc since the roughness depth was different for each. The balance disc was supported by two leaf-spring flexures made from beryllium copper and heat treated. The fixed ends of the flexures were fastened to the aluminum transformer housing which made up the base of the balance and which was firmly secured to the plate body with a steel base plate.

A Schaevitz linear-variable differential transformer was secured with epoxy cement in the aluminum housing directly beneath the balance disc between the flexures and was oriented with its axis in the flow direction. The small transformer core was mounted on a brass screw which passed through the transformer and which was suspended from the disc itself by two aluminum T-bars. Any movement of the disc relative to the base of the balance thus caused the core position to change within the transformer changing the coupling between the primary and secondary windings. Because of the flat shape of the flexures, any lateral displacement of the balance or transformer core was negligible. Adequate viscous damping of the balance disc was obtained by the use of silicone damping fluid placed in the small gap between the flat top of the transformer housing and the back of the balance disc itself. All of the

electrical leads from the balance penetrated the balance base plate and were led through the channel in the back of the test plate to external instrumentation. The differential transformer was connected to a Schaevitz model PC-1 instrument which provided excitation for the transformer primary winding as well as amplification and rectification of the transformer secondary winding output which was printed-out by a Brown recording potentiometer. In one test series, both the balance disc and transformer housing were instrumented with thermocouples whose outputs were measured and recorded by a Brown recording potentiometer.

With the balance installed in the model, the radial clearance between the plate surface and the balance disc was about 0.002-in. The entire balance mechanism was adjusted so that the disc would be approximately centered during testing. To compensate for the changing drag with roughness, different thickness flexures were used such that the applied drag would cause the disc to move approximately one half of the allowable full travel. This provided adequate tolerance for the drag changes occurring due to the variation in Reynolds number and heat transfer rate accompanying the changes in air supply temperatures, as well as for those due to the lack of prior knowledge of the drag to be obtained with each rough surface.

Alignment of the floating element with the flat plate surface was accomplished by means of eight adjusting screws between the bottom of the plate body and the balance base plate in conjunction with the above-mentioned depth gage, Fig. 10. Misalignment was limited to less than 0.0002-in. For both the balance and the calorimeter, it was possible to maintain the best alignment at the disc leading edge.

Because the tests were conducted under conditions of substantial heat transfer from the air to the plate and balance, thermally induced changes in

characteristics of the balance during its operation were unacceptable unless accurate calibrations and appropriate corrections could be made. The basic design of the balance mechanism did not incorporate any special method to avoid errors which might result from temperature changes or gradients in the balance except that it was constructed symmetrically. For this reason, an effort was made to calibrate the device as a unit, realizing that both electrical and mechanical effects could be present. Using a conventionally assembled balance under conditions of slow, uniform heating and cooling or even at different stable temperatures, no reliable correlation between balance temperature and balance output could be determined. The most undesirable characteristic was an unpredictable zero shift which persisted to a large and variable degree even when the balance was again stabilized at its original temperature. Tests of the balance sensitivity (change in output versus change in load) at various temperatures within the range to be expected under test conditions, however, showed only small variations. Static thermal tests of the Schaevitz transformer were also made which indicated only a small phase shift between primary and secondary voltages with changing temperature. This is in agreement with the findings of the Schaevitz Company. Measurements of the temperature of the transformer housing during actual tunnel testing indicated that any resulting variation in sensitivity would not be significant. On the other hand, the large and rapid zero shift, which was not attributable to electrical changes, could not be tolerated.

Consideration of the high sensitivity of the balance makes it a apparent that even very small thermo-mechanical changes could result in large errors in output. For example, the over-all sensitivity of the balance circuit used during these tests resulted in a recorder output of 1/10 of a millivolt for a transformer core movement of 10 microinches. This output

represents 1 - 2% of the local shear force measured. For this reason, the balance was carefully assembled and then tested under rigorous thermal conditions before it was installed in the plate and used. Specifically, the complete balance was connected electrically to the same circuits and recorders used during testing, and the sensitivity of the entire unit was adjusted to the operating value or higher. Next the balance was heated and cooled at the disc surface, causing temperature gradients to arise in the flexures of a nature corresponding to those which might occur during heat transfer runs. This was done both with the balance under no load and under a static load equivalent to the nominal shear force to be measured. Such testing indicated very clearly that unpredictable thermo-mechanical zero shift could exceed 10% of the full-scale output, but that this could be avoided by the proper selection or combination of flexures. This latter process was essentially one of trial and error, since even the sequence of tightening the flexure retaining screws could influence the final results. By this method, however, it was possible to limit the change in output of the balance mechanism to 1% of full scale for rapid temperature changes in excess of 100°F. This figure is within the nominal accuracy of the recording equipment itself.

Because installation of the balance in the test plate introduced stresses in the balance base plate, the balance was reconnected to the recording circuit after installation in the model and was further tested by heating and cooling the disc. If no further zero shift occurred, the base of the balance was sealed with rubber cement and the model was installed in the test section. It is important to remark here that when the model was used during conditions of heat transfer, any zero shift was very apparent since the shear force was expected to remain essentially constant during the steady portion

of the run. Also of significance in maintaining a high degree of accuracy with the skin friction balance was the fact that the elapsed time between obtaining the balance prerun zero reading and the shear force reading during a run was relatively short. Nominally, the elapsed time between the beginning of the run and the data point acquisition was 45 seconds, while the balance output actually became stable within 20 seconds after the beginning of the run. During this time, the balance disc and transformer housing temperatures increased approximately 75°F and 25°F respectively under the most adverse heating conditions. Zero shift or drift due to external instruments and recorders was insignificant after a two-hour warm-up period.

6. Boundary Layer Survey System

The fact that the operating time of the tunnel was short posed severe restrictions on direct measurements within the boundary layer. It was consequently necessary to use a survey system whose dynamic response would permit some satisfactory number of measurements to be completed during a single run. Such a requirement implies a compromise between such quantities as probe size and strength, and the closest approach of the probe center line to the model surface. Such a compromise was possible concerning pressure surveys, but conditions were too stringent to allow for the development of a temperature survey device. Since only pressure surveys were made, calculation of many boundary layer parameters necessarily depended upon an adequate theoretical velocity-temperature relationship as discussed in Data Reduction.

The total pressure probes used in these experiments were made from round, stainless steel hypodermic tubing with outside diameters ranging from 0.020 to 0.036-in. The choice of retaining a round tube entrance was influenced by the desire to correlate the results with other work done at

DRL concerning surface pitot tubes (Refs. 43 and 44). To obtain a survey probe with a small entrance diameter, yet with adequate strength, short lengths of smaller tubing were telescoped and silver-soldered into the main probe tubing which was 0.098-in. in diameter. The large tubing was further soldered into the double-wedge shaft of the drive mechanism discussed below. To avoid bending of the probe under dynamic loading, particularly when the probe was weakened by high temperatures, the elbow of the probe was stiffened with a thin, steel web which was also silver-soldered in place. See Fig. 11. The length of the unstiffened probe tip was then only about one-half inch. Tests and observations of the probe tip position indicated that no significant deflections occurred during testing.

In order to complete 15-20 pitot pressure readings through the bound boundary layer during a single run, a steady-state probe reading had to be obtained within one to two seconds after the probe was moved from its previous position. From this, it is apparent that the dynamic response of the entire pressure measuring system was critical. The components of the system external to the tunnel consisted of a Statham strain-gage pressure transducer and an Offner Type-R Dynograph, with short lengths of flexible tubing used to connect the probe and transducer. The pressure transducer was temperature compensated and had a differential pressure range of ±20 psi requiring a reference pressure source. Generally atmospheric pressure was used as the reference since the range of pressures to be determined (0-40 in. Hg) made this method feasible. The Offner Dynograph included strain-gage couplers, amplifiers, and an eight-channel recorder which also provided both a time marker and an event marker. The pressure survey system provided an overall sensitivity of 1.5-in. mercury per centimeter of pen deflection with excellent

stability and repeatability. The external system was calibrated using a conventional mercury manometer which limited the accuracy of the entire system to approximately ±0.05-in. of mercury. The frequency response of the transducer-recorder combination was at least one order of magnitude greater than was required and presented no limitation to the response of the entire system.

In the final analysis, the diameter and length of the probe tip were the limiting factors in the system response. It was determined by experiment that adequate response could be obtained with a probe diameter as small as 0.028-in., but small differences in probe construction proved to be very critical, so that actual use of the probe was necessary to determine its true performance. It might be noted that one 0.020-in. diameter probe constructed in the above manner had a marginally satisfactory response, but when improvements were attempted, further dynamic tests always gave less satisfactory results. In addition, the strength of the 0.020-in. diameter tubing was marginal at the high temperatures encountered during test runs.

The probe drive mechanism used in these tests was that described in detail in Ref. 45. The device is shown in Fig. 11 installed through the floor of the tunnel. The double wedge containing the probe extends through a threaded shaft and an access hole in the tunnel floor to the vicinity of the plate. This shaft is fitted with a concentric ratchet wheel which can be rotated in increments of 1/50 of a revolution by a solenoid-operated plunger, each increment in turn moving the probe downward from the plate an additional 0.001-in. The solenoid is energized through a common telephone dial switch which will provide the number of electrical impulses selected by the dial number. Thus, probe movements from 0.001 through 0.010-in. could be selected.

Three modifications to this apparatus were made to permit a complete pressure survey of the boundary layer during a single run. First, an escapement was added to the device to permit manual movement of the probe in 0.025-in. increments. This was necessary since movement of the probe with the solenoid consumed two seconds per 0.010-in. Since only the measurements near the model surface were necessary at close intervals, measurements further away from the model where the pressure gradient dimininished could be made at time-saving 0.025-in. intervals. Second, the probe drive mechanism was electrically insulated from the tunnel by the use of Micarta sleeves and gaskets. A dry-cell operated light was installed on the dial console to indicate electrical contact between the model and the probe so as to provide a positive indication of the departure of the probe from the model surface. Third, the solenoid operation was converted from 115 volts AC to 24 volts DC in order to isolate it electrically from other pressure instrumentation, thereby eliminating the electrical interference which otherwise occurred.

B. Surface Roughness

In general, it might be said that there are two categories of uniformly distributed surface roughness: one which could be designated closely spaced roughness, and the other, widely spaced roughness, which in the limit becomes a set of protuberances. Experimental results obtained with each of these could be widely divergent (Ref. 2). In the first case, at least one roughness parameter is necessary to relate different sizes of the same surface configuration. In the second, at least two are necessary, since both roughness spacing and size are individually important. To limit the possible geometric variations, and because of its inherently more fundamental nature, the first category was used in the present investigation. In addition, the restriction to a one-parameter family was maintained.

The principal aim of the experimental program was to determine the influence of uniform surface roughness on skin friction and heat transfer under the available flow conditions. Because this would constitute an extension of available experimental knowledge, it was considered desirable to obtain results which might be related to the results of previous investigations. The obvious choice of uniform sand-grain roughness would perhaps have allowed for the most extensive comparison with previous work. Among other things, however, consideration of the requirement for an isothermal surface and for the use of calorimetric techniques essentially eliminated the use of suitable grain-like materials. Although a highly conductive surface may be made by using fused metal grains or by suitable photoengraving and electroplating techniques, there is actually no assurance that the resulting grain diameter would be equivalent to the same sand-grain diameter (Ref. 33). The next most obvious roughness choice was the transverse V-groove or thread roughness. The chief advantage of this roughness lies in its application to bodies of revolution and several investigations have been made using such surfaces (Refs. 26, 36, and 37). Also, there is evidence that this type of roughness compares closely in effect with sand grain-type roughness (Refs. 26 and 27). For these reasons, the surface roughness configuration chosen for these experiments was the transverse V-groove. An apex angle of 90° was selected on the basis of a general similarity with sand grain roughness. The groove depth was thus constrained to be one-half of the groove spacing or "pitch", and the longitudinal cross section of the surface was saw-toothed in appearance (See Figs. 6, 8, and 9.).

To maintain this roughness as a one-parameter family irrespective of roughness size, each cross section had to remain the same. Experimentation with the conventional machinability of copper quickly demonstrated that even

for an optimum depth, the quality of the V-groove was unsatisfactory. A three-dimensional waviness was difficult to avoid, and for the 90° apex angle in particular, it was not always possible to prevent the copper from folding over into the adjacent groove. Another disadvantage of conventional machining, of course, was the ultimate destruction of the model unless replating was attempted. In addition, any dulling of the sharp cutting bit would affect the shape and depth of the roughness. As an alternative, a method of rolling or impressing the V-grooves in the surface was developed in which the plate, skin-friction balance disc, and calorimeter disc were coated with a thin layer of tin-lead solder to provide a surface amenable to forming. Because this method is somewhat unique and may be useful in other similar experiments, a discussion of the process and attendant problems is deemed worthwile.

Prior to the application of the solder the copper plate body was thoroughly cleaned with dilute acid. Each of the cutouts for instrumentation was fitted with a cylindrical asbestos plug which extended above the plate surface, and the edges of the plate were similarly dammed with asbestos to allow the solder to melt on the surface and flow to the edges. The entire copper plate was heated to a temperature above the melting point of the solder (446°F) and the solder was melted directly on the plate surface. At all edges of the plate, the solder tended to round-off slightly due to surface tension requiring application of a thick layer of solder, some of which could be removed later. At the outside edges of the plate, a slight rounding-off was not considered serious since the plate sides were to be butted against the tunnel wall and would be well submerged in the wall boundary layer. Great care, however, was necessary with the edges of the cutouts for the calorimeter and skin-friction balance. When the plate had cooled, these edges were peened and milled so that they presented a smooth continuation

of the cutout itself. Cylindrical brass plugs, the thickness of the copper plate, which would fit snugly into the two instrumentation cutouts were similarly heated and coated with solder. These were later peened and turned down to diameter in a lathe and were inserted into the cutouts so as to be flush with the plate bottom. At this point in the process, the entire surface of the model was covered with a thick, nonuniform layer of solder.

With the plugs in both instrumentation cutouts, the plate was bolted onto a 1-in. thick steel plate which was machined to the contour of the bottom of the copper plate body. This steel plate was used to assure adequate stiffness of the model during the process of impressing the V-groove roughness into the surface. The model was then mounted in a shaping machine, and the entire leaded surface was machined flat and smooth in a conventional manner, leaving a thickness of approximately 0.030-in. of solder. This coating was thick enough to permit application and removal of several sizes of roughness before recoating became necessary. While the plate remained fixed in the shaper, the cutting tool was relaced with a hard steel roller 3-in. in diameter and 1/2-in. wide, whose periphery contained 6 to 10 cycles of the desired V-groove roughness which had been cut into the roller with a high-precision lathe. The shaper drove this roller transversely across the plate surface causing the roller to turn without slipping. After traversing the plate in both directions, the roller was automatically stepped in a direction down the plate a distance equal to the selected pitch of the V-grooves. In this manner, each surface groove was reimpressed by each of the several grooves in the roller, resulting in a clean replication of the final groove cut into the roller itself. The rough surface extended from 1-in. behind the instrumentation cutouts to within 1/2-in. of the tripper strip (See Fig. 7.). In order to achieve good results, it was determined experimentally that the penetration of the roller into the

flat surface should be just equal to the depth of the particular V-groove. The steel plate was next removed from the model and the two plugs were driven out of the instrumentation cutouts from the top. This left an extremely clean and square edge with no distortion of the roughness on the plate itself.

In a corresponding but inverse manner, the skin-friction balance disc and calorimeter disc were processed. In each case here, however, a special mating copper plate was used into which each disc fitted snugly. Each of these parts was coated with solder separately and the mating surfaces squared off on a milling machine or lathe, whichever was appropriate. The V-grooves were then impressed in the surface of each exactly as they were in the case of the main plate body. Care was taken to begin the roughness at the same distance from the edge of the disc as was used for the plate itself so that alignment of the V-grooves would be possible when the final installation in the model was made. Here, each finished disc was driven from the mating plate by a 1/4-in. diameter bolt inserted through a tapped hole located in the mating plate behind the disc. In this manner, the disc edges remained clean and square, although the corresponding edges on the mating plate were turned up slightly.

After the plate surface was completed for the first roughness, the static pressure taps were redrilled from the back. Stainless steel tubing 0.060-in. in diameter was then fitted into place for each of the three taps and aluminum side panels for the coolant passages were installed. These were all held in place satisfactorily with Armstrong epoxy cement. Iron-constantan thermocouples with teflon insulated leads were next installed in the wells which extended to a location 0.050-in. from the copper-lead interface at five stations along the plate centerline. On all models, a 1/2-in. wide tripper-strip made of No. 80 grit cloth was secured across the forward edge of the plate body with epoxy cement. See Fig. 7.

C. Test Procedures

The test procedures that were followed in the experimental program were not separately unique; but because of the simultaneous measurement of local skin friction and local heat transfer, they represented a departure from previous techniques. In addition, the boundary layer surveys which had to be completed during the short run time of the tunnel required some procedures not in general use.

Because of the short run time, several (3-7) runs were made for each valve of T_w/T_1 and plate roughness condition to assure repeatability of the data. Measurements which were made routinely during each run, such as the model temperature and various flow properties, are not discussed further in this section. The following paragraphs describe the test procedures used to obtain the experimental results presented in this report.

1. Heat Transfer Measurements

During the steady-flow portion of each heat-transfer run, the cooling probe was extended manually to a mechanical "stop", placing one tip approximately 1/16-in. from the surface of the model at the leading edge of the calorimeter disc. Ten cubic centimeters of cold water were then injected onto the calorimeter using the pressure differential across the tunnel wall. The injected water spread out in a thin layer covering the calorimeter and vaporized, rapidly cooling the calorimeter below the temperature of the plate body which was maintained near 555°R. The probe was then retracted and turned downstream so that it could not influence the flow over the test surface. That it did no influence the flow was indicated by the measured static pressure downstream of the test station which showed no effect when the probe was retracted. After cooling ceased, the calorimeter temperature increased

rapidly in its approach to the recovery temperature and was recorded continuously using a recorder speed of 8 inches per minute, see Fig. 12. When the temperature had exceeded the plate temperature by a wide margin, the run was terminated. To maintain a constant plate temperature during each run, cold water was forced through both cooling passages under 60 psi pressure.

2. Skin Friction Measurements

During all heat transfer runs, the injection of cooling water at the calorimeter was necessary. When the tunnel flow conditions were steady, the cooling probe was extended to the model causing shock wave interference with the flow over the skin friction balance which changed the balance output by 10 to 20 percent. When the probe was subsequently retracted, the balance output rapidly stabilized. Under adiabatic flow conditions when the cooling probe was not generally used, the balance output stabilized within the first 20 seconds of run time and remained sensibly constant during the run. The skin friction balance output was printed at 2-second intervals from 10 seconds before each run until well after the tunnel was shut down.

The cooling probe was designed to cool both the balance disc and the calorimeter and was used in this manner for many of the runs, particularly for those during which the balance disc and transformer housing temperatures were measured. This cyclic heating and cooling of the balance disc had no significant effect on the balance output. As a consequence of this, cooling of the balance disc was not always accomplished.

The entire skin friction balance system was calibrated after each run using a simple dead-weight method. A fine thread was glued to the balance disc and was led aft approximately parallel to the plate surface and over a

small pulley with glass bearings to a weight pan. The balance output was recorded while the pan was both loaded and unloaded with analytical balance weights. The disc and plate surface were carefully cleaned with acetone after each calibration was complete. Because the model test surface faced downward, few problems were encountered in keeping the balance disc gap free from obstructions.

3. Boundary Layer Surveys

Because of interaction between the pitot pressure probe and the model instrumentation, boundary layer surveys could not be made simultaneously with heat transfer and skin friction measurements. Several surveys were made, however, under each of the five flow conditions investigated for each of the four model configurations.

Before each survey run, the tip of the pitot probe was adjusted to touch the surface of the plate so that a downward movement of 0.001 or 0.002-in. would move it from the surface. After the run was started and the pitot pressure was observed to be constant, the probe drive mechanism was actuated in steps of 0.001-in. until the probe was 0.002 to 0.003-in. from the plate. Several steps of 0.002 or 0.003-in, were then used, after which the probe was retracted manually in 0.025-in. increments through the remainder of the boundary layer--approximately 0.250-in. in all. Departure of the probe tip from the test surface was indicated by a light on the probe control box and/or by a change in the pitot pressure reading as observed on the Offner recorder. An event marker on the recorder was used to indicate the number of thousandths of an inch probe movement for those increments less than 0.025-in. The pressure instrumentation was calibrated using a vacuum pump and mercury manometer either immediately before or after each run.

IV. DATA REDUCTION

The conversion of experimental measurements to useful forms is prerequisite to an effective examination of the experimental results. The choice of the relationships used in data reduction can, of course, influence the final results and must be made with care. In their application, all necessary principles and assumptions should be made clear, otherwise the limitations of the results may be obscured. In the present investigation, the measured data were reduced using conventional methods throughout, complicated only slightly by the need for consideration of the model surface roughness. The following sections describe the methods and assumptions used in the reduction of flow data, heat transfer data, and skin friction data as well as those used to determine the roughness dimensions. The methods used to calculate boundary layer parameters from the pitot pressure surveys are also discussed. Flow visualization and electronic computation are mentioned.

A. Flow Data

The flow properties which were measured during all runs were the total pressure, p_o, the total temperature, T_o, and the static pressure, p_1. Both p_o and T_o were measured in the tunnel settling chamber, and it was assumed that they remained constant along the test surface of the model outside the boundary layer. Static pressures were measured at three stations along the model center line and, according to the usual analysis of the boundary layer momentum equations, were assumed to remain constant across the boundary layer. For the smooth model, the static pressure measurements were essentially the same at each station while for the rough-surfaced model, a maximum variation of a few hundredths of an inch of mercury occurred between steady-state measurements at different stations. This variation in static pressure was only

of about the same extent as the actual variation which could occur during a run and the average value was used in reducing data. It should be noted that the two upstream static pressure taps were located on the rough portion of the plate while the remaining tap was located on a smooth portion aft of the test station. This was done to avoid dependence on the unproven measurements of static pressure which might be influenced by the surface roughness.

Using the pressure ratio, p_1/p_o, the free-stream Mach number was determined from the isentropic relation

$$\frac{p_1}{p_o} = \left(1 + \frac{\gamma-1}{2} M_1^2\right)^{-\frac{\gamma}{\gamma-1}} \tag{78}$$

as tabulated in Ref. 46. With few exceptions the resulting free-stream Mach number was 4.90 ± 1% for runs in which the survey probe was not used. With p_o, p_1, and the calibrated value of T_o, and using the equation of state for a perfect gas, the remaining unknown free-stream and stagnation properties were deduced from the tabulated isentropic relations of Ref. 46.

The Reynolds number per foot for each run was calculated using the free-stream properties as determined above and the following viscosity-temperature relationship:

$$\mu_1 = \mu_w \left(\frac{T_1}{T_w}\right)^{\omega} \quad . \tag{79}$$

This relationship has enjoyed widespread use because of its manageable analytical form and its validity over a wide range of temperatures for some constant value of ω. Here the value of ω was selected from Ref. 26 for each value of T_w/T_1 to give results corresponding to Sutherland's viscosity-temperature formula (Ref. 47). Another viscosity-temperature relationship

has been proposed by Fiore (Ref. 48) as being more accurate for static temperatures in the range of 50-200°R, as determined from recent measurements. This alternate relation is

$$\mu_1 = 0.80469 \times 10^{-9} T_1 \quad . \tag{80}$$

For the zero heat-transfer runs ($T_1 \approx 106°R$), use of Eq. (80) would result in Reynolds numbers approximately 5% lower than those using Eq. (79), while for the heat-transfer runs there would be no significant difference.

B. Heat Transfer Data

In compressible boundary layer flow, heat transfer is related to the difference between the surface temperature and the recovery, or adiabatic wall temperature. Although an attempt was made to maintain a constant plate temperature, some variation did occur during high rates of heat transfer. Specifically, the surface temperature near the apex of the leading edge wedge increased to values which were 10 to 45°F higher than the remaining plate surface. The thermocouple which measured the wedge surface temperature was located only 2.0-in. from the leading edge of the model (See Fig. 6). At the remaining stations, 5.6, 7.3, 10.8, and 12.5-in. from the leading edge, the measured temperatures agreed to within 10°F. Since most of the plate surface upstream of the test station was essentially isothermal, the temperature rise at the leading edge and the insulating tripper strip were assumed to have no effect on the local conditions at the test station. During the steady portion of runs at high rates of heat transfer, the temperature of the plate as a whole rose only slightly with time, not exceeding 10°F per minute.

The adiabatic wall temperature was calculated from

$$T_{aw} = T_1 \left(1 + r \frac{\gamma-1}{2} M_1^2\right) \quad . \tag{81}$$

Here r is defined as the recovery factor and was taken to be 0.88. This value appears to be valid for the rough surfaces investigated as well as for the smooth.

Heat transfer rates and coefficients were determined using the measured time rate of calorimeter temperature increase and the following relationship which equates the reat of heat gained by the calorimeter to the rate of heat transferred to the calorimeter from the stream.

$$q = (mc)_c \frac{dT_c}{dt} = hA_c \left(T_{aw} - T_c\right) \quad . \tag{82}$$

This equation defines the heat transfer coefficient, h, based on the temperature difference $(T_{aw} - T_c)$. The appropriate value of T_c used here was taken to be the calorimeter temperature when it was equal to the temperature of the adjacent plate as measured at two stations near the calorimeter. Agreement of these measured temperatures was within 1°F, and the calorimeter temperature was assumed to be uniform throughout. This was also the temperature at which dT_c/dt was measured in order to avoid large errors due to heat exchange between the calorimeter disc and the plate body (Ref. 49). See Fig. 12. Values of dT_c/dt ranged from 80 to 300°F per min. A conservative evaluation of heat transfer between the tunnel wall and the calorimeter indicate that the effects of radiation were negligible at the temperatures experienced.

The actual calculations were made to determine the nondimensional Stanton number, C_h, defined by

$$C_h = \frac{h}{\rho_1 U_1 c_p} \quad .$$

Thus, using Eq. (82),

$$C_h = \frac{(mc)_c \frac{dT_c}{dt}}{\rho_1 U_1 C_p A_c \left(T_{aw} - T_w\right)} \tag{83}$$

where

A_c is the projected surface area of the calorimeter disc.

c_p is the specific heat of air at a constant pressure and was taken to be constant at a value of 0.240 Btu/lb°F for the small static temperature range experienced.

$(mc)_c$ is the heat capacity of the calorimeter.

The determination of $(mc)_c$ for the calorimeter requires a brief discussion. For the solid copper calorimeter, m was simply the mass of the calorimeter determined to within ±0.1% by weighing on an analytical balance and using a value g = 32.17 ft/sec^2. The specific heat, c, was taken to be 0.092 Btu/lb°F (Ref. 50). For calorimeters with a roughness applied, the copper disc was weighed and measured before and after application of the solder coating to determine the weight of each material. A composite value of $(mc)_c$ was then calculated as follows:

$$(mc)_c = (m_{cu}c_{cu} + m_s c_s) \tag{84}$$

The specific heat of solder was taken to be 0.041 Btu/lb°F (Ref. 50,. Nominal weights of the copper disc and the solder coating were 17 and 1.7 gms respectively.

C. Skin Friction Data

The reduction of skin friction balance data was very straightforward. The balance output was printed at two-second intervals from 10 seconds before each run until well after the tunnel was shut down. The balance output reading used to determine wall shear stress was that taken at the

time the calorimeter and wall temperatures were equal. Since the balance output was generally steady, however, it value was not very sensitive to the point of selection. From the calibration curve for the appropriate run, the balance output data point was converted to units of force. The wall shear stress was calculated by dividing this force by the projected area of the balance disc, that is,

$$\tau_w = \frac{\text{Force}}{\text{Area}} \quad .$$

The local skin friction coefficient was calculated from this result using the free-stream dynamic pressure, $1/2\ \rho_1\ u_1^2$, so that

$$C_f = \frac{\tau_w}{\frac{1}{2}\cdot\rho_1\ u_1^2} \quad . \tag{85}$$

Balance calibrations were completed after each run as described in Test Procedures. In general, the balance sensitivity remained constant from run to run, and any hysteresis was found to be less than one percent of the full scale output. Because the greatest temperature changes within the balance mechanism occurred when the tunnel was being shut down and because the balance sensitivity remained constant, the zero output reference was always taken as the no-load output measured in still air just before the run.

During many runs when the skin friction balance disc was cooled, both the disc and transformer housing temperatures were measured. An example of the temperature history of each is illustrated in Fig. 12. No significant changes in measured skin friction occurred as a result of this cyclic heating and cooling, indicating that the step temperature effect at the disc and the thermal extension or contraction of the balance flexures were not significant. This agrees with the findings of Ref. 51 which are based on smooth

plate measurements. From considerations of the repeatability of skin friction measurements, it is felt that the accuracy of the balance system is ±2 percent.

Mean skin friction coefficients were calculated from the momentum integral equation:

$$C_F = \frac{2\theta}{x}$$

For this investigation, the values calculated in this manner also include momentum losses due to the leading edge and tripper strip. For this reason, and the fact that no laminar or transition regions are accounted for, they can only be considered approximate. This situation is covered further in Discussion of Results.

D. Roughness Size

The roughness spacing or pitch, P, was controlled automatically by the machine that impressed the V-grooves and was extremely uniform. Microscopic measurements of 0.0001-in. accuracy showed no variation in pitch from the stated values, P = 0.005, 0.010, and 0.030-in. used here.

The roughness height, H, was nominally one-half of the pitch. The top and bottom of the roughness grooves formed clean right angles without ridges, waviness, or three-dimensional effects, see Figs. 8 and 9. The peak-to-valley height measured microscopically was less than the nominal value by no more than 0.0005-in. This is probably significant only for the smallest pitch used; viz., 0.005-in. Since the pitch and depth are geometrically related, a roughness height of P/2 was used in the reduction of data.

E. Pressure Survey Data

For various reasons it was not always possible to completely traverse the boundary layer well into the free stream and, thus, to obtain the

free-stream pitot pressure for each run. Because of this, two different methods were used to reduce the pressure survey data to Mach number distributions. The first method employed the measured static pressure and pitot pressure to determine the ratio, p_{o_2}/p_1, which in turn was used to find the local Mach number from the Rayleigh pitot formula:

$$\frac{p_{o_2}}{p_1} = \left[\frac{(\gamma + 1)\, M^2}{2}\right]^{\frac{\gamma}{\gamma-1}} \left[\frac{\gamma + 1}{2\gamma\, M^2 - (\gamma - 1)}\right]^{\frac{1}{\gamma-1}} . \qquad (87)$$

Because of experimental errors, particularly in measurements of p_1, the calculated local Mach number did not always converge exactly on the free-stream Mach number at the edge of the boundary layer; however, the variation was generally less than 1%. The second method employed was based on an average free-stream Mach number determined from

$$\frac{p_{o_2}}{p_o} = \left[\frac{(\gamma + 1)\, M_1^{\,2}}{(\gamma - 1)\, M_1^{\,2} + 2}\right]^{\frac{\gamma}{\gamma-1}} \left[\frac{\gamma + 1}{2\gamma\, M_1^{\,2} - (\gamma - 1)}\right]^{\frac{1}{\gamma-1}} \qquad (88)$$

for those runs where free-stream pitot pressures were available. An average Mach number for each different plate configuration was calculated. Using this average Mach number, the static pressure was determined for each run from the more accurate value of p_o. With this static pressure and the measured pitot pressure, the Rayleigh pitot formula was again used to find the local Mach number distribution within the boundary layer. Although the second method produced slightly better convergence with the free-stream Mach number at the outer edge of the boundary layer, agreement between the results of the two methods was generally within 1%. The boundary layer survey data presented in this report are those calculated following the second method. It may be noted that both Eqs. (87) and (88) are tabulated in Ref. 46.

An average boundary layer Mach number distribution was determined for each combination of roughness and temperature ratio, T_w/T_1, that was investigated (20 in all). With the appropriate average free-stream Mach number and the Crocco temperature-velocity relation, Eq. (47), the velocity distribution through the boundary layer was calculated for each case. Using these results the integrands of the momentum thickness expression and others were calculated, plotted, and the integrals determined graphically.

F. Schlieren Data

During many runs, a single schlieren photograph of the test region was taken; also, many runs were observed through the schlieren optical system. No attempt was made to utilize the photographs for quantitative analysis.

G. Electronic Computation

Following the above calculations, basic data from all runs were reduced to useful form utilizing the CDC 1604 digital computer at The University of Texas Computation Center. The computer program was written to provide systematic calculation of the necessary parameters for each appropriate run, as well as corresponding theoretical values following Van Driest, Ref. 15; Sommer and Short, Ref. 21; and Fenter, Ref. 26.

V. DISCUSSION OF RESULTS

The experimental results obtained in this investigation can be categorized broadly as skin friction measurements, boundary layer survey measurements, and heat transfer measurements. They are discussed here in this order because of the dependence of each suceeding topic on the previous one. The results are compared with available theory, and a limited extension of Goddard's theory is presented which accounts for the observed effects of heat transfer on rough-plate skin friction. The influence of roughness on boundary layer velocity profiles is presented and is shown to be qualitatively, if not quantitatively, the same as for the incompressible case. Heat transfer data are given in coefficient form but are also combined with the skin-friction results to determine validity of Reynolds analogy under the test conditions. All data are presented in both graphical and tabular form, and a quantitative indication of the limited scatter of the local skin-friction and heat-transfer measurements is included. A comparison of the Reynolds number based on measured plate length with that determined from R_θ and C_f is also given. Except at the highest heat transfer rates with the rough models, the correspondence is nearly one-to-one. When applicable, the data are displayed using the Reynolds number based on R_θ and C_f.

A. Skin Friction Results

In order to provide a basis for the evaluation of rough plate data and to determine the accuracy of the experimental apparatus by comparing measurements with established theory, a smooth plate model was tested under the full range of flow conditions available. The experimental skin friction coefficients for the smooth plate are plotted against the Reynolds number in

Fig. 13. For comparison, the corresponding curves from the theories of Van Driest (Ref. 17) and Sommer and Short (Ref. 21) are also plotted and the agreement is seen to be very satisfactory. It should be mentioned again that because the Mach number was fixed, the unit Reynolds number varied with the air supply temperature. Since the plate temperature was maintained essentially constant, however, the variation of R_x with T_w/T_1 was unique. As a consequence, the theoretical values can be plotted unambiguously against either R_x or T_w/T_1 according to the actual flow conditions experienced. In Fig. 13 the two extreme experimental temperature ratios are shown at the corresponding Reynolds numbers. The theoretical curve for an adiabatic plate is also included to indicate clearly the effect of heat transfer to the plate on the skin friction coefficient. A summary of smooth plate data is presented in Table III where the number of measurements made for each flow condition is given, as well as both the average deviation from the arithmetic mean value and the percentage deviation. The latter values are direct indications of the scatter of the measured data which is generally less than two percent.

The influence of increasing surface roughness on the local skin friction coefficient can be seen in Fig. 14. The smooth plate data are included here as a reference along with the corresponding theoretical prediction of Spalding and Chi (Ref. 18). Little increase above the smooth plate results was obtained for the roughness of P = 0.005-in. Based on a roughness height, H, equal to P/2, the nondimensional roughness height defined by

$$\frac{U_\tau H}{\nu_w}$$

ranged from 6.0 to 6.6, increasing with increasing heat transfer. Only a small effect for this roughness is thus expected, since the smooth-plate

nondimensional laminar sublayer thickness is approximately 11.5, and according to Harkness (Ref. 52), increases slightly with heat transfer to the plate. The fact that the present roughness is two-dimensional and not three-dimensional, as is sand-grain roughness, may alter the effective value of the parameter $U_\tau H/\nu_w$; however, it has been found by several investigators (Refs. 26, 27) that the V-groove roughness corresponds reasonably closely to sand-grain roughness of the same size. This point is discussed at length below.

Again referring to Fig. 14, it can be seen that the roughness of P = 0.010-in. caused the values of C_f to increase markedly above those for the smooth plate. The nondimensional roughness heights for this surface were from 12.9 to 13.4 and placed the surface well into the transitionally rough regime which extends to values of $U_\tau K/\nu_w$ from 70 to 100 where K is the equivalent sand-grain size, see Fig. 1. For the roughness of P - 0.030-in., the increase in C_f was about 50% over the corresponding smooth-plate values. The nondimensional roughness heights in this case varied from 43.6 to 47.4 when determined using the V-groove height. The experimental skin friction coefficients for all surfaces are also plotted in Fig. 15 against the nondimensional roughness height. This is a cross plot of the results given in Fig. 14 for several heat-transfer conditions. It appears from this figure that C_f remains near the smooth plate value until some minimum roughness height is reached. That is, the surface remains aerodynamically smooth for a roughness size less than some critical value. This nondimensional value is approximately between three and four, and seems to be affected only slightly by the presence of heat transfer. The effect of heat transfer on the initial increase in C_f is more pronounced, although the increase at $U_\tau H/\nu_w = 11.5$ is

about 10% for each case examined here. The average experimental skin friction coefficients and the average deviations of the measurements for the rough plates are given in Tables IV, V, and VI; it can be seen that the average scatter in the measured data generally remains less than two percent.

For arbitrary rough surfaces in high-speed flow, the comparison of experimental data with theory is not as simple as for smooth surfaces. If the surface is in the fully rough flow regime, a determination of the equivalent roughness must first be made to allow for comparison with theory; however, if it is in the transitionally rough regime, no well-established theory is presently available to be used. For an initial comparison, the theoretical predictions of both Fenter and Goddard with K = 0.015-in. are plotted in Fig. 14. Again the theoretical values correspond to the flow conditions experienced in this investigation. For a 90° V-groove roughness, Fenter suggests that K = 0.63H, which would improve the agreement between his theory and the data for P = 0.030-in.; however, this small value of K implies that $U_\tau K/\nu_w \approx 28$. According to Fenter the transitionally rough regime extends between the values of 5 and 100, so that further consideration of the equivalent roughness in terms of his theory would not be meaningful.

The theory of Goddard for sand-roughened surfaces in compressible flow has been experimentally verified over a wide range of Mach numbers under zero heat-transfer conditions. From Fig. 14 it can be seen that the experimental skin friction coefficient for the present adiabatic case with H = 0.015-in. is greater than that predicted by Goddard for a fully rough surface with K = 0.015-in. This trend for a two-dimensional roughness is in agreement with results of Wade (Ref. 36) whose experiments were conducted at Mach 2.48 with cone-cylinder models having a V-groove roughness. Using both the smooth and rough-plate data, the ratios $(C_f/C_{fi})_{exp}$ and $(C_F/C_{Fi})_{exp}$ are shown in

Fig. 16 plotted against H for the adiabatic case. For increasing values of roughness height, H, the ratios $(C_f/C_{fi})_{exp}$ and $(C_F/C_{Fi})_{exp}$ decrease and appear to approach an asymptotic value of approximately 0.21. Following the method presented in THEORY, this result was compared with the experimental value of T_l/T_{aw} and the equivalent roughness, K, was calculated from Eq. (68) to be 1.82H. For the roughness of H = 0.015-in., analysis of the boundary layer velocity distributions which are discussed below also indicates that the effects of the V-groove roughness on skin friction are approximately equivalent to those of sand-grain roughness.

The behavior of $(C_f/C_{fi})_{exp}$ with increasing roughness is shown in Fig. 17 for different heat transfer conditions along with the values of the applicable temperature ratio T_l/T_w. Although for increasing H, each value of $(C_f/C_{fi})_{exp}$ appears to approach a constant value in these coordinates, each value is no longer in excess of the corresponding T_l/T_w. In fact there is a consistent decrease in the value of the asymptotes as T_l/T_w increases. That is, for increasing heat transfer to the plate, the measured skin friction became increasingly less than that predicted by Eq. (57). Although from this and Eq. (68), it might be argued that the imposed heat transfer alters the equivalent roughness, it seems more fundamental to retain the equivalence according to the type of roughness and to explain the observations in terms of the flow conditions. In this way, any conclusions obtained are less likely to be limited to the specific surface roughness under consideration.

Using the equivalent roughness height determined from the zero heat transfer measurements, the values of C_{fi} were recalculated. Then with the experimental values of C_f, the ratio C_f/C_{fi} was formed and plotted against H as before to determine the asymptote for each heat-transfer case. The

resulting values are shown plotted against the experimental temperature ratios, T_l/T_w, in Fig. 18. As assured by the selected equivalent roughness, $K = 1.83H$, the zero heat-transfer result falls on the line through the origin which respresent Eq. (57) while the remaining heat-transfer results lie below it. From a physical point of view this type of variation might be expected because, according to the physical argument leading to Eqs. (56) or (60), the fluid density affecting the surface drag is that existing in the vicinity of the roughness elements. For the adiabatic plate, the temperature gradients near the roughness elements must be very small so that the wall value of the density, and consequently the use of T_l/T_w in Eq. (60) are reasonable first approximations. In the heat-transfer case, however, a large temperature (and density) gradient must exist near the plate surface. This gradient under the heat transfer conditions of the present experimental investigation was always positive, since the plate temperature was maintained below the recovery temperature. As a result of this and the constant pressure boundary layer, the fluid density in the neighborhood of the roughness elements, $\bar{\rho}_K$, was less than the related wall value. Rather than using ρ_w as a first approximation to $\bar{\rho}_K$ when a temperature gradient exists at the surface, therefore, it is more appropriate to use a value intermediate between those corresponding to the temperatures T_w and T_{aw}. Using the experimental data at hand, an expression is derived below for $\bar{\rho}_K$ based on this argument. In a sense, it is a reference temperature method, the generality of which can be determined only by comparison with further experimental data.

It is assumed that Eq. (60),

$$\frac{C_f}{C_{fi}} = \frac{\bar{\rho}_K}{\rho_l} \quad ,$$

is valid to first order and that it reduces to Eq. (57) for the adiabatic plate. The simplest expression for $\bar{\rho}_K$ which satisfies this requirement is

$$\bar{\rho}_K = \rho_{aw} + \lambda\left(\rho_w - \rho_{aw}\right) \tag{89}$$

or

$$\frac{\bar{\rho}_K}{\rho_1} = \frac{\rho_{aw}}{\rho_1} + \lambda\left(\frac{\rho_w}{\rho_1} - \frac{\rho_{aw}}{\rho_1}\right) \tag{90}$$

where ρ_{aw} is the density corresponding to T_{aw}, and λ is an unspecified function. If Eq. (90) is rewritten using Eq. (8), then

$$\frac{T_1}{\bar{T}_K} = \frac{T_1}{T_{aw}} + \lambda\left(\frac{T_1}{T_w} - \frac{T_1}{T_{aw}}\right) \quad , \tag{91}$$

or

$$\frac{C_f}{C_{fi}} - \frac{T_1}{T_{aw}} = \lambda\left(\frac{T_1}{T_w} - \frac{T_1}{T_{aw}}\right) \quad . \tag{92}$$

This expression is simply the function $C_f/C_{fi} = \lambda\, T_1/T_w$ under a translation of both coordinates which, from Fig. 18, is seen to be virtually a straight line of slope 0.635. Therefore, for the conditions investigated, λ is a constant and is equal to 0.635. Equation (92) can be written for C_f/C_{fi} explicitly as

$$\frac{C_f}{C_{fi}} = (1 - \lambda)\,\frac{T_1}{T_{aw}} + \lambda\,\frac{T_1}{T_w} \quad . \tag{93}$$

For $\lambda = 0.635$ this becomes

$$\frac{C_f}{C_{fi}} = 0.365\,\frac{T_1}{T_{aw}} + 0.635\,\frac{T_1}{T_w} \tag{94}$$

where, of course, (T_1/T_{aw}) can be written as a function of the free-stream Mach number and the recovery factor, if desired. Because λ shows no dependence on T_1/T_w or R_x over the range investigated and because Eq. (93)

inherently accounts for the effects of both the Mach number M_1 and temperature ratio T_w/T_1, it may have a more general application than can be ascertained from the present data. Assuming for the moment that the value of λ remains constant, the skin friction predictions of Eqs. (57) and (94) can be compared for various Mach numbers and temperature ratios. This is shown in Fig. 19 for $T_w = T_{aw}$ and $T_w = T_1$. Both results are the same for the adiabatic plate but differ considerably for $T_w = T_1$ where Goddard's expression predicts no change in skin friction due to compressibility. The assumption that λ is an absolute constant, of course, is highly speculative; however, from physical considerations, it might be expected to remain near the value determined above, since that value defines $\bar{\rho}_K$ to be approximately midway between the ρ_w and ρ_{aw}.

Because the drag of roughness elements in a boundary layer is largely dependent on the local dynamic pressure, there arises the possibility that some quantitative measurements of skin friction may be made directly with a surface pitot pressure tube. Since boundary layer surveys were made during this investigation, a limited number of data were available for this purpose. Pitot pressures were measured with a 0.028-in. diameter probe lying on the top of the roughness elements which were themselves 0.015-in. high for the only case considered here. The Mach number at the probe centerline was found from the Rayleigh pitot formula as described in DATA REDUCTION and was used to determine the corresponding local-dynamic pressure q from

$$q = \frac{1}{2} \gamma \, p_1 \, M^2$$

The values of the ratio of q/q_1 to $(q/q_1)_{aw}$ are compared in the brief table below with values of C_f/C_{faw} which were determined from the skin-friction balance measurements for the same roughness and temperature ratio.

T_w/T_1	C_f/C_{faw}	$\left(\frac{q}{q_1}\right) \div \left(\frac{q}{q_1}\right)_{aw}$	% Difference
3.80	1.16	1.32	+ 13.8
3.55	1.21	1.19	- 1.5
3.18	1.27	1.20	- 5.4
2.91	1.32	1.37	+ 3.8

Although the number of measurements was limited, the fair agreement indicates that this method deserves further attention. This is particularly true because of the difficulty of making boundary-layer measurements in the presence of heat transfer.

Mean skin friction coefficients, C_F, were calculated using the boundary layer pressure survey data as described in DATA REDUCTION. These values are plotted in Fig. 20 against the Reynolds number. It should be recalled that these measurements include the effects of the leading edge and tripper strip; however, for all four model configurations these effects should have been the same. Referring to Fig. 20 it can be seen that the only configuration which does not enter the turbulent transition region at the lower test Reynolds numbers is the smooth one. In some instances, the drag of the rough plate at high rates of heat transfer is actually less than for the smooth plate at the same values of R_x and T_w/T_1 because of delayed transition. A similar effect was found by James (Ref. 37) for rough cylinders on which the length of the laminar boundary layer was increased by 10-15% for certain optimum roughness heights. One possible explanation of this phenomenon is that the increased intermittency of the turbulent boundary layer of a rough surface (Ref. 53) causes the time-averaged momentum losses to be decreased. If this is the case, the effect would only be significant for short bodies but might find useful application in internal aerodynamics.

According to Czarnecki and Monta (Ref. 54), who carried out experiments on a roughened ogival cylinder at Mach numbers of 1.61 and 2.01, a large part of the measured drag was found to be supersonic wave drag. Their models, however, cannot be described as having closely spaced roughness elements which is a significant factor in this respect. In the present case, neither the static pressure measurements made along the plate nor the schlieren photographs indicated the presence of wave drag. Three typical schlieren photographs taken under different heat transfer conditions for the case of the rough plate with P = 0.030-in. are shown in Figs. 21, 22, and 23.

B. Boundary Layer Survey Results

The results of the boundary layer surveys are presented in Tables VII through X for the 20 different heat transfer and roughness combinations tested. The momentum thickness for each case is included, as well as the appropriate value of U_τ which was calculated using the wall shear stress measured with the skin friction balance. To calculate the boundary layer velocity profiles, use was made of the Crocco energy relation, Eq. (47), valid for a Prandtl number equal to unity. The resulting velocity profiles are shown in Figs. 24 through 28 for the different heat transfer conditions experienced. In each case the effect of increased roughness was to flatten the inner portion of the profile leaving the outer portion and the boundary layer thickness relatively unaffected. This is comparable to the usual incompressible results. The effect of increasing heat transfer on the velocity profiles is apparent if the figures are considered consecutively. As the temperature ratio T_w/T_1 decreases, the profiles for the smooth-plate coalesce with those for the smallest roughness, while those for the two larger roughnesses are not affected to any great extent. This is

probably because of increased viscous effects at the higher temperatures near the wall which remain important only for small roughness sizes. Plotted on a logarithmic scale, this variation in velocity profiles is seen to be a vertical shift in the nondimensional velocity distribution as predicted in Chapter II, see Figs. 29 and 30. This shift may be used to compare the effects of the present V-groove roughness with the shift experienced using sand-grain roughness in incompressible flow as given by Eq. (36). Although the velocity distribution in a compressible flow with heat transfer is given by an equation of the form of Eq. (50), the shift due to increasing roughness can be determined with good accuracy from the plot of u/U_τ vs U_τ/ν_w, provided the Mach number and temperature ratio are the same for the profiles considered. This was also found to be true for the zero heat-transfer case by Goddard (Ref. 27). Following this procedure, the shift in velocity profile for each rough surface was determined using the smooth-plate velocity profile for the same temperature ratio, T_w/T_1, as the reference. The results are compared with Eq. (36) in Fig. 31 and are seen to be approximately the same as those predicted for the incompressible boundary layer of a sand grain roughened surface.

C. Heat Transfer Results

The experimental values of C_h for all model configurations are given in Tables III through VI and are plotted against the Reynolds number in Fig. 32. The estimated value of C_h for the smooth plate as suggested by Van Driest (Ref. 15) is also included and is in fair agreement with the smooth-plate measurements. The variation of C_h with R_x is seen to be qualitatively the same as that of C_f which is shown in Fig. 14. There was little increase in C_h for the roughness of height 0.0025-in., even though the physical surface

area of the plate and calorimeter was increased over the smooth-surface area by approximately 40%. Further increases in C_h of about the same magnitude were obtained when the roughness height was again increased to 0.005-in. and then to 0.015-in. The behavior of C_h with increasing nondimensional roughness height is shown in Fig. 33 which is a cross plot from Fig. 32. A comparison of Figs. 15 and 33 shows a striking difference in the behaviors of C_f and C_h with increasing roughness; this is discussed further below.

The values of C_f and C_h from each test run were combined in accordance with Eq. (62) to determine the experimental Reynolds analogy factors. The average of these values for each flow condition and model configuration is also given in Tables III through VI, along with the average deviation of the individual measurements from the stated average value. These deviations are, in general, less than 5%, as is the case for the heat transfer measurements themselves. The experimentally determined values of S for the smooth plate are shown in Figs. 34, 35, and 36 plotted against M_1, R_x, and $(T_{aw} - T_w)$ respectively along with smooth plate data from the indicated references. Although the data were obtained over a wide range of flow parameters, as indicated from the figures, the variations in S are no greater than the probable experimental errors.

In Fig. 37 the experimental Reynolds analogy factors are plotted against T_w/T_1 and it can be seen that the values 0.8 to 0.85, suggested by Eckert (Ref. 32), constitute a fair approximation. The effect of increasing roughness on S is seen to be small for the smaller roughness sizes. The roughness of P = 0.030-in., however, increases the value of S significantly to an average value near unity, which corresponds to the simple Reynolds analogy, Eq. 61. That the analogy factor is not likely to remain near unity for

further increases in roughness, is apparent from Figs. 15 and 33. This may also be seen clearly if, for the experimental conditions, S is plotted against the roughness height as in Figs. 38. For the type of roughness employed here, it appears that the Reynolds analogy factor will increase in direct proportion to the roughness height throughout the transitionally rough flow regime. For greater roughness heights, it seems likely that it will increase directly with the skin friction coefficient since, as indicated in Fig. 33, C_h may approach a nearly constant value.

D. The Effective Reynolds Number

Having determined R_θ and C_f experimentally, the effective Reynolds number for each of the 20 test conditions was calculated from Eqs. (75) and (77) by use of the curves of Figs. 3 and 4. These values are shown in Figs. 39-42, plotted against the Reynolds number based on the measured length to the test station. The good agreement for the smooth plate indicates that the effective turbulent origin is very near the leading edge and that, for the particular configuration, the Reynolds number based on the length x is adequate for use over all the flow conditions used. For the rough plate at high rates of heat transfer, however, there may be a 5 to 10% variation in the length of the turbulent boundary layer; therefore, the actual plate length should not be used in calculating R_x.

VI. CONCLUSIONS

Certain conclusions can be drawn from the experimental observations made in this study which may, of course, be limited to the flow regimes investigated. These are as follows:

1. The experimental results, in general, indicate the desirability and feasibility of using the direct measuring skin friction balance in nonadiabatic, compressible flow for both smooth and rough surfaces.
2. From the results obtained in this investigation, it appears that the effects of surface roughness on the compressible turbulent boundary layer with heat transfer remain similar to those observed in low-speed flow if the nonuniform fluid density is accounted for in some approximate manner.
3. The effects of the V-groove roughness used in the present tests correspond closely to those of a uniformly distributed sand-grain roughness.
4. It does not appear that supersonic wave drag is a factor in the skin friction drag of the type of surface employed in this investigation.
5. Quantitative skin friction predictions can be made for a rough surface with a compressible turbulent boundary layer and with heat transfer by the use of the incompressible relations and the concept of a reference temperature if the equivalent sand-grain roughness of the surface is known.
6. The present measurements indicated that the maximum roughness height which will cause no increase in skin friction is approximately 1/4 to 1/2 of the smooth plate laminar sublayer thickness and that the

extent of the fully rough regime is comparable to that for the incompressible case if the wall value of the density is used in the friction velocity.

7. From considerations of the increase in skin friction with increase in roughness height, it appears that the skin friction law must be of a similar form for both compressible and incompressible flow even in the presence of heat transfer.

8. With increasing roughness, heat transfer to the rough surface is increased, as is the skin friction, but to a different degree which depends on the roughness regime of the flow as described below in terms of Reynolds analogy.

9. The Reynolds analogy factor, which is relatively insensitive to changes in the flow parameters, appears to remain valid as long as the roughness height is less than twice the laminar sublayer thickness. For roughness in excess of this value, the analogy factor increases directly with the roughness height until the fully rough regime is reached, after which it is probable that it increases approximately with C_f, that is, it appears that C_h may reach a relatively constant value for large roughness heights.

REFERENCES

1. Clauser, F. H., "Turbulent Boundary Layer", Advances In Applied Mechanics, Vol. IV, ed. by H. L. Dryden and T. von Kármán, Academic Press Inc., 1956, pp. 1-21.

2. Schlichting, H., Boundary Layer Theory, McGraw-Hill Book Co., 1960, Chapters XVIII-XXI, pp. 457-565.

3. Van Driest, E. R., "Turbulent Boundary Layer in Compressible Fluids", Journal of the Aeronautical Sciences, Vol. 18, No. 3, March, 1951.

4. Deissler, R. G., and Loeffler, A. L., "Analysis of Turbulent Flow and Heat Transfer on a Flat Plate at High Mach Numbers with Variable Fluid Properties", NASA TR R-17, 1959.

5. Prandtl, L., "The Mechanics of Viscous Fluids", Aerodynamic Theory, Div. G, Vol. III, ed. by W. F. Durand, Reprinted Edition 1934.

6. von Kármán, T., "Mechanical Similitude and Turbulence", NACA TN-611, March, 1931.

7. von Kármán, T., "Turbulence and Skin Friction", Journal of the Aeronautical Sciences, Vol. 1, pp. 1-20, January, 1934.

8. Schoenherr, K. E., "Resistance of Flat Surfaces Moving Through a Fluid", Transactions of the Society of Naval Architects and Marine Engineers, Vol. 40, 1932.

9. Bertram, M. H., "Calculations of Compressible Average Turbulent Skin Friction", NASA TR R-123, 1962.

10. Coles, D., "The Law of the Wake in the Turbulent Boundary Layer", Journal of Fluid Mechanics, Vol. 1, Part 2, July, 1956.

11. Schultz-Grunow, F., "Neues Reibungswiderstandsgesetz fur glatte Platten", Luftfahrtforschung, Vol. 17, No. 8, August, 1940, pp. 219-246 (translation available as "New Frictional Resistance Law for Smooth Plates", NACA TM-986, September, 1941).

12. Prandlt, L., and Schlichting, H., "Das Widerstandgesetz rauher Platten", Werft, Reedereie, Hafen Jahrg. 15, Heft 1, January 1934, p. 1., (translated as "The Resistance Law for Rough Plates", David Taylor Model Basin Translation 258, September, 1955).

13. Clutter, D. W., "Charts for Determining Skin-Friction Coefficients on Smooth and on Rough Flat Plates at Mach Numbers up to 5.0 with and without Heat Transfer", Report No. ES 29074, Douglas Aircraft Division, Long Beach, California, April 15, 1959.

14. Droblenkov, V. F., "The Turbulent Boundary Layer on a Rough Curvilinear Surface", NACA TM 1440, September, 1958.

15. Van Driest, E. R., "Convective Heat Transfer in Gases", Turbulent Flows and Heat Transfer, Vol. V High Speed Aeordynamics and Jet Propulsion, ed. by C. C. Lin, Princeton University Press, 1959, pp. 370-395.

16. Wilson, R. E., "Turbulent Boundary-Layer Characteristics Supersonic Speeds--Theory and Experiment", Journal of the Aeronautical Sciences, Vol. 17, No. 9, September, 1950.

17. Van Driest, E. R., "The Problem of Aerodynamic Heating", Aeronautical Engineering Review, October, 1956, pp. 26-41.

18. Spalding, D. B., and Chi, S. W., "The Drag of a Compressible Turbulent Boundary Layer on a Smooth Flat Plate with and without Heat Transfer", Journal of Fluid Mechanics, Vol. 18, Part 1, January, 1964.

19. Rubesin, M. W., and Johnson, H. A., "A Critical Review of Skin-Friction and Heat-Transfer Solutions of the Laminar Boundary Layer of a Flat Plate", ASME Trans., Vol. 71, No. 4, May, 1949, p. 383.

20. Fischer, W. W., and Norris, R. H., "Supersonic Convective Heat-Transfer Correlation from Skin-Temperature Measurements on a V-2 Rocket in Flight", ASME Trans., Vol. 71, No. 5, July, 1949, pp. 457-470.

21. Sommer, S. C., and Short, B. J., "Free-Flight Measurements of Turbulent-Boundary-Layer Skin Friction in the Presence of Severe Aerodynamic Heating at Mach Numbers from 2.8 to 7.0", NACA TN-3391, March, 1955.

22. Eckert, E. R. G., "Survey of Heat Transfer at High Speeds", Wright Air Development Center TR- 54-70, April, 1954.

23. Monaghan, R. J., "On the Behavior of Boundary Layers at Supersonic Speeds", Fifth International Aeronautical Conference, (Los Angeles, California, June 20-23, 1955), Inst. Aero. Sci., Inc., 1955, pp. 277-315.

24. Peterson, J. B., Jr., "A Comparison of Experimental and Theoretical Results for the Compressible Turbulent-Boundary-Layer Skin Friction with Zero Pressure Gradient", NASA D-1795, March, 1963.

25. Spalding, D. B., "A New Analytical Expression for the Drag of a Flat Plate Valid for Both the Turbulent and Laminar Regimes", Int. Journal Heat and Mass Transfer, Vol. 5, p. 1133.

26. Fenter, F. W., "The Turbulent Boundary Layer on Uniformly Rough Surfaces at Supersonic Speeds", Report No. DRL-468, CM-941, Defense Research Laboratory, The University of Texas, Austin, Texas, January, 1960 (also Ph.D. dissertation in Aerospace Engineering).

27. Goddard, F. E., Jr., "Effect of Uniformly Distributed Roughness on Turbulent Skin-Friction Drag at Supersonic Speeds", Journal of the Aero/Space Sciences, Vol. 26, No. 1, January, 1959.

28. Liepmann, H. W., and Goddard, F. E., Jr., "Note on the Mach Number Effect Upon the Skin Friction of Rough Surfaces", Journal of the Aeronautical Sciences, Vol. 24, No. 10, p. 784, October, 1957.

29. Prandtl, L., and Tietjens, O. G., Applied Hydro and Aeromechanics, McGraw-Hill Book Co., Inc., New York, 1934.

30. Colburn, A. P., "A Method of Correlating Forced Convection Heat Transfer Data and Comparison with Fluid Friction", American Inst. of Chem. Engrs., Trans., Vol. XXIX, 1933, pp. 174-210.

31. Rubesin, M. W., "A Modified Reynolds Analogy for Compressible Turbulent Boundary Layer on a Flat Plate", NACA TN-2917, March, 1953.

32. Eckert, E. R. G., "Survey on Heat Transfer at High Speeds", ARL-189, Aeronautical Research Laboratory, Wright-Patterson Air Force Base, Ohio, December, 1961.

33. Hastrup, R. C., Sabersky, R. H., Bartz, D. R., and Noel, M. B., "Friction and Heat Transfer in a Rough Tube at Varying Prandtl Numbers", Jet Propulsion, Vol. 28, No. 4, April, 1958, pp. 259-262.

34. Nikuradse, J., "Laws of Flow in Rough Pipes", NACA TM-1292, 1950.

35. Seiff, A., "Examination of the Existing Data on the Heat Transfer of Turbulent Boundary Layers at Supersonic Speeds from the Point of View of Reynolds Analogy", NACA TN-3284, 1954.

36. Wade, J. H. T., "An Experimental Investigation of the Effects of Surface Roughness on the Drag of a Cone-Cylinder Model at a Mach Number of 2.48", University of Toronto, Institute of Aerophysics, Report No. 34, September, 1955.

37. James, C. S., "Boundary-Layer Transition on Hollow Cylinders in Supersonic Free Flight as Affected by Mach Number and a Screwthread Type of Surface Roughness", NASA MEMO 1-20-59A, February, 1959.

38. Moore, D. R., "Drag Effects of Surface Roughness at High Reynolds Numbers, M = 2.8", Report No. 0-71000/4R-16, Ling-Temco-Vought, Inc., Dallas, Texas, June, 1964.

39. Harkness, J. L., "The Design of a Three-Dimensional Intermittent Flow Hypersonic Wind Tunnel", Report No. DRL-197, Defense Research Laboratory, The University of Texas, Austin, Texas, January, 1949 (also Master's thesis in Aeronautical Engineering).

40. Hartwig, W. H., "Theory, Design, and Performance of a 420 kw Electrical Heater for Automatic Control of Stagnation Temperature in a Blow-Down Wind Tunnel", Report No. DRL-383, AFOSR TN-56-163, Defense Research Laboratory, The University of Texas, Austin, Texas, June, 1956 (also Ph.D. dissertation in Electrical Eng.).

41. Weiler, J. E., "A Storage-Type Air Heater for an Intermittent-Flow Supersonic Wind Tunnel", Report No. DRL-393, AFOSR TN-56-572, Defense Research Laboratory, The University of Texas, Austin, Texas, 7 November 1956.

42. Cole, C. H., Jr., "The Design and Evaluation of a Constant Temperature Flat Plate", Report No. DRL-474, Defense Research Laboratory, The University of Texas, Austin, Texas, January, 1962 (also Master's thesis in Aerospace Engineering).

43. Moore, D. R., "Velocity Similarity in the Compressible Turbulent Boundary Layer with Heat Transfer", Report No. DRL-480, Defense Research Laboratory, The University of Texas, Austin, Texas, April, 1962 (also Ph.D. dissertation in Aerospace Engineering).

44. Westkaemper, J. C., and Hill, O., "Summary of Studies on the Measurement of Local Skin Friction by Means of the Surface Impact or Preston Tube", Report No. DRL-513, CR-9, Defense Research Laboratory, The University of Texas, Austin, Texas, February 18, 1964.

45. Lacy, J. R., "Interference Effects Between Total-Pressure Probes in the Boundary Layer of a Supersonic Wind Tunnel", Report No. DRL-420, AFOSR TN-58-6, Defense Research Laboratory, The University of Texas, Austin, Texas, January, 1958 (also Master's thesis in Mechanical Engineering).

46. Ames Research Staff, "Equations, Tables, and Charts for Compressible Flow", NACA Report 1135, 1953.

47. Handbook of Supersonic Aerodynamics, NAVORD Report 1488, Vol. 5, U. S. Navy Bureau of Ordnance, GPO Washington, D. C., 1953, p. 1510.10a-2.

48. Fiore, A. W., "An Equation for the Coefficient of Viscosity at Low Temperatures", OAR Research Review, Office of Aerospace Research, Vol. II, No. 19, December 2, 1963.

49. Westkaemper, J. C., "An Experimental Evaluation of the Insulated-Mass Technique of Measuring Heat Transfer at High Velocities", Report No. DRL-439, CF-2765, Defense Research Laboratory, The University of Texas, Austin, Texas, January, 1959 (also Master's thesis in Mechanical Engineering).

50. Handbook of Chemistry and Physics, 43rd Edition, 1961, ed. by C. D. Hodgman, The Chemical Rubber Publishing Co., Cleveland, Ohio, p. 2320.

51. Westkaemper, J. C., "Step-Temperature Effects on Direct Measurements of Drag", AIAA Journal, Vol. 1, No. 7, July, 1963, p. 1708.

52. Harkness, J. L, "The Effect of Heat Transfer on Turbulent Boundary Layer Skin Friction", Report No. DRL-436, CM-940, Defense Research Laboratory, The University of Texas, Austin, Texas, 2 June 1959.

53. Schubauer, G. B., and Tchen, C. N., "Turbulent Flow", Turbulent Flows and Heat Transfer, Vol. V, Section B, ed. by C. C. Lin, Princeton University Press, Princeton, N. J., 1959, pp. 75-195.

54. Czarnecki, K. R., and Monta, W. J., "Boundary-Layer Velocity Profiles and Skin Friction Due to Surface Roughness on an Ogive Cylinder at Mach Numbers of 1.61 and 2.01", NASA TN D-2048, December, 1963.

55. Pappas, C. C., "Measurement of Heat Transfer in the Turbulent Boundary Layer on a Flat Plate in Supersonic Flow and Comparison With Skin-Friction Results", NACA TN-3222, 1954

56. Fallis, W. B., "Heat Transfer in the Transitional and Turbulent Boundary Layers on a Flat Plate at Supersonic Speeds", Rep. No. 19, University of Toronto, Inst. of Aerophysics, May, 1952.

TABLE I

VALUES OF F_c AT VARIOUS M_1 AND T_w/T_1

(from Spalding, Ref. 18)

T_w/T_1 \ M_1	0	1	2	3	4
1	1.0000	1.0295	1.1167	1.2581	1.4494
2	1.4571	1.4867	1.5744	1.7176	1.9130
3	1.8660	1.8956	1.9836	2.1278	2.3254
4	2.2500	2.2796	2.3678	2.5126	2.7117
5	2.6180	2.6477	2.7359	2.8812	3.0813
6	2.9747	3.0044	3.0927	3.2384	3.4393
8	3.6642	3.6938	3.7823	3.9284	4.1305
10	4.3311	4.3608	4.4493	4.5958	4.7986
12	4.9821	5.0117	5.1003	5.2470	5.4504
14	5.6208	5.6505	5.7391	5.8860	6.0898
16	6.2500	6.2797	6.3683	6.5153	6.7196
18	6.8713	6.9010	6.9897	7.1368	7.3413
20	7.4861	7.5157	7.6045	7.7517	7.9564

T_w/T_1 \ M_1	5	6	7	8	9
1	1.6871	1.9684	2.2913	2.6542	3.0562
2	2.1572	2.4472	2.7809	3.1564	3.5725
3	2.5733	2.8687	3.2092	3.5929	4.0184
4	2.9621	3.2611	3.6066	3.9964	4.4290
5	3.3336	3.6355	3.9847	4.3792	4.8174
6	3.6930	3.9971	4.3493	4.7477	5.1905
8	4.3863	4.6937	5.0505	5.4549	5.9050
10	5.0559	5.3657	5.7259	6.1347	6.5904
12	5.7088	6.0204	6.3832	6.7955	7.2556
14	6.3491	6.6621	7.0271	7.4422	7.9058
16	6.9795	7.2937	7.6603	8.0778	8.5444
18	7.6019	7.9170	8.2851	8.7045	9.1737
20	8.2175	8.5334	8.9027	9.3238	9.7952

TABLE II

VALUES OF F_{rx} AT VARIOUS M_1 AND T_w/T_1

(from Spalding, Ref. 18)

T_w/T_1 \ M_1	0	1	2	3	4
1	1.0000	1.1023	1.3562	1.6631	1.9526
2	0.2471	0.2748	0.3463	0.4385	0.5326
3	0.1061	0.1185	0.1512	0.1947	0.2410
4	0.0576	0.0645	0.0829	0.1079	0.1352
5	0.0356	0.0399	0.0516	0.0677	0.0856
6	0.0240	0.0269	0.0349	0.0460	0.0586
8	0.0127	0.0143	0.0187	0.0248	0.0319
10	0.0077	0.0087	0.0114	0.0153	0.0198
12	0.0052	0.0058	0.0076	0.0102	0.0133
14	0.0036	0.0041	0.0054	0.0073	0.0095
16	0.0025	0.0030	0.0040	0.0054	0.0071
18	0.0021	0.0023	0.0031	0.0041	0.0054
20	0.0016	0.0018	0.0024	0.0033	0.0043

T_w/T_1 \ M_1	5	6	7	8	9
1	2.1946	2.3840	2.5262	2.6301	2.7038
2	0.6178	0.6902	0.7493	0.7962	0.8327
3	0.2849	0.3239	0.3572	0.3847	0.4072
4	0.1620	0.1865	0.1497	0.2264	0.2418
5	0.1036	0.1204	0.1355	0.1487	0.1600
6	0.0715	0.0837	0.0949	0.1048	0.1135
8	0.0394	0.0466	0.0535	0.0597	0.0653
10	0.0246	0.0293	0.0339	0.0382	0.0421
12	0.0166	0.0200	0.0233	0.0264	0.0292
14	0.0120	0.0144	0.0168	0.0192	0.0214
16	0.0104	0.0108	0.0127	0.0145	0.0162
18	0.0069	0.0084	0.0099	0.0113	0.0127
20	0.0054	0.0066	0.0079	0.0091	0.0102

TABLE III
SKIN FRICTION AND HEAT TRANSFER DATA
SMOOTH PLATE

M_1	T_w/T_1	R_x $\times 10^{-7}$	T_r °R	C_f $\times 10^3$	ΔC_f $\times 10^3$	ΔC_f %	No. of Runs	C_h $\times 10^3$	ΔC_h $\times 10^3$	ΔC_h %	No. of Runs	S	ΔS	ΔS %	No. of Runs
4.88	5.21	1.415	559	1.016	0.012	1.22	6								
4.93	4.22	0.845	740	1.248	0.049	3.90	3	0.652	0.006	0.98	2	0.989	0.000	0.00	1
4.91	3.83	0.759	828	1.282	0.030	2.34	4	0.714	0.021	2.91	3	0.891	0.015	1.73	3
4.93	3.76	0.613	900	1.379	0.018	1.31	3	0.798	0.181	2.27	3	0.868	0.009	1.07	3
4.90	3.67	0.765	799	1.246	0.013	1.08	4	0.741	0.013	1.73	4	0.841	0.013	1.57	4
4.93	3.41	0.521	992	1.446	0.007	0.47	2	0.869	0.032	3.74	2	0.832	0.070	8.47	2
4.92	3.33	0.615	919	1.360	0.011	0.82	3	0.832	0.015	1.83	3	0.818	0.022	2.68	3
4.91	3.03	0.560	997	1.367	0.024	1.78	3	0.865	0.032	3.71	4	0.790	0.023	2.94	3

TABLE IV

SKIN FRICTION AND HEAT TRANSFER DATA

ROUGH PLATE P=0.005 in.

M_1	T_w/T_1	R_x $\times 10^{-7}$	T_r $^\circ R$	C_f $\times 10^3$	ΔC_f $\times 10^3$	ΔC_f %	No. of Runs	C_h $\times 10^3$	ΔC_h $\times 10^3$	ΔC_h %	No. of Runs	S	ΔS	ΔS %	No. of Runs
4.87	5.17	1.501	558	1.050	0.003	0.28	5								
4.85	3.94	1.014	726	1.204	0.019	1.58	4	0.661	0.012	1.88	4	0.911	0.020	2.15	4
4.84	3.59	0.843	814	1.297	0.025	1.96	5	0.760	0.040	5.21	7	0.828	0.018	2.21	5
4.85	3.18	0.670	913	1.393	0.018	1.28	5	0.833	0.049	5.85	7	0.835	0.036	4.29	5
4.87	2.97	0.564	997	1.478	0.018	1.20	3	0.907	0.028	3.08	5	0.810	0.014	1.76	3

TABLE V
SKIN FRICTION AND HEAT TRANSFER DATA
ROUGH PLATE P=0.010 in.

M_1	T_w/T_1	R_x $\times 10^{-7}$	T_r °R	C_f $\times 10^3$	ΔC_f $\times 10^3$	ΔC_f %	No. of Runs	C_h $\times 10^3$	ΔC_h $\times 10^3$	ΔC_h %	No. of Runs	S	ΔS	ΔS %	No. of Runs
4.84	5.15	1.532	541	1.114	0.021	1.85	5								
4.88	3.94	0.919	728	1.324	0.027	2.04	4	0.786	0.018	2.26	5	0.847	0.009	1.04	4
4.87	3.66	0.842	785	1.371	0.014	1.00	3	0.801	0.034	4.31	3	0.848	0.035	4.19	3
4.87	3.55	0.750	816	1.435	0.004	0.28	3	0.847	0.023	2.73	4	0.848	0.016	1.85	3
4.89	3.25	0.621	901	1.530	0.009	0.58	6	0.904	0.013	1.47	6	0.837	0.008	0.98	6
4.91	2.99	0.502	997	1.671	0.019	1.17	4	1.015	0.020	1.95	5	0.819	0.009	1.16	4

TABLE VI
SKIN FRICTION AND HEAT TRANSFER DATA
ROUGH PLATE P=0.030 in.

M_1	T_w/T_1	R_x $\times 10^{-7}$	T_r °R	C_f $\times 10^3$	ΔC_f $\times 10^3$	ΔC_f %	No. of Runs	C_h $\times 10^3$	ΔC_h $\times 10^3$	ΔC_h %	No. of Runs	S	ΔS	ΔS %	No. of Runs
4.87	5.21	1.347	542	1.490	0.016	1.10	7								
4.89	3.75	0.830	748	1.704	0.026	1.54	4	0.862	0.032	3.71	4	0.990	0.032	3.21	4
4.89	3.56	0.740	795	1.789	0.025	1.41	6	0.920	0.516	5.61	6	0.976	0.057	5.87	6
4.90	3.21	0.604	891	1.922	0.016	0.82	6	1.003	0.046	4.54	6	0.961	0.045	4.66	6
4.90	2.87	0.450	1007	2.110	0.048	2.29	5	1.097	0.059	5.35	5	0.966	0.060	6.17	5

TABLE VIIa

BOUNDARY LAYER SURVEY DATA

(Smooth Plate)

$M_1 = 4.91$ $\quad \frac{T_w}{T_1} = 5.186$ $\quad R_x = 1.318 \times 10^7$

$T_o = 607°R$ $\quad T_1 = 104°R$ $\quad x = 0.957$ ft

$\Theta = 8.07 \times 10^{-3}$ in. $\quad T_{aw} = 541°R$ $\quad u_1 = 2459$ ft/ sec

$U_\tau = 126.0$ ft / sec

y (inches)	$\frac{U_\tau y}{\nu_w}$	$\frac{M}{M_1}$	$\frac{\bar{u}}{u_1}$	$\frac{\bar{u}}{U_\tau}$
0.018	41.90	0.375	0.698	13.61
0.020	46.56	0.395	0.720	14.04
0.025	58.20	0.428	0.752	14.66
0.030	69.84	0.458	0.779	15.19
0.035	81.48	0.482	0.799	15.58
0.050	116.40	0.535	0.837	16.32
0.075	174.60	0.611	0.881	17.18
0.100	232.80	0.687	0.916	17.86
0.125	291.00	0.765	0.944	18.41
0.150	349.20	0.842	0.966	18.84
0.175	407.40	0.910	0.982	19.15
0.200	465.60	0.960	0.992	19.35
0.225	523.80	0.985	0.997	19.44
0.250	582.00	0.993	0.999	19.48
0.275	640.20	0.995	0.999	19.48

TABLE VIIb

BOUNDARY LAYER SURVEY DATA
(Smooth Plate)

$M_1 = 4.91$ $\quad \frac{T_w}{T_1} = 3.779$ $\quad R_x = 0.7915 \times 10^7$

$T_o = 824.2°R$ $\quad T_1 = 141.6°R$ $\quad x = 0.943$ ft

$\Theta = 9.42 \times 10^{-3}$ in. $\quad T_{aw} = 739°R$ $\quad u_1 = 2865$ ft/sec

$U_\tau = 137.8$ ft/sec

y (inches)	$\frac{U_\tau y}{\nu_w}$	$\frac{M}{M_1}$	$\frac{\bar{u}}{u_1}$	$\frac{\bar{u}}{U_\tau}$
0.014	36.59	0.377	0.657	13.66
0.016	41.81	0.389	0.671	13.95
0.020	52.27	0.426	0.712	14.81
0.025	65.33	0.455	0.740	15.39
0.030	78.40	0.482	0.765	15.91
0.035	91.47	0.500	0.781	16.24
0.050	130.66	0.541	0.813	16.91
0.075	195.99	0.613	0.861	17.91
0.100	261.33	0.693	0.903	18.78
0.125	326.66	0.770	0.935	19.44
0.150	391.99	0.848	0.962	20.01
0.175	457.33	0.924	0.983	20.44
0.200	522.66	0.975	0.995	20.69
0.225	587.99	0.994	0.999	20.78
0.250	653.32	1.001	1.000	20.79
0.275	718.66	1.002	1.001	20.82
0.300	783.99	1.002	1.001	20.82

TABLE VIIc

BOUNDARY LAYER SURVEY DATA

(Smooth Plate)

$M_1 = 4.91$ $\quad \frac{T_w}{T_1} = 3.503$ $\quad R_x = 0.6870 \times 10^7$

$T_o = 894.1°R$ $\quad T_1 = 153.6°R$ $\quad x = 0.943$ ft

$\Theta = 9.82 \times 10^{-3}$ in. $\quad T_{aw} = 799°R$ $\quad u_1 = 2984$ ft/ sec

$U_\tau = 141.9$ ft/ sec

y (inches)	$\frac{U_\tau y}{\nu_w}$	$\frac{M}{M_1}$	$\frac{\bar{u}}{u_1}$	$\frac{\bar{u}}{U_\tau}$
0.014	36.83	0.384	0.658	13.84
0.016	42.09	0.394	0.670	14.09
0.020	52.61	0.423	0.702	14.76
0.025	65.76	0.465	0.744	15.65
0.030	78.91	0.490	0.766	16.11
0.035	92.06	0.509	0.782	16.44
0.050	131.52	0.553	0.816	17.16
0.075	197.28	0.618	0.860	18.09
0.100	263.04	0.690	0.898	18.88
0.125	328.80	0.768	0.932	19.59
0.150	390.56	0.842	0.958	20.14
0.175	460.32	0.916	0.980	20.61
0.200	526.08	0.972	0.994	20.90
0.225	591.84	0.990	0.998	20.99
0.250	657.60	0.999	1.000	21.03
0.275	723.36	1.001	1.000	21.03
0.300	789.12	1.002	1.000	21.03

TABLE VIId

BOUNDARY LAYER SURVEY DATA
(Smooth Plate)

$M_1 = 4.91$ $\quad \frac{T_w}{T_1} = 3.166$ $\quad R_x = 0.5680 \times 10^7$

$T_o = 994.8°R$ $\quad T_1 = 170.9°R$ $\quad x = 0.943$ ft

$\Theta = 10.35 \times 10^{-3}$ in. $\quad T_{aw} = 905°R$ $\quad u_1 = 3148$ ft/ sec

$U_\tau = 147.6$ ft/ sec

y (inches)	$\frac{U_\tau y}{\nu_w}$	$\frac{M}{M_1}$	$\frac{\bar{u}}{u_1}$	$\frac{\bar{u}}{U_\tau}$
0.014	37.17	0.392	0.658	10.04
0.016	42.41	0.403	0.672	10.34
0.020	53.10	0.440	0.711	15.17
0.025	66.38	0.480	0.750	16.00
0.030	79.65	0.502	0.770	16.43
0.035	92.93	0.521	0.786	16.77
0.050	132.75	0.560	0.816	17.41
0.075	199.13	0.624	0.858	18.30
0.100	265.51	0.700	0.899	19.18
0.125	331.89	0.770	0.930	19.84
0.150	398.86	0.841	0.956	20.39
0.175	464.60	0.904	0.976	20.82
0.200	531.01	0.961	0.991	21.14
0.225	597.40	0.983	0.996	21.25
0.250	663.77	0.995	0.999	21.31
0.275	730.15	0.996	0.999	21.31
0.300	796.53	0.997	0.999	21.31

TABLE VIIe

BOUNDARY LAYER SURVEY DATA

(Smooth Plate)

$M_1 = 4.91$ $\quad \frac{T_w}{T_1} = 2.782$ $\quad R_x = 0.4955 \times 10^7$

$T_o = 1148.4°R$ $\quad T_1 = 197.3°R$ $\quad x = 0.943$ ft

$\Theta = 11.08 \times 10^{-3}$ in. $\quad T_{aw} = 1021°R$ $\quad u_1 = 3382$ ft/ sec

$U_\tau = 145.0$ ft/ sec

y (inches)	$\frac{U_\tau y}{\nu_w}$	$\frac{M}{M_1}$	$\frac{\bar{u}}{u_1}$	$\frac{\bar{u}}{U_\tau}$
0.014	38.48	0.399	0.656	15.30
0.016	43.98	0.411	0.670	15.62
0.020	54.97	0.450	0.712	16.60
0.025	68.71	0.482	0.743	17.33
0.030	82.45	0.504	0.763	17.79
0.035	96.20	0.522	0.779	18.17
0.050	137.43	0.561	0.809	18.87
0.075	206.14	0.631	0.857	19.98
0.100	274.85	0.703	0.897	20.92
0.125	343.56	0.771	0.929	21.67
0.150	412.27	0.839	0.954	22.25
0.175	480.99	0.897	0.973	22.69
0.200	549.70	0.943	0.985	22.97
0.225	618.41	0.968	0.992	23.13
0.250	687.12	0.978	0.995	23.20
0.275	755.84	0.990	0.998	23.27
0.300	824.55	0.990	0.998	23.27

TABLE VIIIa

BOUNDARY LAYER SURVEY DATA

(Rough Plate P = 0.005-in.)

$M_1 = 4.95$ $\quad \frac{T_w}{T_1} = 5.089$ $\quad R_x = 1.412 \times 10^7$

$T_o = 643.7°R$ $\quad T_1 = 109.1°R$ $\quad x = 0.974$ ft

$\Theta = 8.11 \times 10^{-3}$ in. $\quad T_{aw} = 558°R$ $\quad u_1 = 2535$ ft/sec

$U_\tau = 126.0$ ft/sec

y (inches)	$\frac{U_\tau y}{\nu_w}$	$\frac{M}{M_1}$	$\frac{\bar{u}}{u_1}$	$\frac{\bar{u}}{U_\tau}$
0.018	43.25	0.401	0.728	14.58
0.020	48.06	0.408	0.735	14.72
0.025	60.07	0.444	0.769	15.40
0.030	72.10	0.470	0.791	15.84
0.035	84.10	0.485	0.803	16.08
0.050	120.15	0.522	0.830	16.62
0.075	180.22	0.594	0.873	17.49
0.100	240.30	0.670	0.910	18.22
0.125	300.37	0.745	0.938	18.78
0.150	360.45	0.824	0.961	19.24
0.175	420.52	0.902	0.980	19.62
0.200	480.60	0.965	0.994	19.90
0.225	540.67	0.996	0.999	20.00
0.250	600.75	1.004	1.000	20.02
0.275	660.82	1.005	1.001	20.04

TABLE VIIIb

BOUNDARY LAYER SURVEY DATA

(Rough Plate P = 0.005-in.)

$M_1 = 4.95$ $\quad \frac{T_w}{T_1} = 4.030$ $\quad R_x = 0.8917 \times 10^7$

$T_o = 814.2°R$ $\quad T_1 = 138.0°R$ $\quad x = 0.974$ ft

$\Theta = 9.67 \times 10^{-3}$ in. $\quad T_{aw} = 728°R$ $\quad u_1 = 2851$ ft/sec

$U_\tau = 145.3$ ft/sec

y (inches)	$\frac{U_\tau y}{\nu_w}$	$\frac{M}{M_1}$	$\frac{\bar{u}}{u_1}$	$\frac{\bar{u}}{U_\tau}$
0.018	44.65	0.398	0.689	13.52
0.020	49.62	0.412	0.704	13.81
0.025	62.02	0.455	0.747	14.66
0.030	74.42	0.490	0.778	15.27
0.035	86.83	0.509	0.794	15.58
0.050	124.04	0.550	0.824	16.17
0.075	186.06	0.610	0.863	16.93
0.100	248.08	0.680	0.899	17.64
0.125	310.10	0.751	0.930	18.25
0.150	372.12	0.823	0.955	18.74
0.175	434.13	0.891	0.975	19.13
0.200	496.16	0.945	0.988	19.39
0.225	558.18	0.982	0.997	19.56
0.250	620.20	0.994	0.999	19.60
0.275	682.22	1.000	1.000	19.62
0.300	744.24	1.002	1.001	19.64

TABLE VIII c

BOUNDARY LAYER SURVEY DATA
(Rough Plate P = 0.005-in.)

$M_1 = 4.95$ $\quad \frac{T_w}{T_1} = 3.649$ $\quad R_x = 0.7564 \times 10^7$

$T_o = 906.8°R$ $\quad T_1 = 153.7°R$ $\quad x = 0.974$ ft

$\Theta = 10.12 \times 10^{-3}$ in. $\quad T_{aw} = 810°R$ $\quad u_1 = 3010$ ft/sec

$U_\tau = 150.8$ ft/sec

y (inches)	$\frac{U_\tau y}{\nu_w}$	$\frac{M}{M_1}$	$\frac{\bar{u}}{u_1}$	$\frac{\bar{u}}{U_\tau}$
0.018	46.07	0.397	0.678	13.53
0.020	51.19	0.411	0.694	13.85
0.025	63.99	0.450	0.734	14.65
0.030	76.79	0.482	0.764	15.25
0.035	89.59	0.507	0.785	15.66
0.050	127.98	0.545	0.814	16.24
0.075	191.97	0.610	0.858	17.12
0.100	255.96	0.680	0.895	17.86
0.125	319.95	0.754	0.929	18.54
0.150	383.94	0.825	0.954	19.04
0.175	447.93	0.892	0.975	19.46
0.200	511.92	0.948	0.988	19.71
0.225	575.91	0.982	0.996	19.88
0.250	639.90	0.992	0.999	19.93
0.275	703.89	0.998	1.000	19.95
0.300	767.88	1.000	1.000	19.95

TABLE VIIId

BOUNDARY LAYER SURVEY DATA

(Rough Plate P = 0.005-in.)

$M_1 = 4.95$ $\quad \frac{T_w}{T_1} = 3.240$ $\quad R_x = 0.6352 \times 10^7$

$T_o = 1030.7°R$ $\quad T_1 = 174.7°R$ $\quad x = 0.974$ ft

$\Theta = 10.03 \times 10^{-3}$ in. $\quad T_{aw} = 913°R$ $\quad u_1 = 3208$ ft/sec

$U_\tau = 146.7$ ft/sec

y (inches)	$\frac{U_\tau y}{\nu_w}$	$\frac{M}{M_1}$	$\frac{\bar{u}}{u_1}$	$\frac{\bar{u}}{U_\tau}$
0.018	45.04	0.411	0.684	14.95
0.020	50.10	0.424	0.698	15.26
0.025	62.63	0.461	0.736	16.09
0.030	75.16	0.471	0.763	16.68
0.035	87.61	0.515	0.784	17.14
0.050	125.26	0.558	0.817	17.86
0.075	187.89	0.619	0.858	18.76
0.100	250.52	0.687	0.895	19.57
0.125	313.15	0.760	0.928	20.29
0.150	375.78	0.830	0.954	20.86
0.175	438.41	0.875	0.974	21.30
0.200	501.04	0.947	0.988	21.60
0.225	563.67	0.980	0.996	21.78
0.250	626.30	0.990	0.998	21.82
0.275	698.93	0.995	0.999	21.84
0.300	751.56	0.998	1.000	21.86
0.325	814.19	1.000	1.000	21.86

TABLE VIIIe

BOUNDARY LAYER SURVEY DATA
(Rough Plate P = 0.005-in.)

$M_1 = 4.95$ $\quad \frac{T_w}{T_1} = 2.993$ $\quad R_x = 0.5457 \times 10^7$

$T_o = 1121.5°R$ $\quad T_1 = 190.1°R$ $\quad x = 0.974$ ft

$\Theta = 10.17 \times 10^{-3}$ in. $\quad T_{aw} = 999°R$ $\quad u_1 = 3347$ ft/ sec

$U_\tau = 159.7$ ft/ sec

y (inches)	$\frac{U_\tau y}{\nu_w}$	$\frac{M}{M_1}$	$\frac{\bar{u}}{u_1}$	$\frac{\bar{u}}{U_\tau}$
0.018	47.67	0.425	0.693	14.53
0.020	52.97	0.441	0.709	14.86
0.025	66.21	0.484	0.751	15.74
0.030	79.45	0.513	0.777	16.29
0.035	92.70	0.535	0.795	16.66
0.050	135.42	0.579	0.828	17.36
0.075	198.63	0.645	0.870	18.24
0.100	264.85	0.715	0.906	18.99
0.125	331.06	0.787	0.937	19.64
0.150	397.27	0.859	0.962	20.16
0.175	463.49	0.921	0.980	20.54
0.200	529.70	0.960	0.990	20.75
0.225	595.91	0.975	0.994	20.84
0.250	662.12	0.980	0.996	20.88
0.275	728.34	0.984	0.996	20.88
0.300	794.55	0.984	0.996	20.88
0.325	860.76	0.984	0.996	20.88

TABLE IXa

BOUNDARY LAYER SURVEY DATA

(Rough Plate P = 0.010-in.)

$M_1 = 4.94$ $\quad \frac{T_w}{T_1} = 5.171$ $\quad R_x = 1.355 \times 10^7$

$T_o = 620.0°R$ $\quad T_1 = 105.4°R$ $\quad x = 0.974$ ft

$\Theta = 8.60 \times 10^{-3}$ in. $\quad T_{aw} = 544°R$ $\quad u_1 = 2487$ ft/ sec

$U_\tau = 134.6$ ft/ sec

y (inches)	$\frac{U_\tau y}{\nu_w}$	$\frac{M}{M_1}$	$\frac{\bar{u}}{u_1}$	$\frac{\bar{u}}{U_\tau}$
0.014	35.98	0.342	0.662	12.24
0.016	41.12	0.347	0.668	12.35
0.020	51.40	0.360	0.684	12.64
0.025	64.25	0.379	0.705	13.03
0.030	77.10	0.400	0.727	13.44
0.035	89.45	0.422	0.749	13.86
0.050	128.50	0.485	0.803	14.14
0.075	192.75	0.555	0.851	15.73
0.100	257.00	0.643	0.898	16.60
0.125	321.25	0.727	0.932	17.23
0.150	385.50	0.807	0.958	17.71
0.175	449.75	0.882	0.977	18.06
0.200	514.00	0.949	0.991	18.32
0.225	578.25	0.977	0.996	18.41
0.250	642.50	0.994	0.999	18.46
0.275	706.75	1.000	1.000	18.48
0.300	771.00	1.000	1.000	18.48

TABLE IXb

BOUNDARY LAYER SURVEY DATA
(Rough Plate P = 0.010-in.)

$M_1 = 4.94$ $\quad \frac{T_w}{T_1} = 3.966$ $\quad R_x = 0.8680 \times 10^7$

$T_o = 798.2°R$ $\quad T_1 = 135.7°R$ $\quad x = 0.953$ ft

$\Theta = 10.12 \times 10^{-3}$ in. $\quad T_{aw} = 706°R$ $\quad u_1 = 2822$ ft/sec

$U_\tau = 145.4$ ft/sec

y (inches)	$\frac{U_\tau y}{\nu_w}$	$\frac{M}{M_1}$	$\frac{\bar{u}}{u_1}$	$\frac{\bar{u}}{U_\tau}$
0.014	38.65	0.366	0.650	12.61
0.016	44.17	0.375	0.661	12.82
0.020	55.21	0.398	0.687	13.33
0.025	69.01	0.419	0.710	13.77
0.030	82.81	0.438	0.729	14.14
0.035	96.61	0.455	0.745	14.45
0.050	138.02	0.502	0.787	15.27
0.075	207.03	0.574	0.840	16.30
0.100	276.04	0.657	0.887	17.21
0.125	345.05	0.732	0.922	17.89
0.150	414.06	0.808	0.950	18.43
0.175	483.07	0.882	0.973	18.88
0.200	552.08	0.950	0.989	19.19
0.225	621.09	0.994	0.999	19.38
0.250	691.10	1.003	1.001	19.42
0.275	759.11	1.010	1.002	19.44
0.300	828.12	1.010	1.002	19.44
0.325	897.13	1.010	1.002	19.44

TABLE IXc

BOUNDARY LAYER SURVEY DATA

(Rough Plate P = 0.010-in.)

$M_1 = 4.94$ $\quad \frac{T_w}{T_1} = 3.597$ $\quad R_x = 0.7046 \times 10^7$

$T_o = 894.7°R$ $\quad T_1 = 152.1°R$ $\quad x = 0.958$ ft

$\Theta = 10.01 \times 10^{-3}$ in. $\quad T_{aw} = 796°R$ $\quad u_1 = 2988$ ft/sec

$U_\tau = 156.3$ ft/sec

y (inches)	$\frac{U_\tau y}{\nu_w}$	$\frac{M}{M_1}$	$\frac{\bar{u}}{u_1}$	$\frac{\bar{u}}{U_\tau}$
0.014	38.76	0.370	0.645	12.33
0.016	44.30	0.381	0.658	12.58
0.020	55.37	0.410	0.692	13.23
0.025	69.21	0.441	0.724	13.84
0.030	83.06	0.459	0.741	14.16
0.035	96.90	0.472	0.754	14.41
0.050	138.42	0.519	0.794	15.18
0.075	207.64	0.596	0.848	16.21
0.100	276.85	0.675	0.893	17.07
0.125	346.06	0.757	0.930	17.78
0.150	415.27	0.834	0.957	18.29
0.175	484.49	0.905	0.978	18.69
0.200	553.70	0.962	0.991	18.94
0.225	622.91	0.992	0.998	19.08
0.250	692.12	1.000	1.000	19.12
0.275	761.34	1.000	1.000	19.12
0.300	830.55	1.000	1.000	19.12

TABLE IXd

BOUNDARY LAYER SURVEY DATA

(Rough Plate P = 0.010-in.)

$M_1 = 4.94$ $\quad \frac{T_w}{T_1} = 3.210$ $\quad R_x = 0.6183 \times 10^7$

$T_o = 1002.4°R$ $\quad T_1 = 170.4°R$ $\quad x = 0.950$ ft

$\Theta = 10.44 \times 10^{-3}$ in. $\quad T_{aw} = 891°R$ $\quad u_1 = 3162$ ft/sec

$U_\tau = 150.1$ ft/sec

y (inches)	$\frac{U_\tau y}{\nu_w}$	$\frac{M}{M_1}$	$\frac{\bar{u}}{u_1}$	$\frac{\bar{u}}{U_\tau}$
0.014	59.17	0.378	0.644	13.57
0.016	44.77	0.390	0.659	13.89
0.020	55.96	0.421	0.691	14.63
0.025	69.95	0.448	0.722	15.21
0.030	83.94	0.470	0.743	15.66
0.035	97.93	0.485	0.757	15.95
0.050	139.89	0.527	0.792	16.69
0.075	209.84	0.603	0.847	17.85
0.100	279.79	0.678	0.890	18.75
0.125	349.74	0.757	0.927	19.53
0.150	419.68	0.836	0.956	20.15
0.175	489.63	0.909	0.978	20.61
0.200	559.58	0.962	0.991	20.88
0.225	629.53	0.984	0.997	21.01
0.250	699.47	0.996	0.999	21.05
0.275	769.42	1.000	1.000	21.07
0.300	839.37	1.000	1.000	21.07

TABLE IXe

BOUNDARY LAYER SURVEY DATA

(Rough Plate P = 0.010-in.)

$M_1 = 4.94$ $\quad \frac{T_w}{T_1} = 2.915$ $\quad R_x = 0.4982 \times 10^7$

$T_o = 1128.2°R$ $\quad T_1 = 191.8°R$ $\quad x = 0.953$ ft

$\Theta = 10.61 \times 10^{-3}$ in. $\quad T_{aw} = 1004°R$ $\quad u_1 = 3355$ ft/sec

$U_\tau = 166.2$ ft/sec

y (inches)	$\frac{U_\tau y}{\nu_w}$	$\frac{M}{M_1}$	$\frac{\bar{u}}{u_1}$	$\frac{\bar{u}}{U_\tau}$
0.014	40.43	0.391	0.651	13.14
0.016	46.20	0.402	0.664	13.41
0.020	57.75	0.439	0.705	14.23
0.025	72.19	0.467	0.733	14.80
0.030	86.63	0.487	0.752	15.18
0.035	101.07	0.507	0.770	15.55
0.050	144.38	0.580	0.876	16.68
0.075	216.58	0.635	0.862	17.40
0.100	288.77	0.706	0.901	18.19
0.125	360.96	0.779	0.933	18.84
0.150	433.15	0.845	0.957	19.32
0.175	505.35	0.912	0.978	19.75
0.200	577.54	0.960	0.990	19.99
0.225	649.73	0.977	0.995	20.09
0.250	721.92	0.980	0.996	20.11
0.275	794.12	0.980	0.996	20.11
0.300	866.31	0.980	0.996	20.11

TABLE Xa

BOUNDARY LAYER SURVEY DATA

(Rough Plate P = 0.030-in.)

$M_1 = 4.95$ $\quad \frac{T_w}{T_1} = 5.211$ $\quad R_x = 1.307 \times 10^7$

$T_o = 607.1°R$ $\quad T_1 = 102.9°R$ $\quad x = 0.937$ ft

$\Theta = 10.81 \times 10^{-3}$ in. $\quad T_{aw} = 536°R$ $\quad u_1 = 2962$ ft/sec

$U_\tau = 154.9$ ft/sec

y (inches)	$\frac{U_\tau y}{\nu_w}$	$\frac{M}{M_1}$	$\frac{\bar{u}}{u_1}$	$\frac{\bar{u}}{U_\tau}$
0.014	40.71	0.290	0.593	9.43
0.016	46.52	0.293	0.597	9.49
0.020	58.15	0.301	0.608	9.66
0.025	72.69	0.318	0.631	10.03
0.030	87.23	0.331	0.649	10.32
0.035	101.77	0.345	0.666	10.59
0.050	145.38	0.392	0.719	11.43
0.075	218.08	0.457	0.780	12.40
0.100	290.77	0.519	0.827	13.14
0.125	363.46	0.598	0.876	13.92
0.150	436.15	0.680	0.914	14.53
0.175	508.85	0.762	0.943	14.99
0.200	581.54	0.843	0.967	15.37
0.225	654.23	0.917	0.984	15.64
0.250	726.93	0.976	0.996	15.83
0.275	799.62	0.997	0.999	15.88
0.300	872.31	1.005	1.001	15.91
0.325	945.00	1.005	1.001	15.91

TABLE Xb

BOUNDARY LAYER SURVEY DATA

(Rough Plate P = 0.030-in.)

$M_1 = 4.95$ $\quad \frac{T_w}{T_1} = 3.754$ $\quad R_x = 0.6857 \times 10^7$

$T_o = 854.9°R$ $\quad T_1 = 144.9°R$ $\quad x = 0.937$ ft

$\Theta = 12.97 \times 10^{-3}$ in. $\quad T_{aw} = 771°R$ $\quad u_1 = 2995$ ft/sec

$U_\tau = 176.8$ ft/sec

y (inches)	$\frac{U_\tau y}{\nu_w}$	$\frac{M}{M_1}$	$\frac{\bar{u}}{u_1}$	$\frac{\bar{u}}{U_\tau}$
0.014	42.52	0.326	0.593	10.05
0.016	48.60	0.330	0.598	10.13
0.020	60.75	0.344	0.617	10.45
0.025	75.94	0.360	0.637	10.79
0.030	91.12	0.371	0.651	11.03
0.035	106.31	0.382	0.664	11.25
0.050	151.87	0.419	0.705	11.94
0.075	227.81	0.482	0.766	12.98
0.100	303.74	0.549	0.819	13.87
0.125	379.68	0.620	0.865	14.65
0.150	455.61	0.696	0.904	15.31
0.175	531.54	0.774	0.937	15.87
0.200	607.48	0.850	0.962	16.30
0.225	683.42	0.920	0.981	16.62
0.250	759.35	0.975	0.995	16.86
0.275	835.28	0.998	1.000	16.94
0.300	911.22	1.000	1.000	16.94

TABLE Xc

BOUNDARY LAYER SURVEY DATA

(Rough Plate P = 0.030-in.)

$M_1 = 4.95$ $\quad \frac{T_w}{T_1} = 3.530$ $\quad R_x = 0.6388 \times 10^7$

$T_o = 909.1°R$ $\quad T_1 = 154.1°R$ $\quad x = 0.937$ ft

$\Theta = 13.51 \times 10^{-3}$ in. $\quad T_{aw} = 815°R$ $\quad u_1 = 3013$ ft/sec

$U_T = 180.9$ ft/sec

y (inches)	$\frac{U_T y}{\nu_w}$	$\frac{M}{M_1}$	$\frac{\bar{u}}{u_1}$	$\frac{\bar{u}}{U_T}$
0.014	42.61	0.317	0.574	9.56
0.016	48.80	0.323	0.582	9.69
0.020	60.99	0.338	0.602	10.03
0.025	76.24	0.353	0.622	10.36
0.030	91.49	0.366	0.639	10.64
0.035	106.74	0.378	0.653	10.87
0.050	152.49	0.415	0.695	11.57
0.075	228.73	0.480	0.760	12.66
0.100	304.98	0.545	0.812	13.52
0.125	381.22	0.618	0.861	14.34
0.150	457.47	0.694	0.901	15.01
0.175	533.71	0.769	0.934	15.56
0.200	609.96	0.842	0.959	15.97
0.225	686.20	0.907	0.978	16.29
0.250	762.45	0.965	0.992	16.52
0.275	838.69	0.996	0.999	16.64
0.300	914.94	1.004	1.001	16.67

TABLE Xd

BOUNDARY LAYER SURVEY DATA

(Rough Plate P = 0.030-in.)

$M_1 = 4.95$ $\quad \frac{T_w}{T_1} = 3.206$ $\quad R_x = 0.5741 \times 10^7$

$T_o = 1004.7°R$ $\quad T_1 = 170.3°R$ $\quad x = 0.937$ ft

$\Theta = 14.13 \times 10^{-3}$ in. $\quad T_{aw} = 899°R$ $\quad u_1 = 3168$ ft/sec

$U_\tau = 180.9$ ft/sec

y (inches)	$\frac{U_\tau y}{\nu_w}$	$\frac{M}{M_1}$	$\frac{\bar{u}}{u_1}$	$\frac{\bar{u}}{U_\tau}$
0.014	40.44	0.305	0.547	9.58
0.016	50.78	0.310	0.554	9.70
0.020	63.48	0.329	0.581	10.17
0.025	79.35	0.347	0.605	10.59
0.030	95.22	0.360	0.622	10.19
0.035	111.09	0.373	0.639	11.19
0.050	158.70	0.414	0.686	12.01
0.075	238.05	0.484	0.756	13.24
0.100	317.40	0.550	0.810	14.18
0.125	396.75	0.619	0.857	15.01
0.150	476.10	0.690	0.896	15.69
0.175	555.45	0.761	0.928	16.25
0.200	634.80	0.833	0.955	16.72
0.225	714.15	0.901	0.976	17.09
0.250	793.50	0.962	0.991	17.35
0.275	872.85	0.992	0.998	17.48
0.300	952.20	1.000	1.000	17.51
0.325	1031.55	1.002	1.001	17.53

TABLE Xe

BOUNDARY LAYER SURVEY DATA
(Rough Plate P = 0.030-in.)

$M_1 = 4.95$ $\quad \frac{T_w}{T_1} = 2.916$ $\quad R_x = 0.4683 \times 10^7$

$T_o = 1120.9°R$ $\quad T_1 = 190.0°R$ $\quad x = 0.937$ ft

$\Theta = 12.84 \times 10^{-3}$ in. $\quad T_{aw} = 1006°R$ $\quad u_1 = 3346$ ft/sec

$U_\tau = 191.3$ ft/sec

y (inches)	$\frac{U_\tau y}{\nu_w}$	$\frac{M}{M_1}$	$\frac{\bar{u}}{u_1}$	$\frac{\bar{u}}{U_\tau}$
0.014	44.23	0.325	0.566	9.20
0.016	50.54	0.335	0.580	10.14
0.020	63.18	0.353	0.604	10.56
0.025	78.97	0.370	0.626	10.95
0.030	94.77	0.390	0.651	11.38
0.050	157.95	0.456	0.723	12.64
0.075	236.92	0.527	0.787	13.76
0.100	315.90	0.601	0.842	14.73
0.125	394.87	0.679	0.887	15.51
0.150	473.85	0.758	0.924	16.16
0.175	552.82	0.831	0.952	16.65
0.200	631.80	0.902	0.975	17.05
0.225	710.77	0.963	0.992	17.35
0.250	789.75	0.986	0.997	17.44
0.275	868.72	0.994	0.999	17.47
0.300	947.70	0.995	0.999	17.47
0.325	1026.67	0.995	0.999	17.47

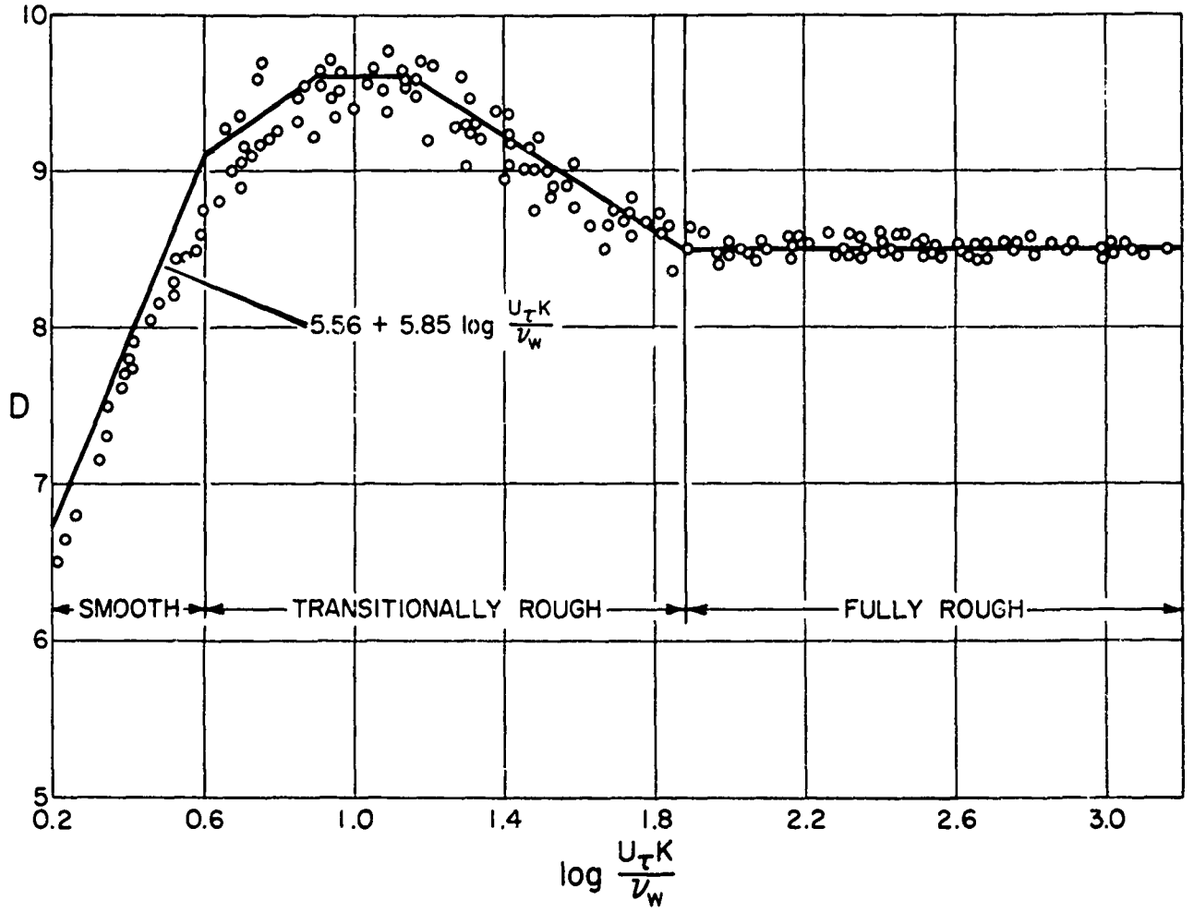

FIGURE 1
NIKURADSE'S ROUGHNESS FUNCTION vs NONDIMENSIONAL ROUGHNESS HEIGHT (Ref. 13)

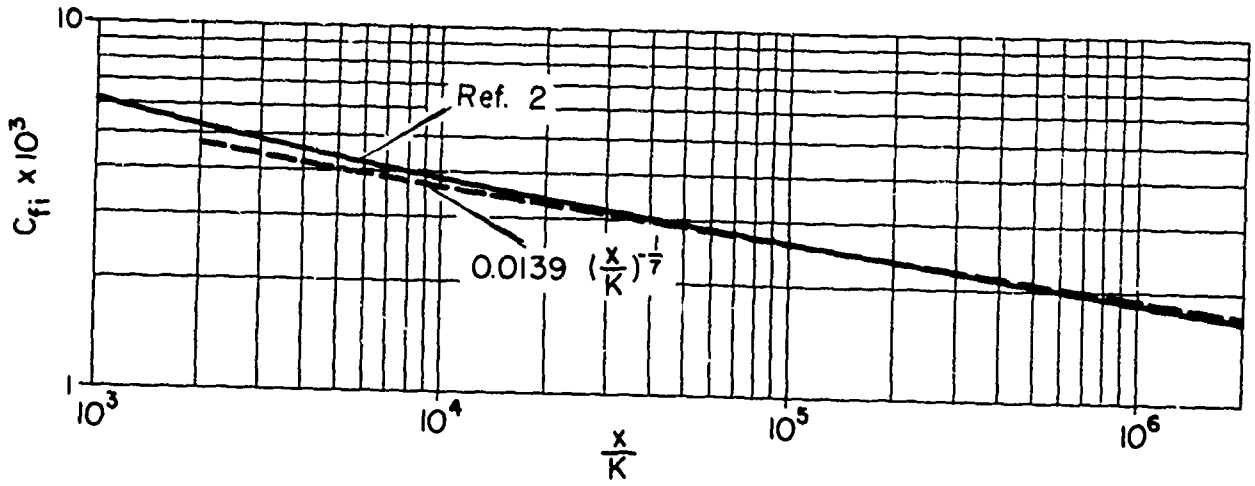

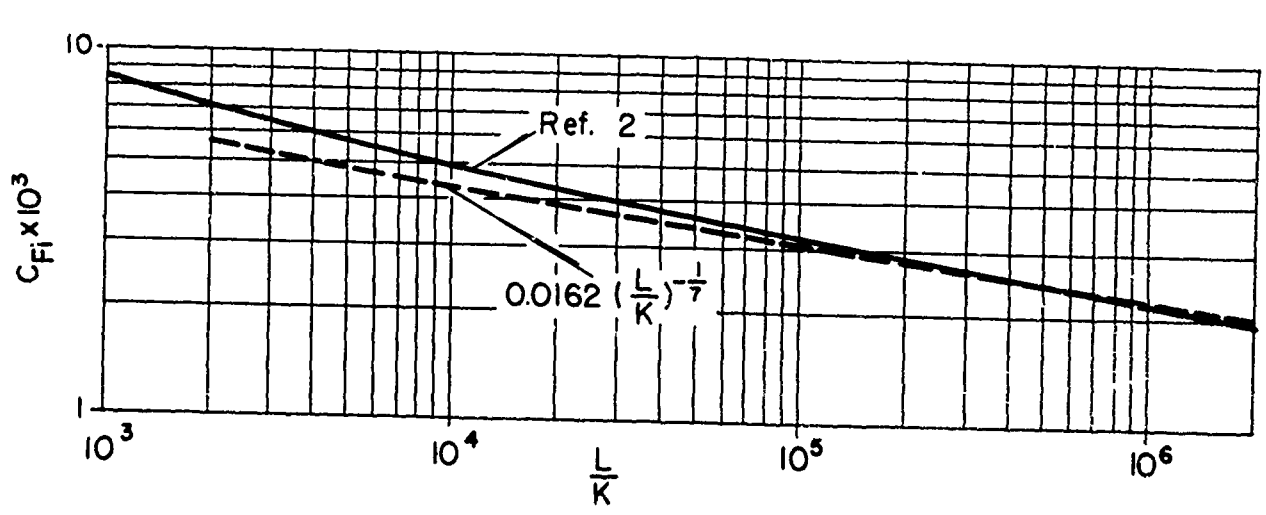

FIGURE 2
THE EFFECT OF RELATIVE ROUGHNESS ON SKIN FRICTION COEFFICIENTS, INCOMPRESSIBLE FLOW (Refs. 2 AND 14)

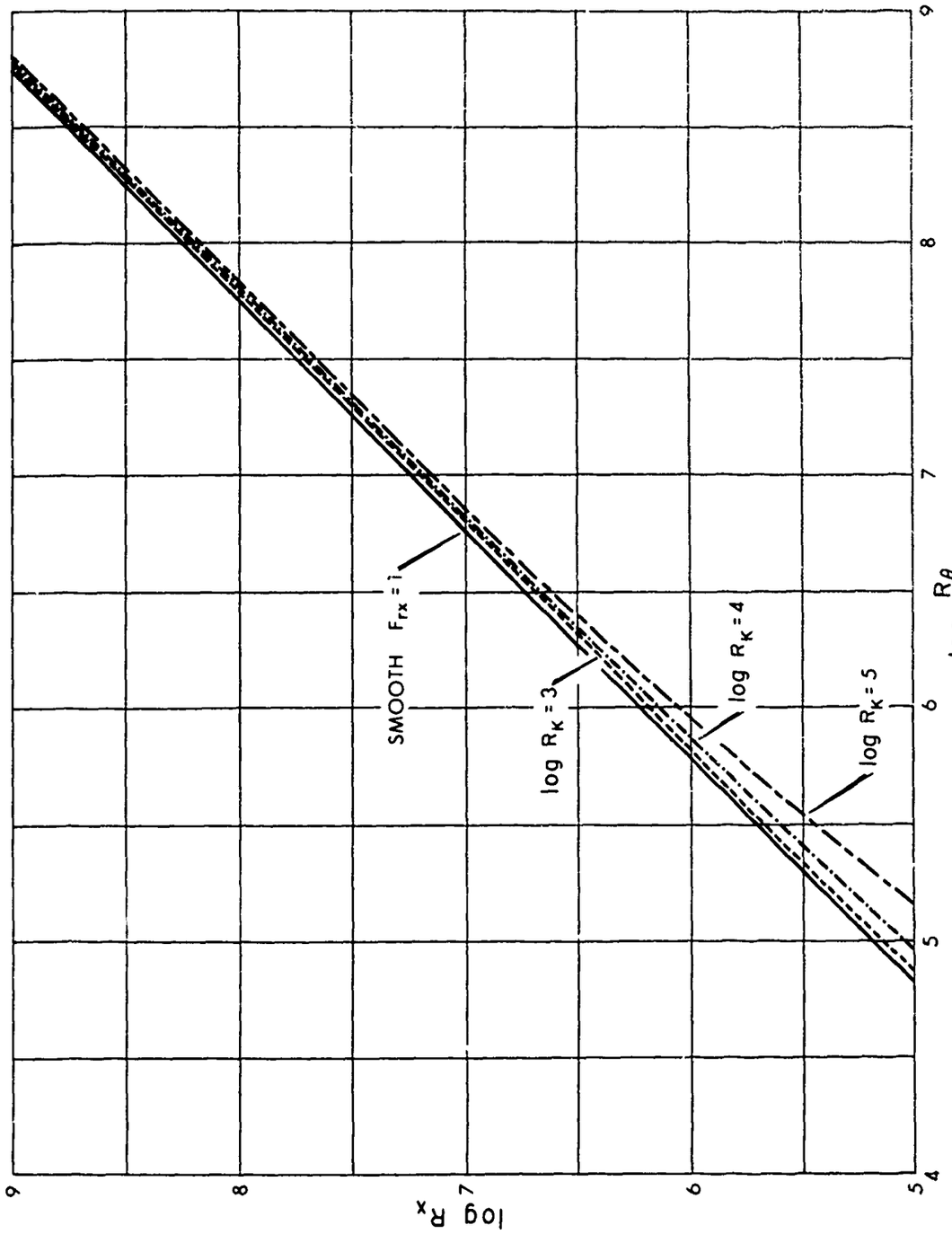

FIGURE 4
THE VARIATION OF R_x WITH $\frac{R\theta}{C_f}$ FOR VARIOUS VALUES OF R_K (ROUGH FLAT PLATES)

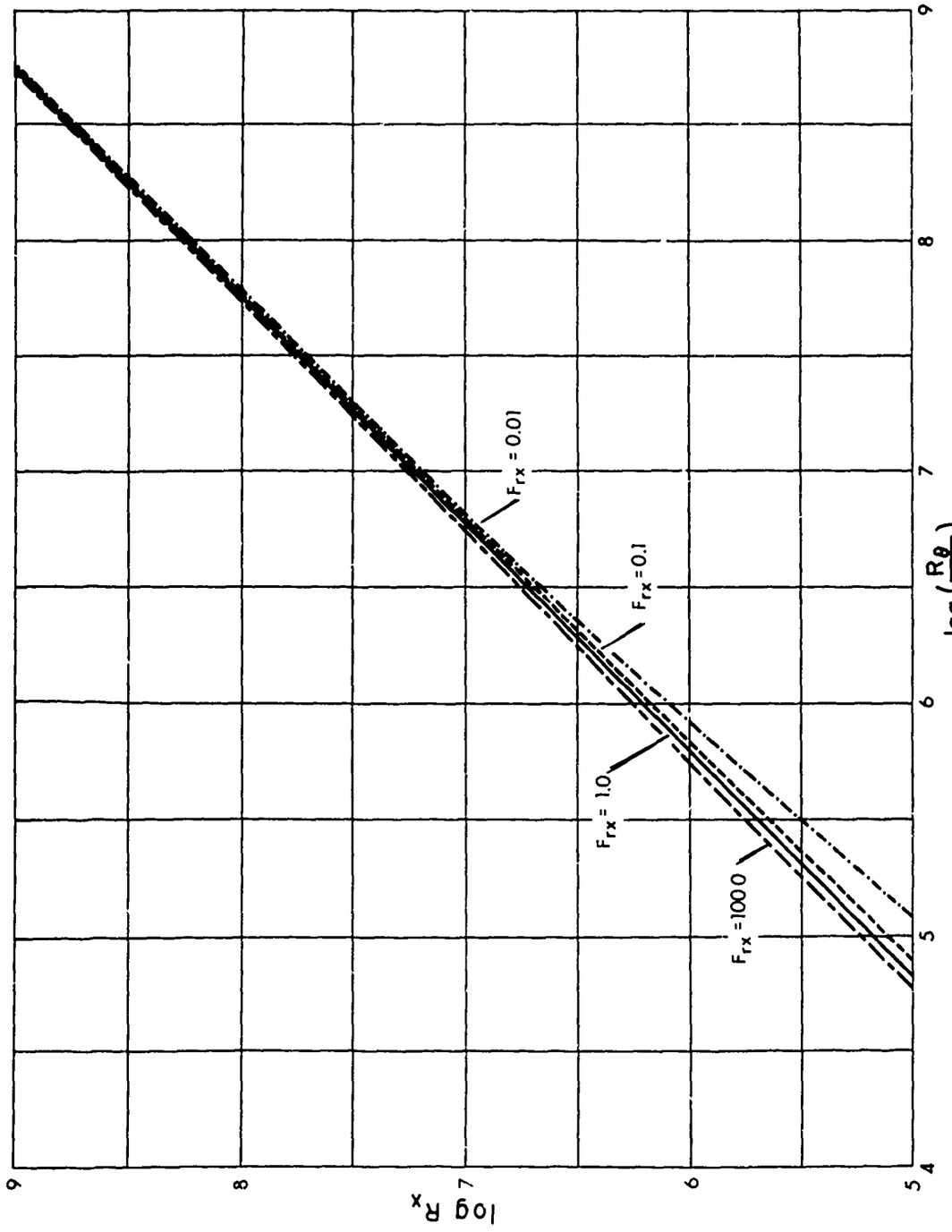

FIGURE 3
THE VARIATION OF R_x WITH $\frac{R\theta}{C_f}$ FOR VARIOUS VALUES OF F_{rx} (SMOOTH FLAT PLATES)

FIGURE 5
WIND TUNNEL CONTROL CONSOLE, PROBE DRIVE CONTROL
OFFNER AND BROWN RECORDERS

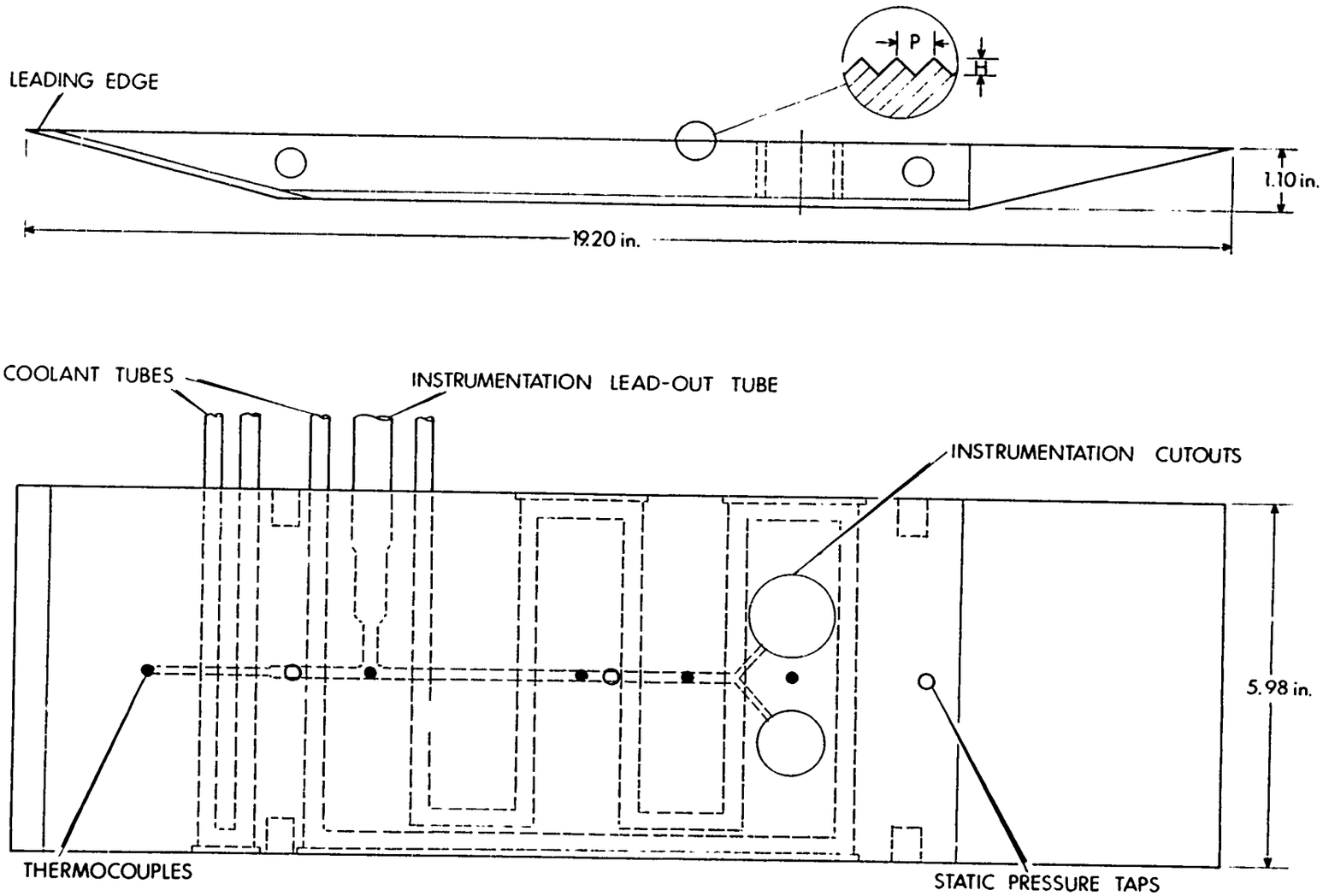

FIGURE 6
FLAT PLATE MODEL

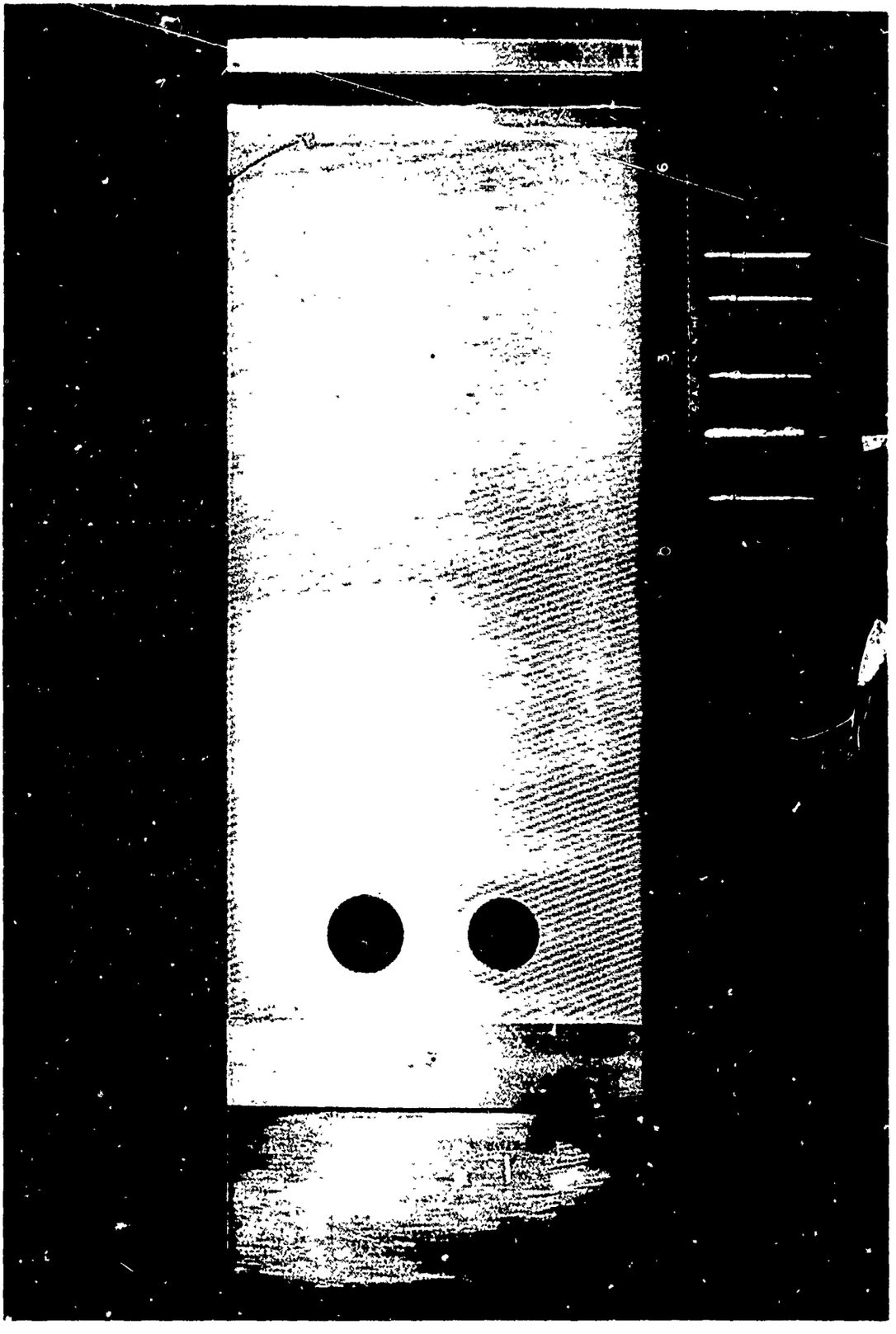

FIGURE 7
ROUGH FLAT PLATE MODEL SHOWING INSTRUMENTATION CUTOUTS

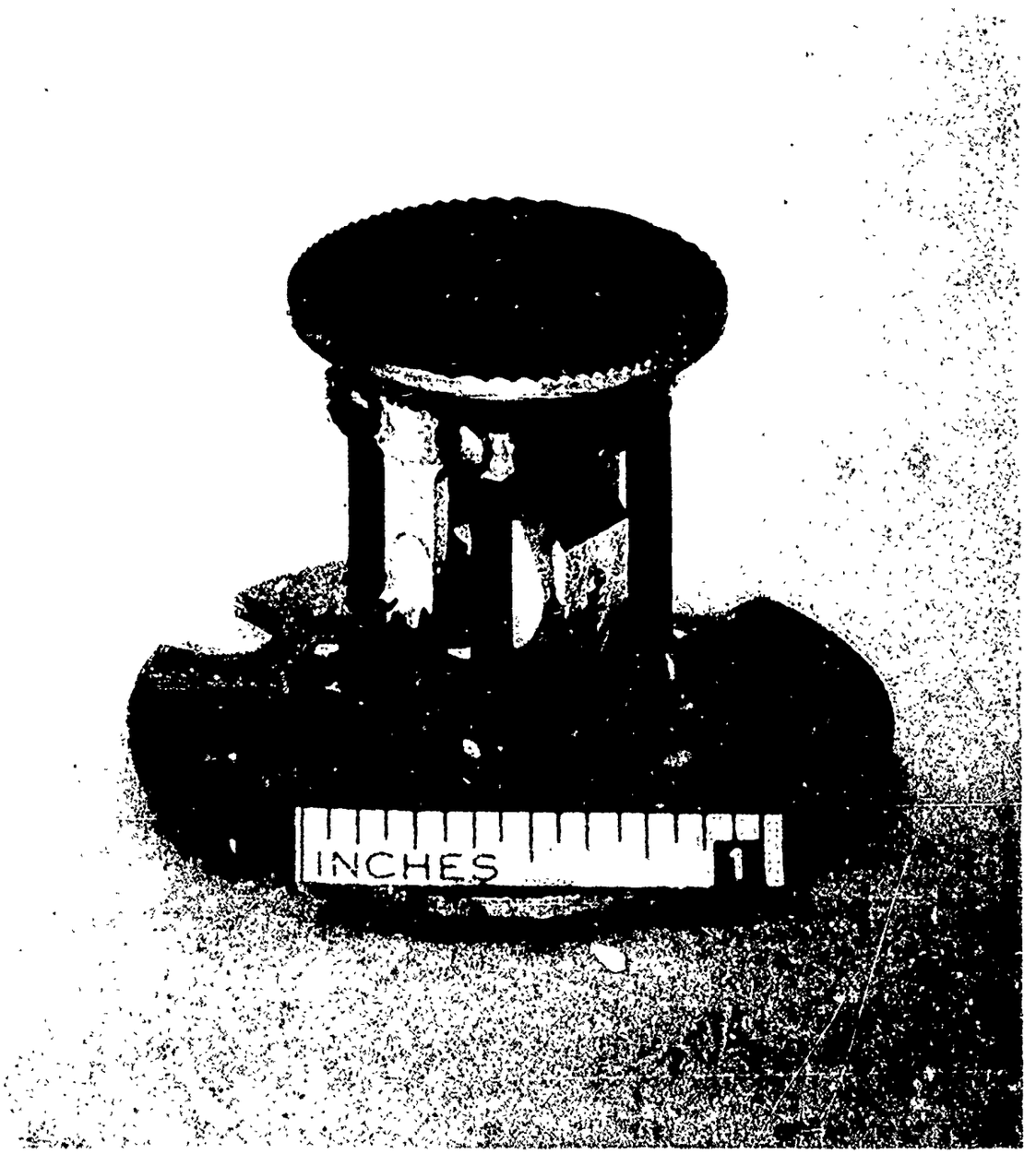

FIGURE 8
SKIN FRICTION BALANCE (DISC ROUGHNESS: P = 0.030 in.)

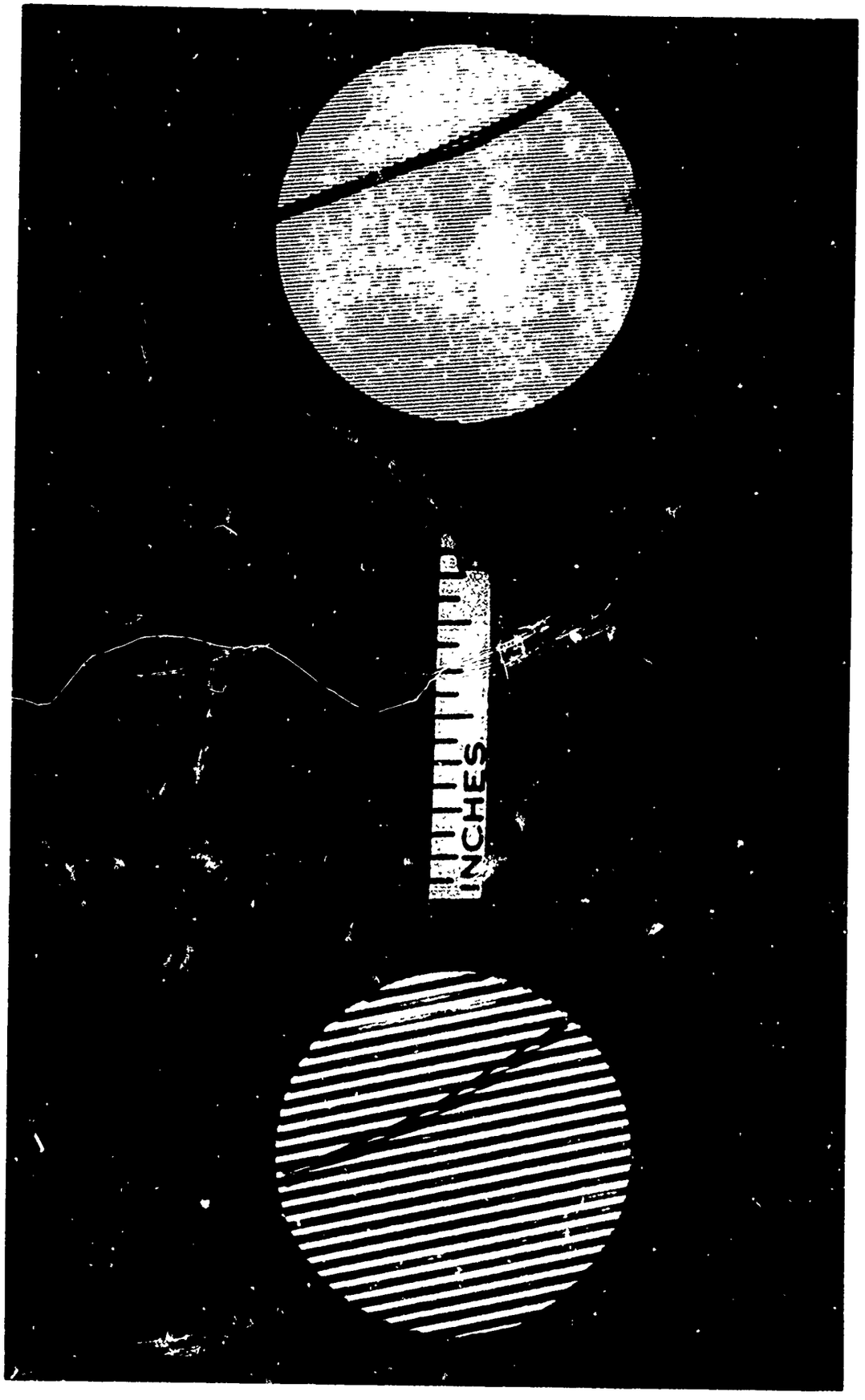

FIGURE 9
CALORIMETER DISCS (P= 0.030-in. AND 0.005-in.)

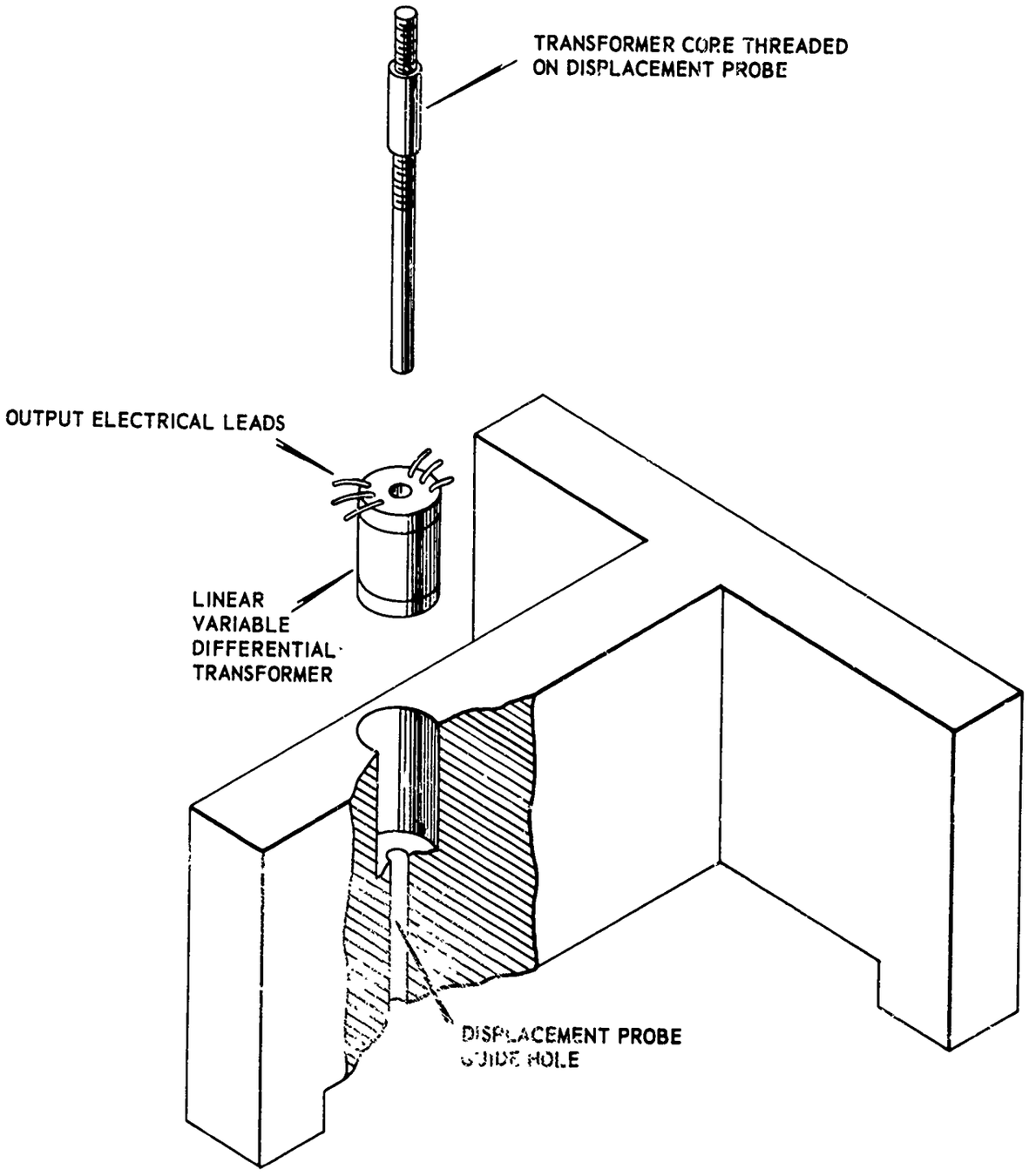

FIGURE 10
EXPLODED VIEW OF DISPLACEMENT GAGE

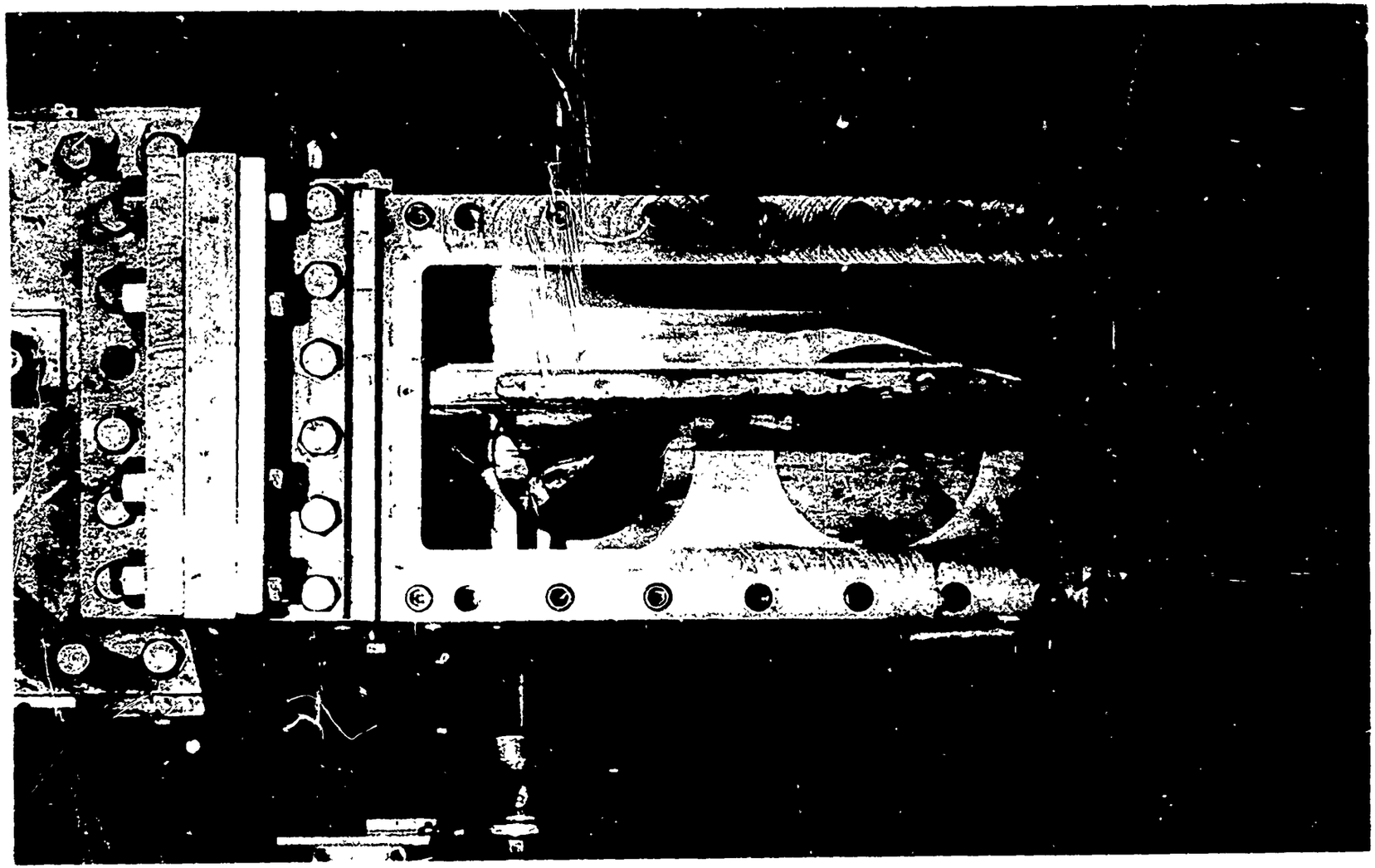

FIGURE 11
ROUGH FLAT PLATE MODEL, SURVEY PROBE
AND DRIVE MECHANISM INSTALLED IN WIND TUNNEL TEST SECTION

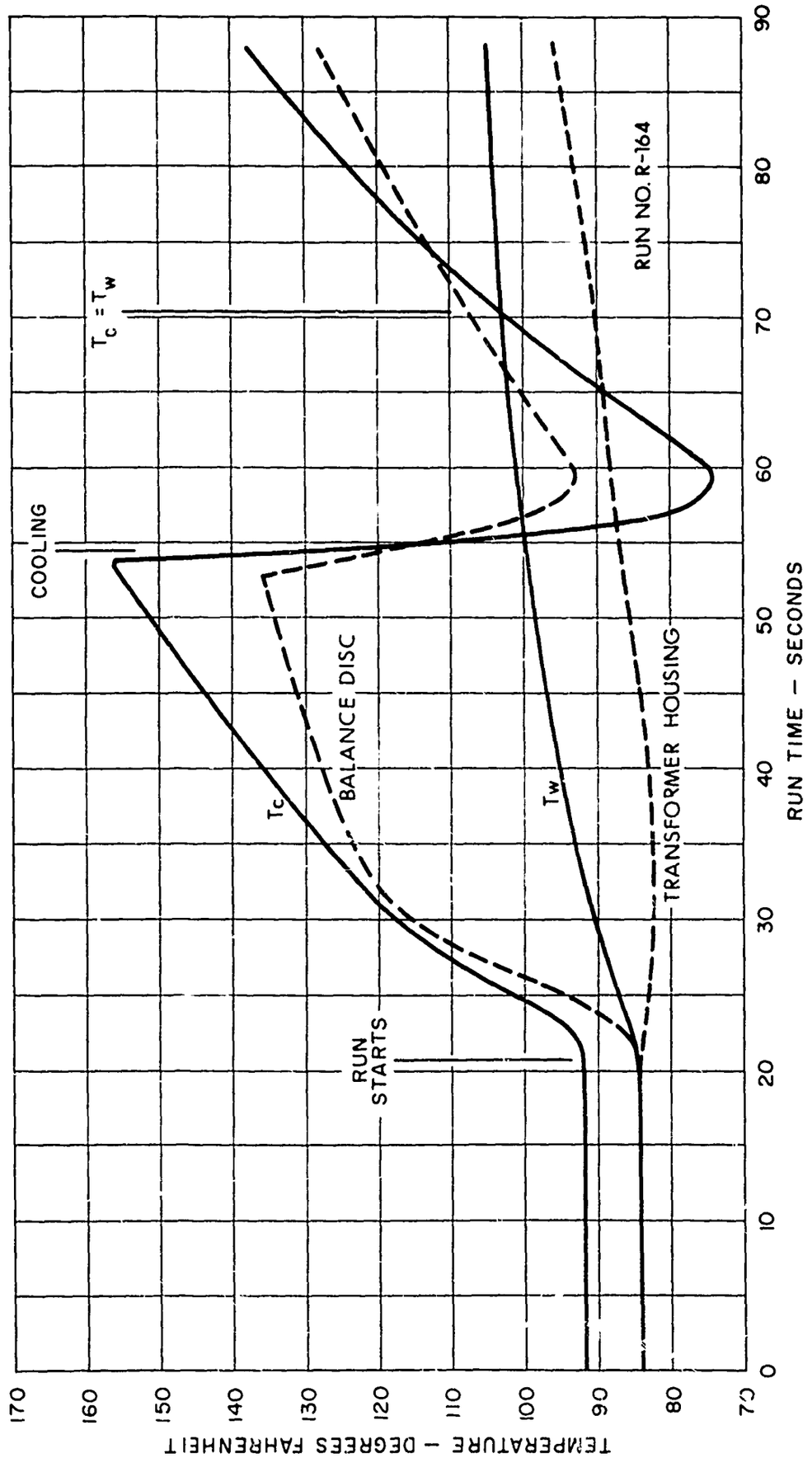

FIGURE 12
TYPICAL TEMPERATURE-TIME HISTORY OF THE CALORIMETER DISC, BALANCE DISC, AND TRANSFORMER HOUSING
($P = 0.010$-in., $T_{aw} = 350$ F)

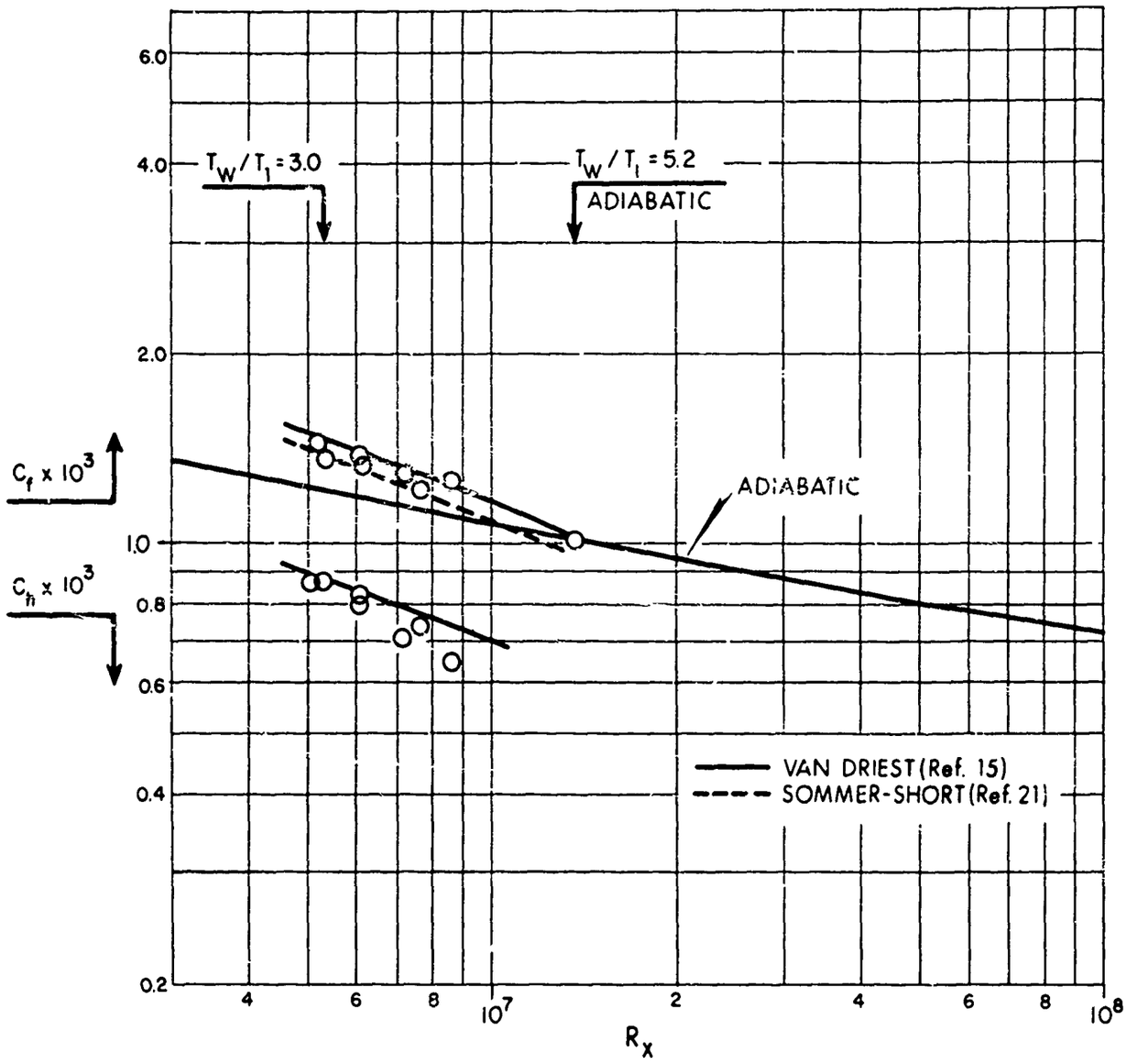

FIGURE 13
COMPARISON OF EXPERIMENTAL LOCAL SKIN FRICTION
AND HEAT TRANSFER COEFFICIENTS
WITH THEORY AT $M_1 = 4.93$ (SMOOTH PLATE)

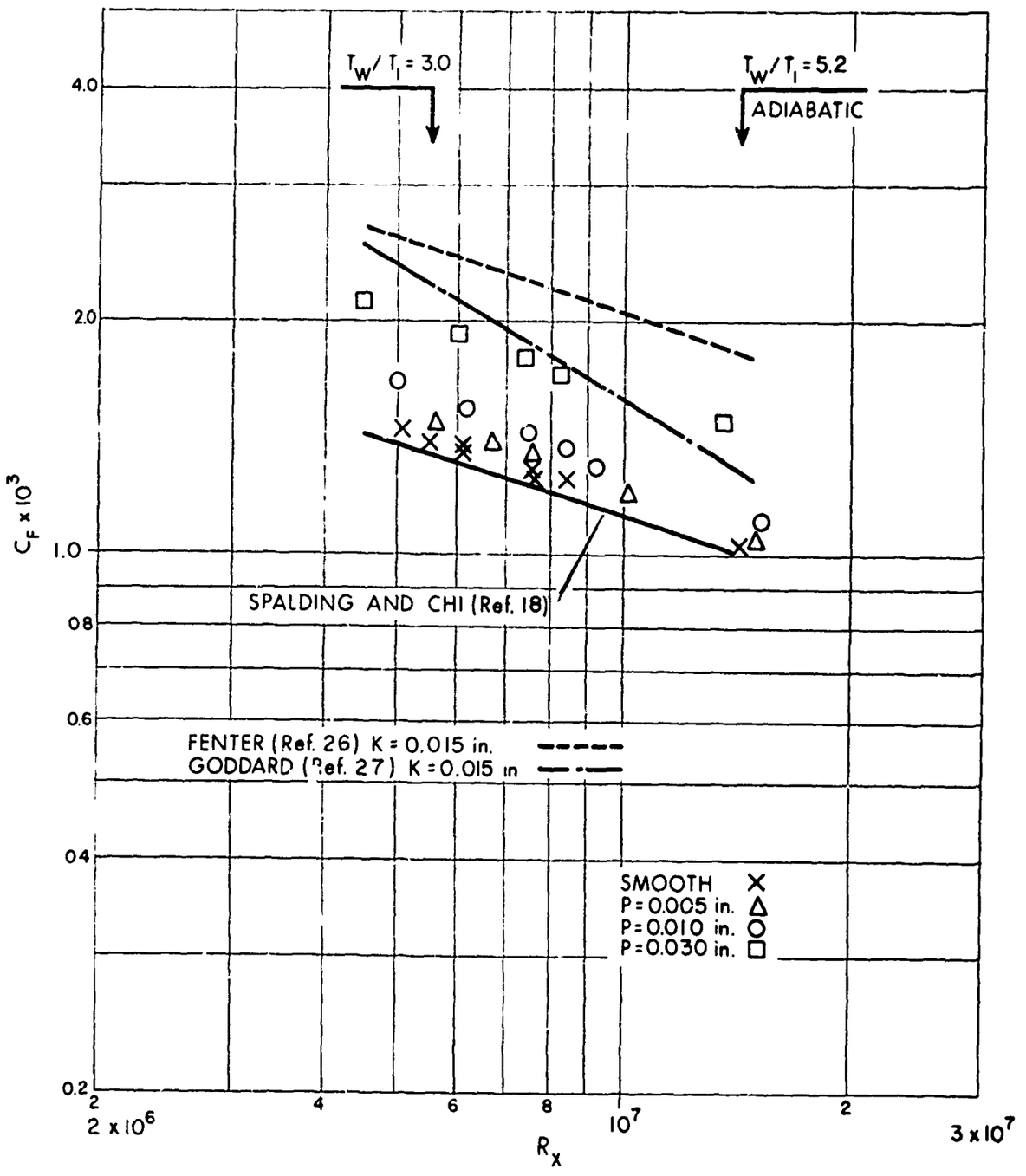

FIGURE 14
COMPARISON OF EXPERIMENTAL LOCAL SKIN FRICTION COEFFICIENTS WITH THEORY AT $M_1 = 4.93$ (SMOOTH AND ROUGH PLATES)

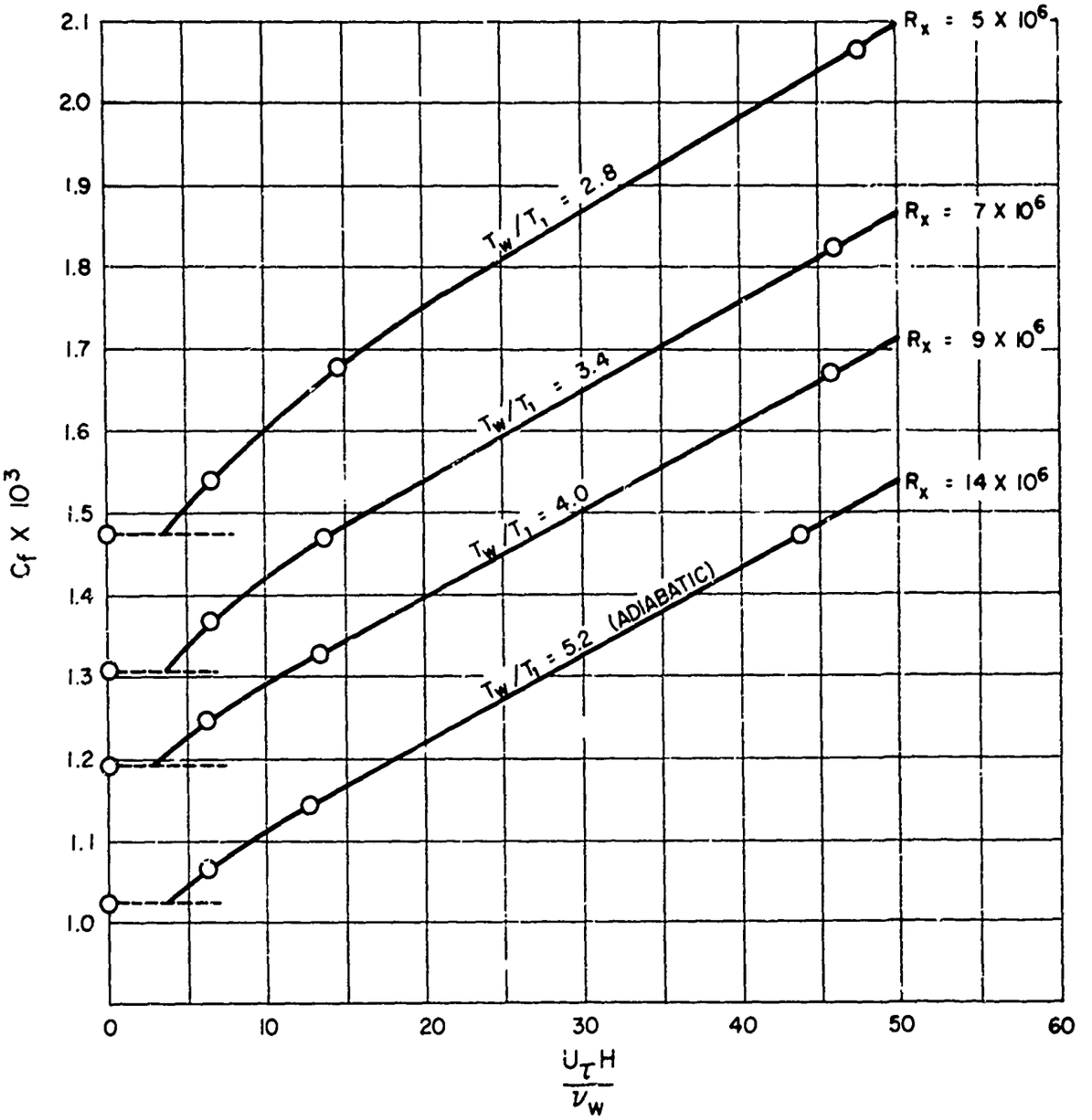

FIGURE 15
VARIATION OF EXPERIMENTAL LOCAL SKIN FRICTION COEFFICIENTS WITH NONDIMENSIONAL ROUGHNESS HEIGHT AT $M_1 = 4.93$

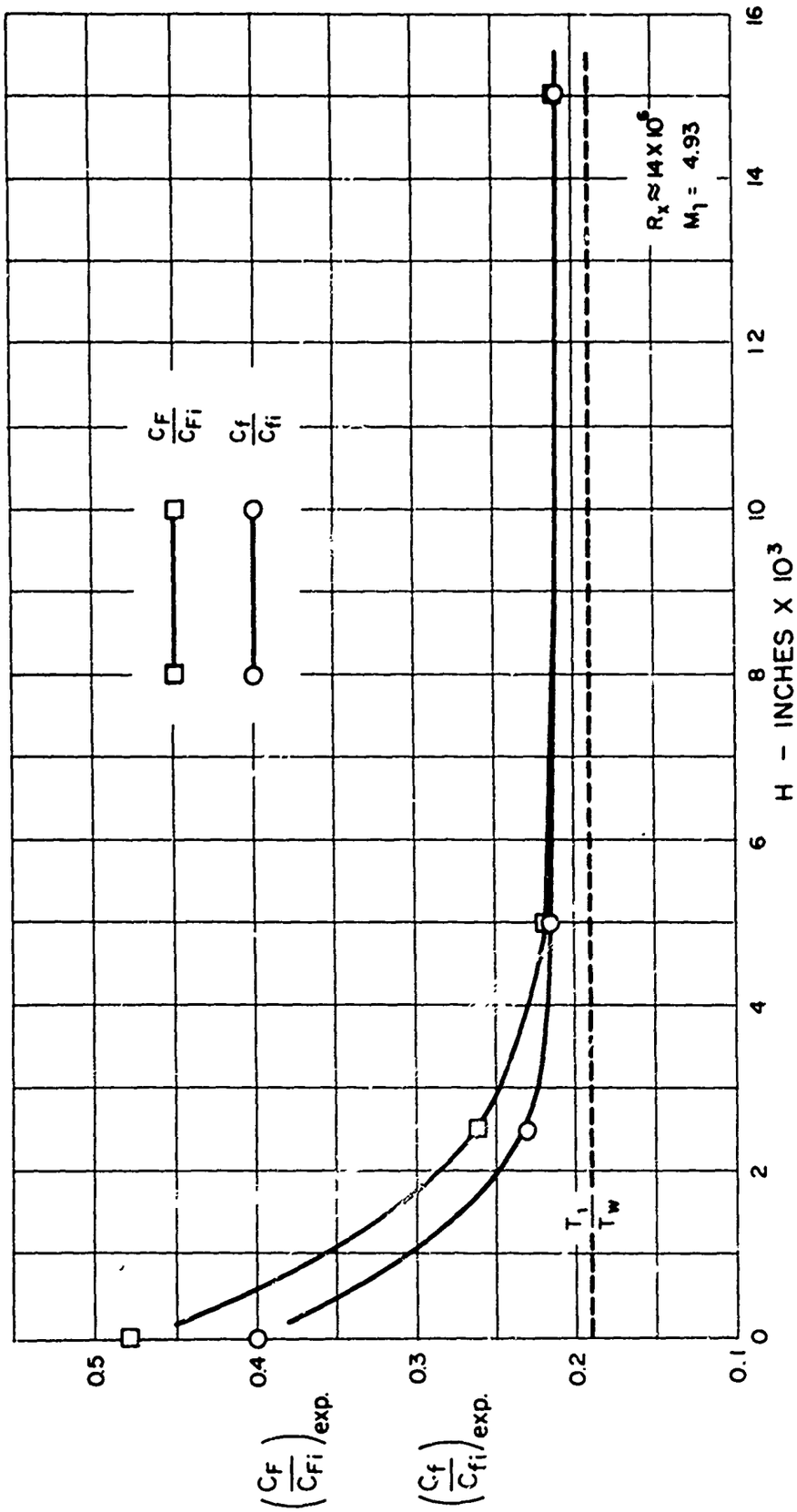

FIGURE 16
VARIATION OF EXPERIMENTAL SKIN FRICTION COEFFICIENT RATIOS WITH ROUGHNESS HEIGHT FOR ZERO HEAT TRANSFER AT $M_1 = 4.93$

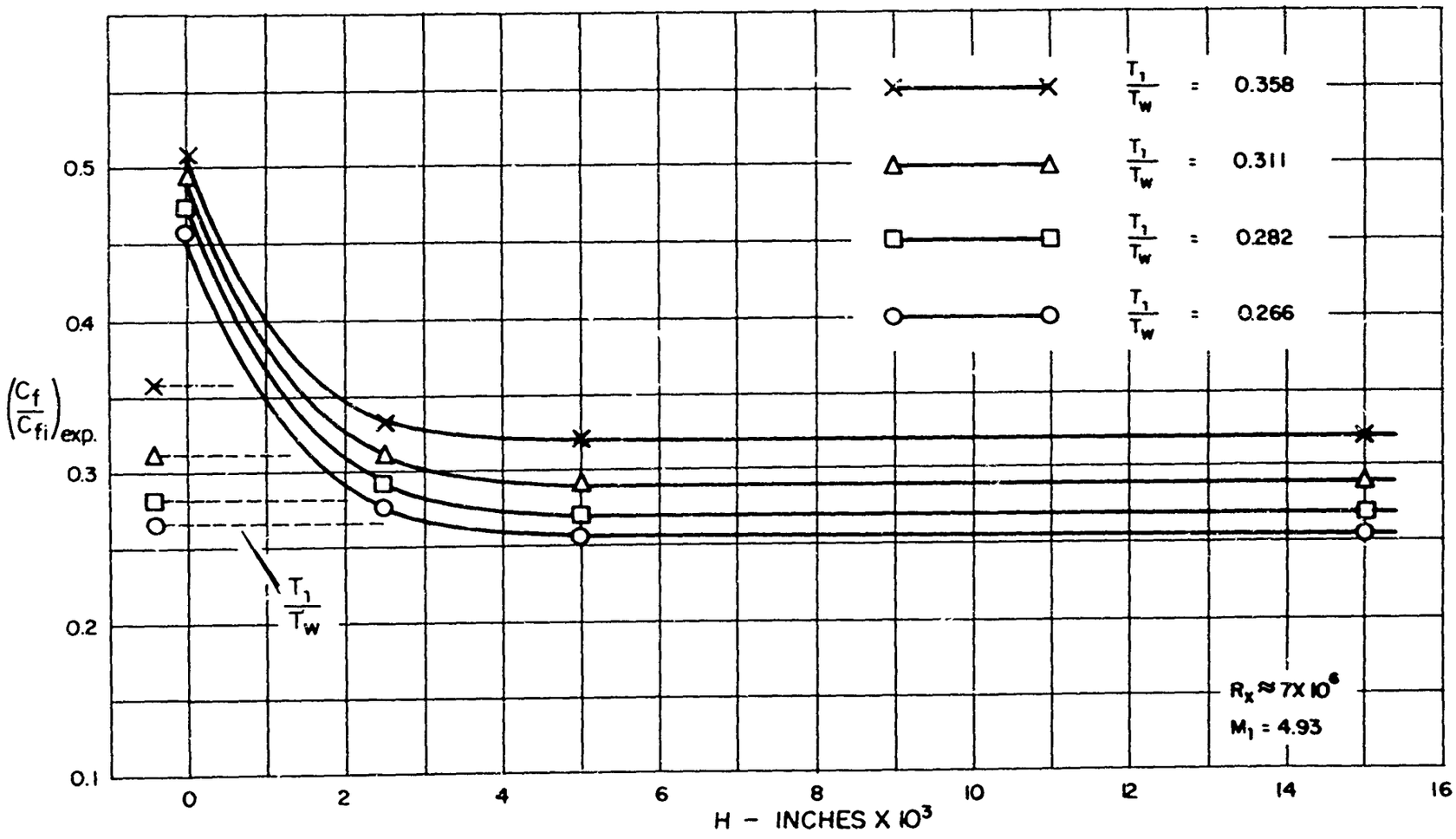

FIGURE 17
VARIATION OF EXPERIMENTAL LOCAL SKIN FRICTION COEFFICIENT RATIOS WITH ROUGHNESS HEIGHT AT $M_1 = 4.93$

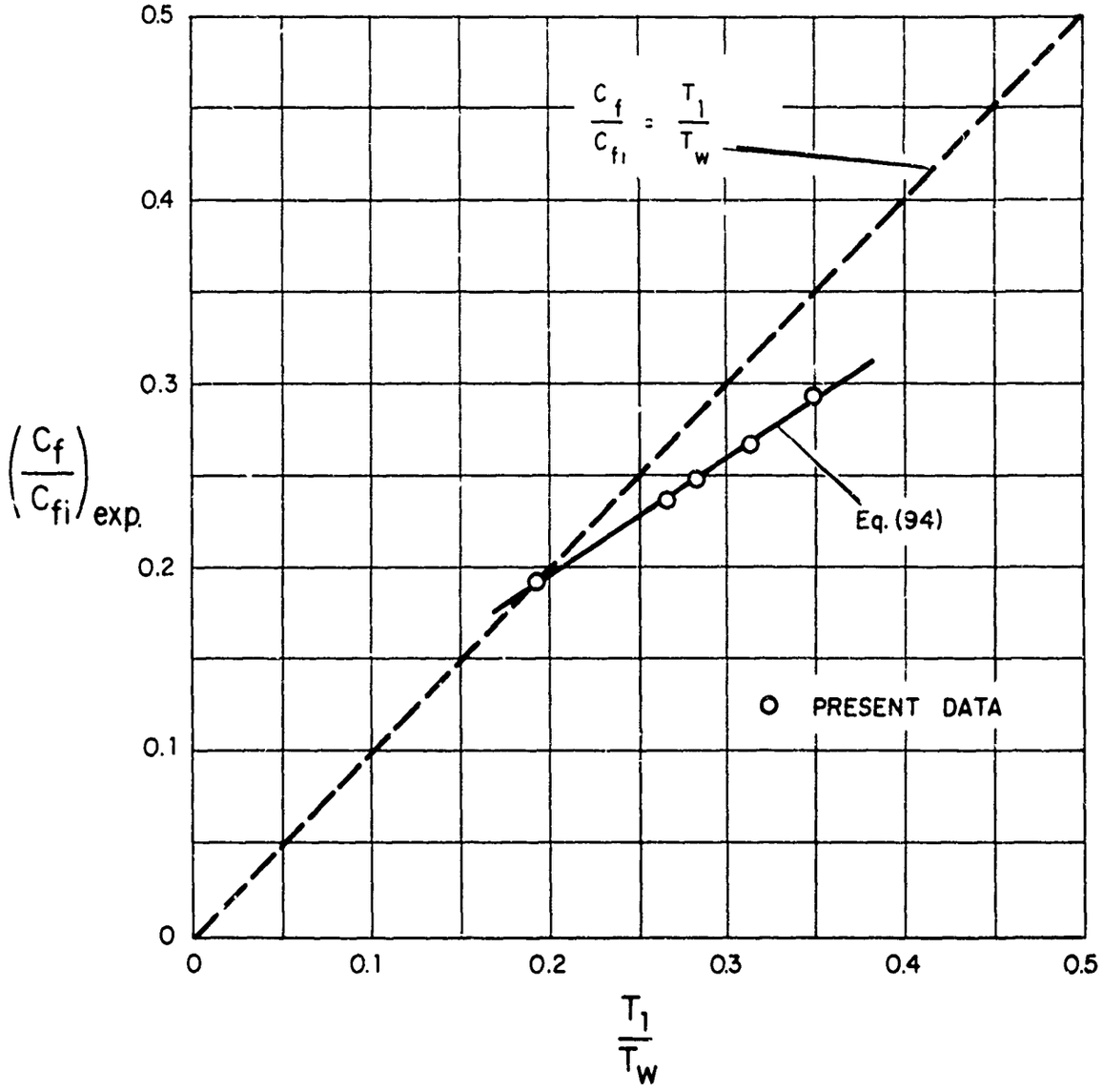

FIGURE 18
VARIATION OF EXPERIMENTAL LOCAL SKIN FRICTION COEFFICIENT RATIOS WITH TEMPERATURE RATIO AT $M_1 = 4.93$

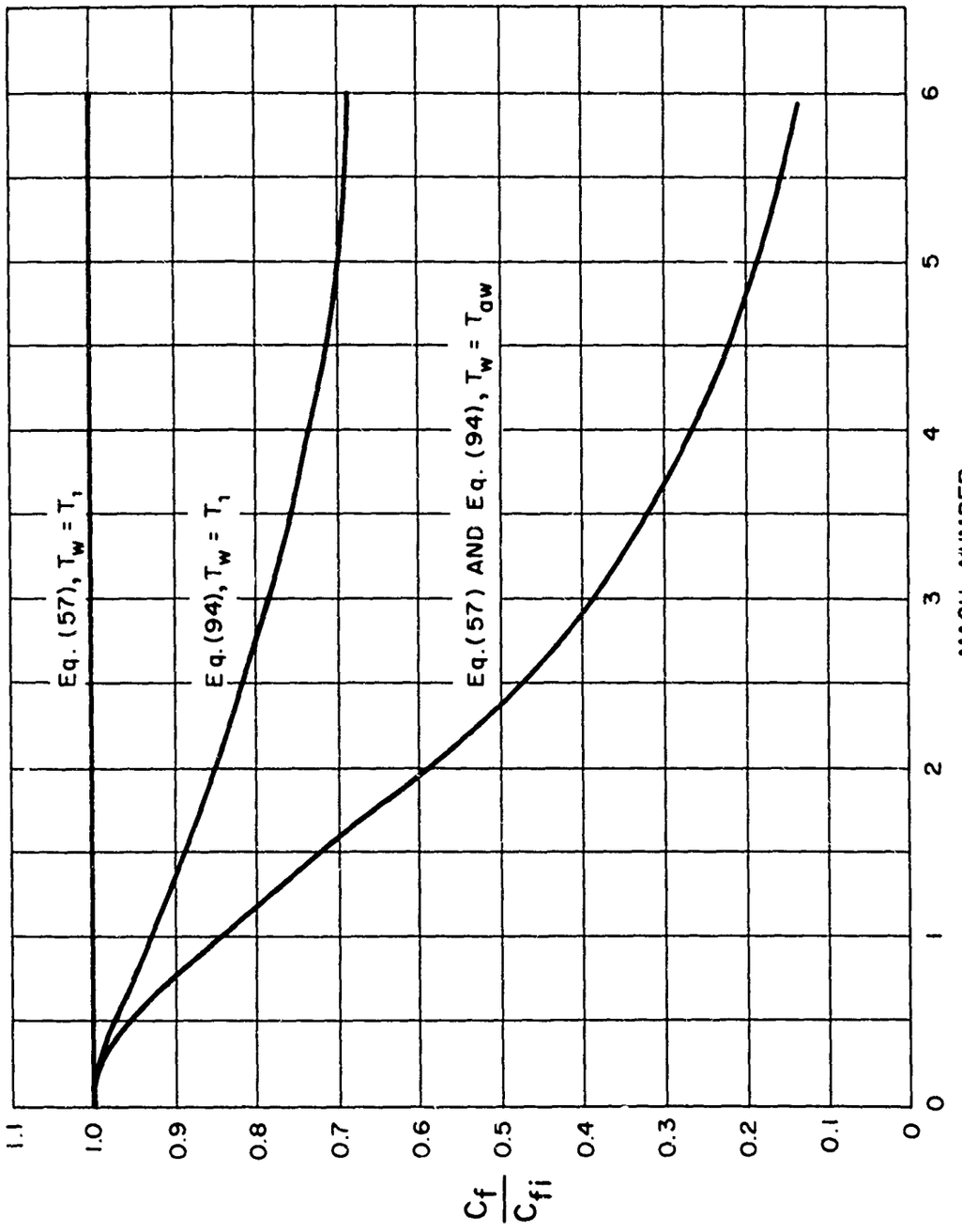

FIGURE 19
THE EFFECT OF MACH NUMBER ON THE LOCAL SKIN FRICTION COEFFICIENT RATIO
(FULLY ROUGH PLATES)

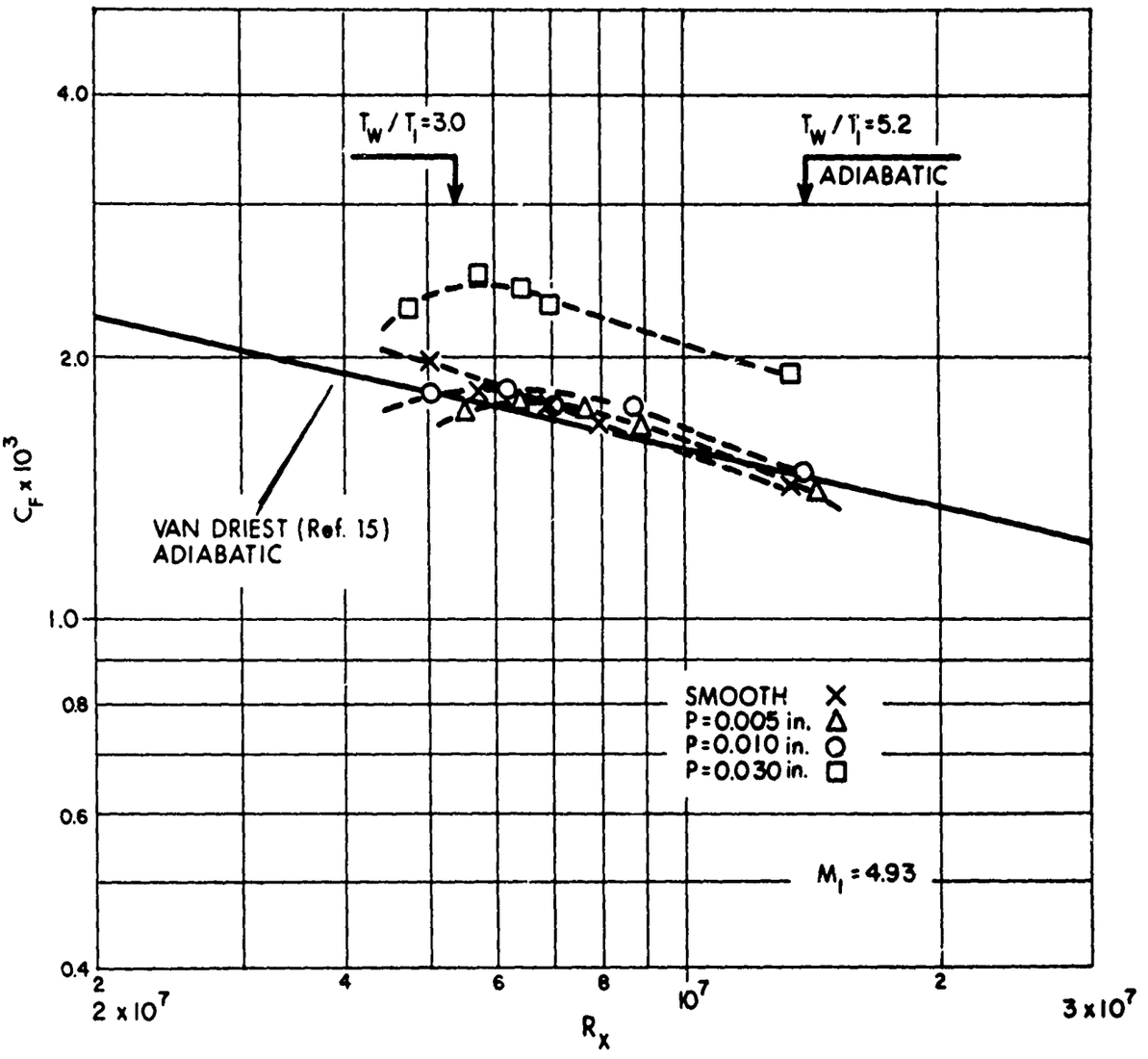

FIGURE 20
EXPERIMENTAL MEAN SKIN FRICTION COEFFICIENTS FOR SMOOTH AND ROUGH SURFACES AT $M_1 = 4.93$

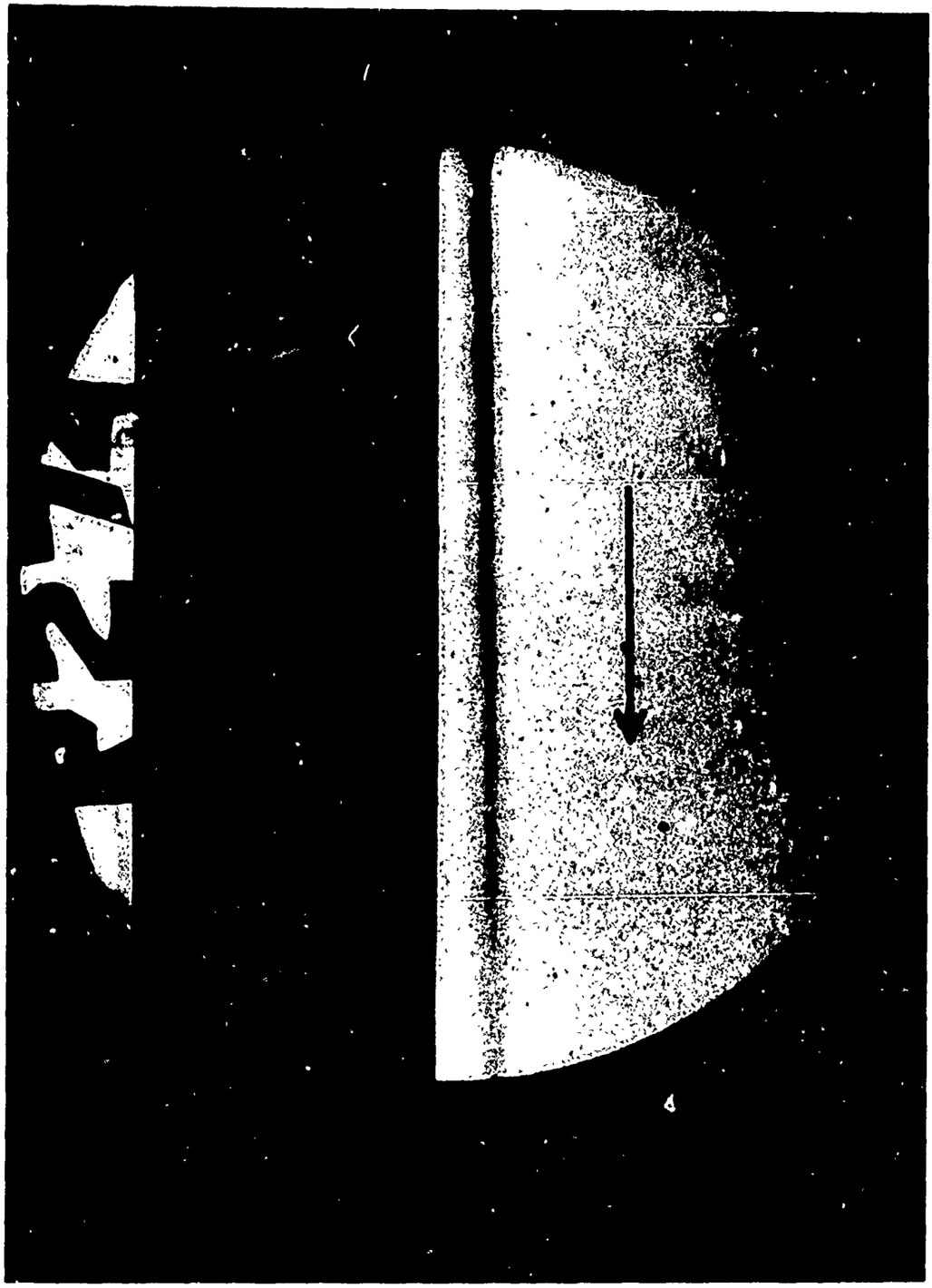

FIGURE 21
SCHLIEREN PHOTOGRAPH OF THE TEST REGION
$M_1 = 4.87$, $R_x = 13.7 \times 10^6$, $T_w/T_1 = 5.18$
(ROUGH PLATE, P = 0.030 - in.)

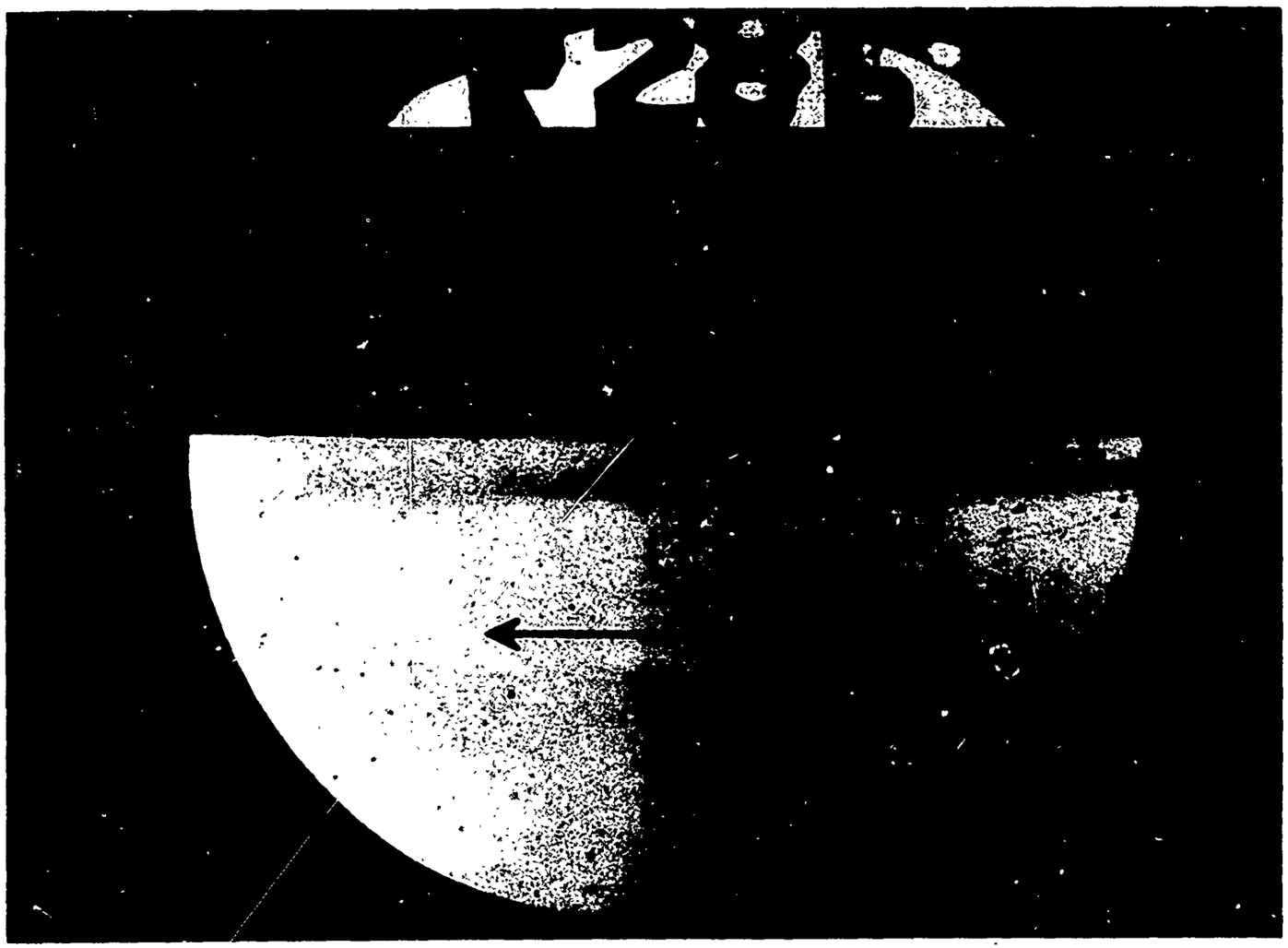

FIGURE 22
SCHLIEREN PHOTOGRAPH OF THE TEST REGION
$M_1 = 4.90$, $R_x = 5.90 \times 10^6$, $T_w / T_t = 3.19$
(ROUGH PLATE, P = 0.030-in.)

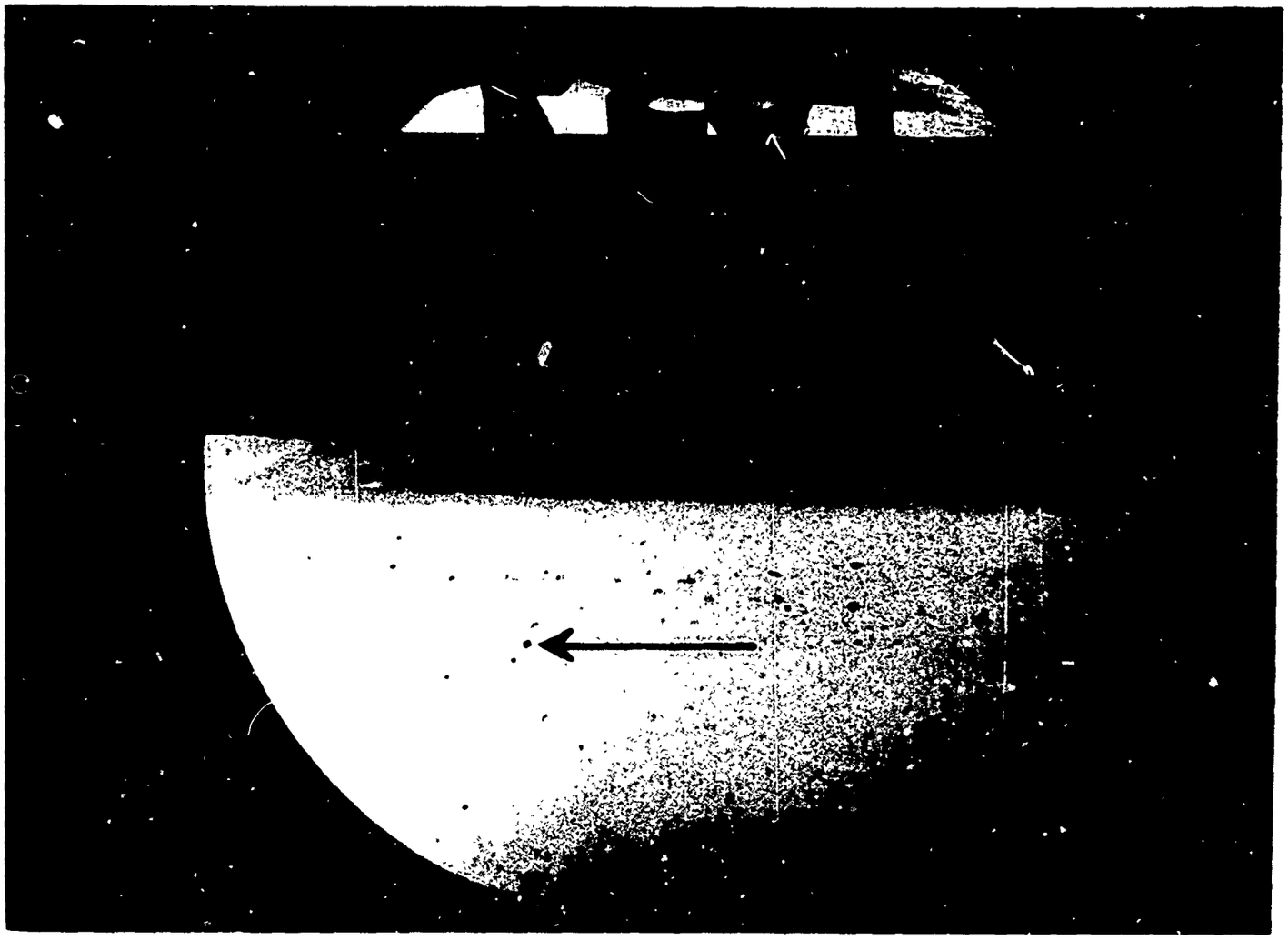

FIGURE 23
SCHLIEREN PHOTOGRAPH OF THE TEST REGION
$M_1 = 4.90$, $R_x = 4.50 \times 10^6$, $T_w / T_1 = 2.93$
(ROUGH PLATE, P= 0.030-in.)

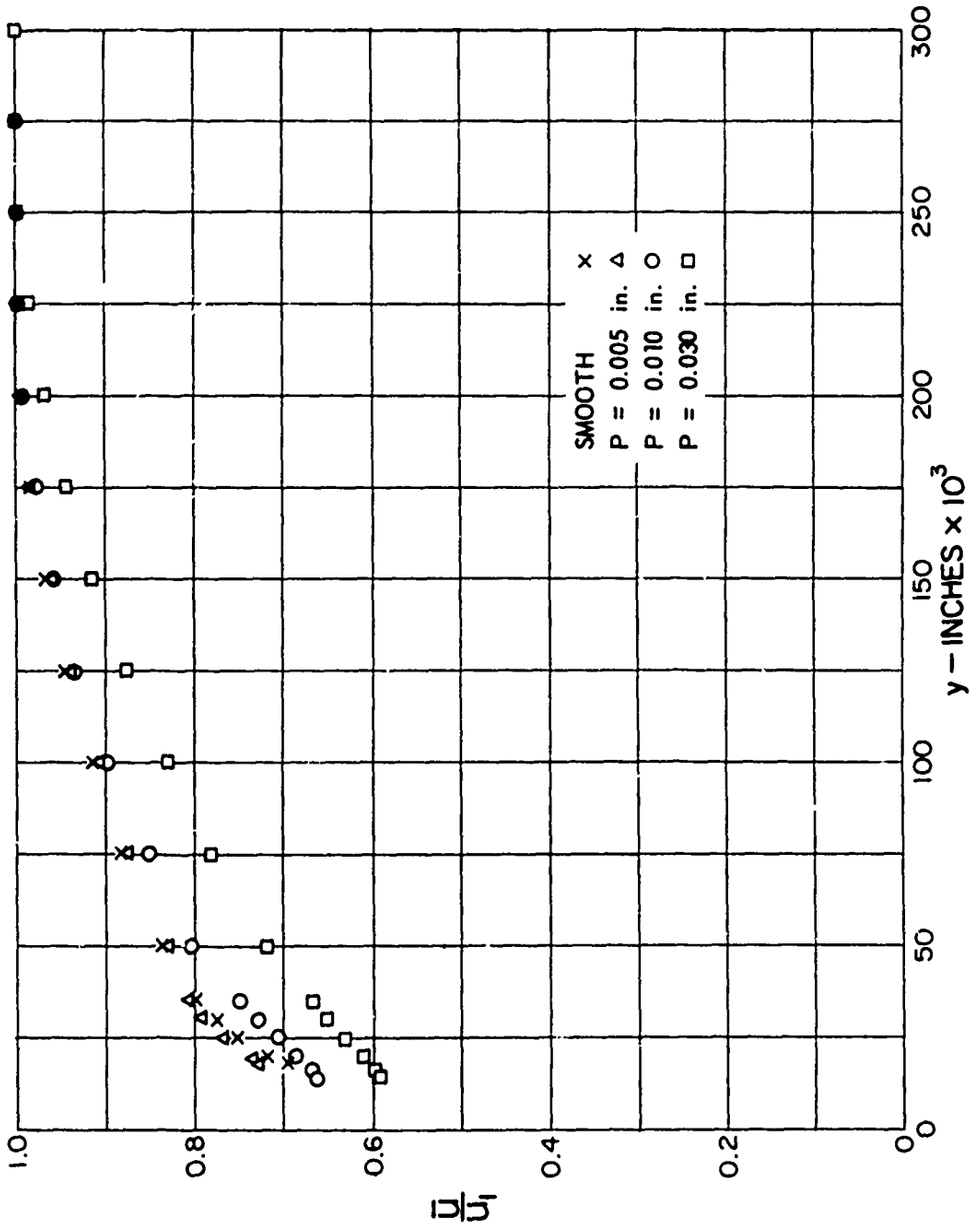

FIGURE 24
VELOCITY RATIO vs DISTANCE FROM THE PLATE SURFACE
FOR VARIOUS DEGREES OF ROUGHNESS
$M_1 = 4.93$, $T_w = T_{aw}$

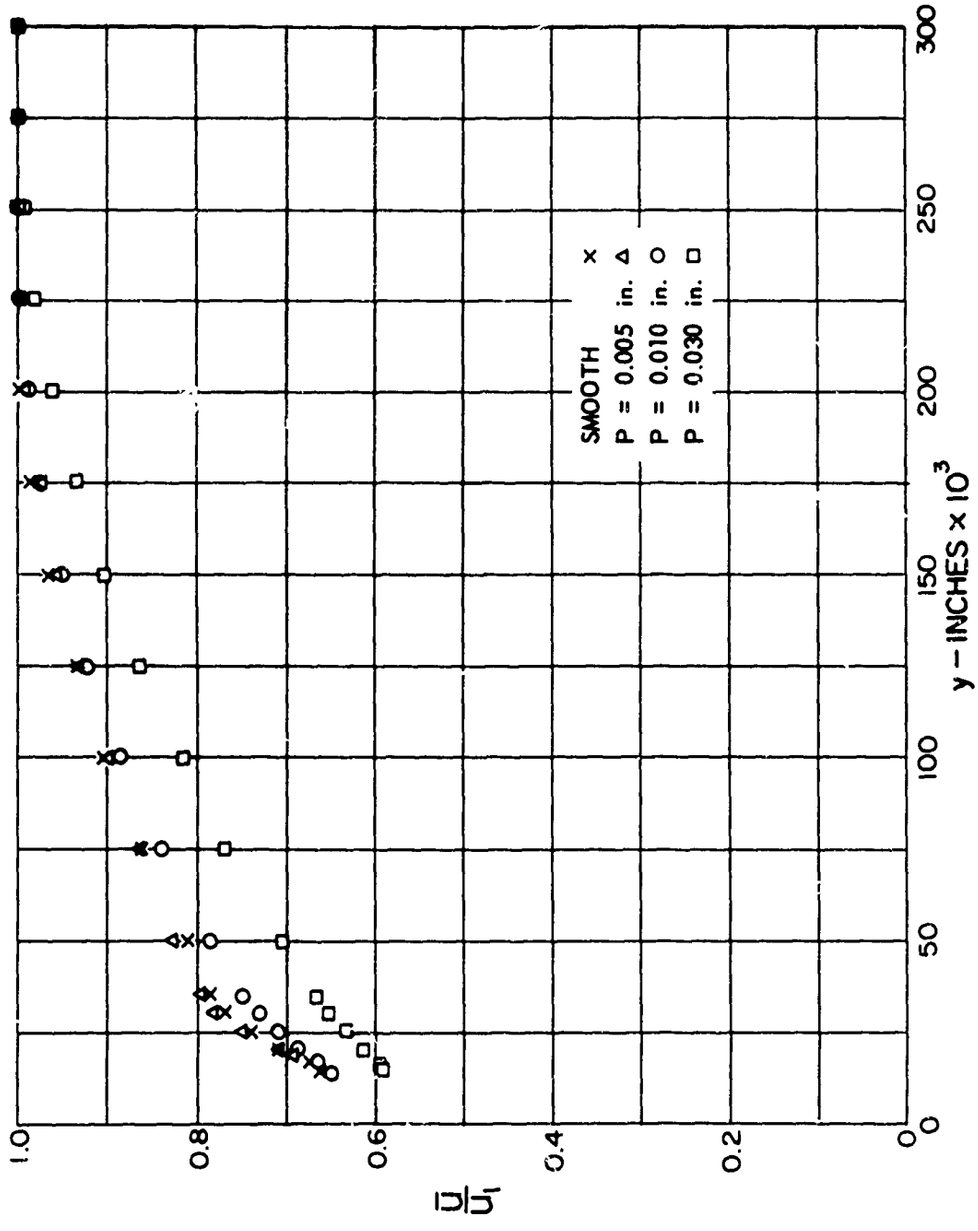

FIGURE 25
VELOCITY RATIO vs DISTANCE FROM THE PLATE SURFACE
FOR VARIOUS DEGREES OF ROUGHNESS
$M_1 = 4.93$, $T_w/T_1 = 3.8$

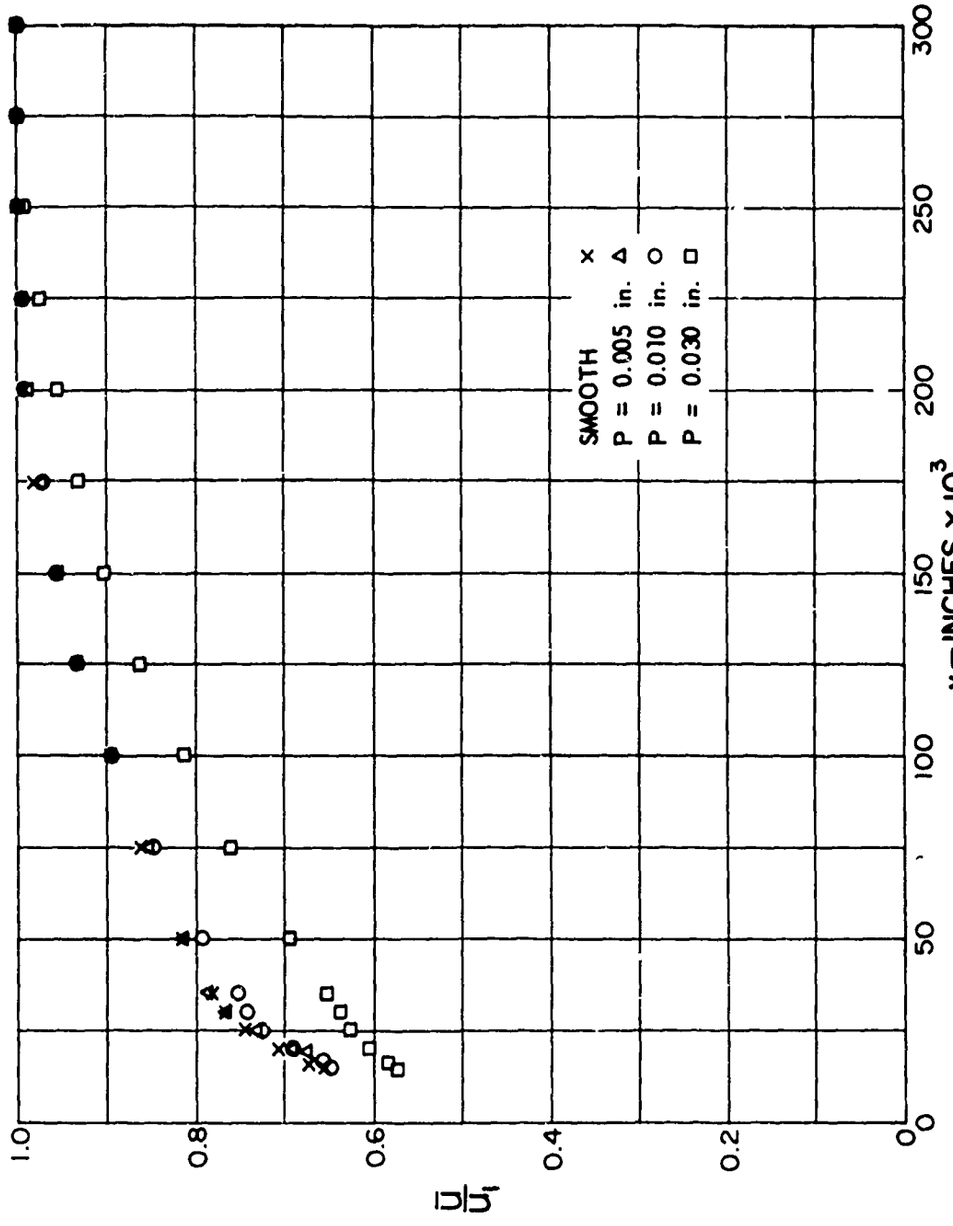

FIGURE 26
VELOCITY RATIO vs DISTANCE FROM THE PLATE SURFACE
FOR VARIOUS DEGREES OF ROUGHNESS
$M_1 = 4.93$, $T_w / T_1 = 3.5$

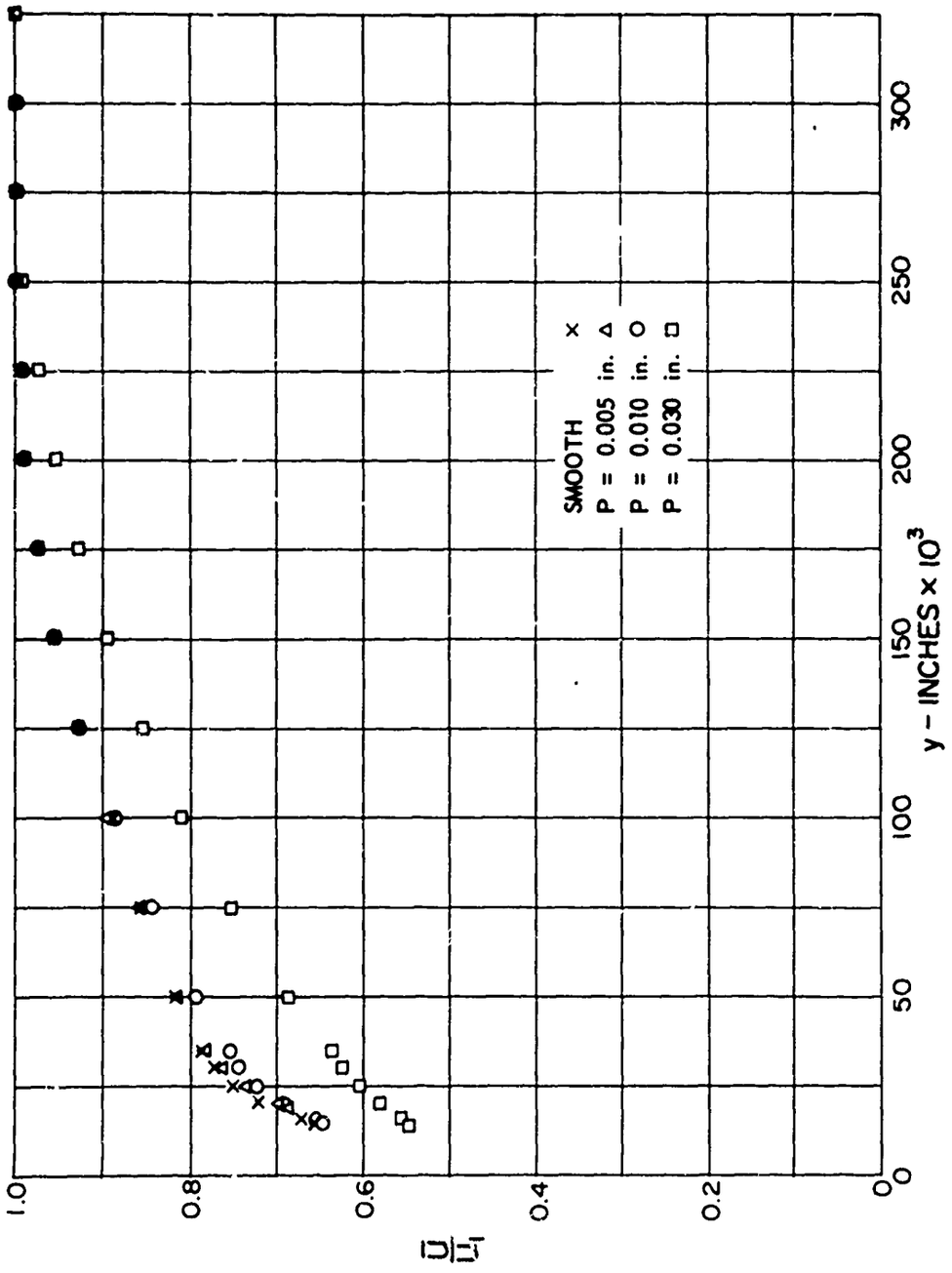

FIGURE 27
VELOCITY RATIO vs DISTANCE FROM THE PLATE SURFACE
FOR VARIOUS DEGREES OF ROUGHNESS
$M_1 = 4.93$, $T_w/T_1 = 3.2$

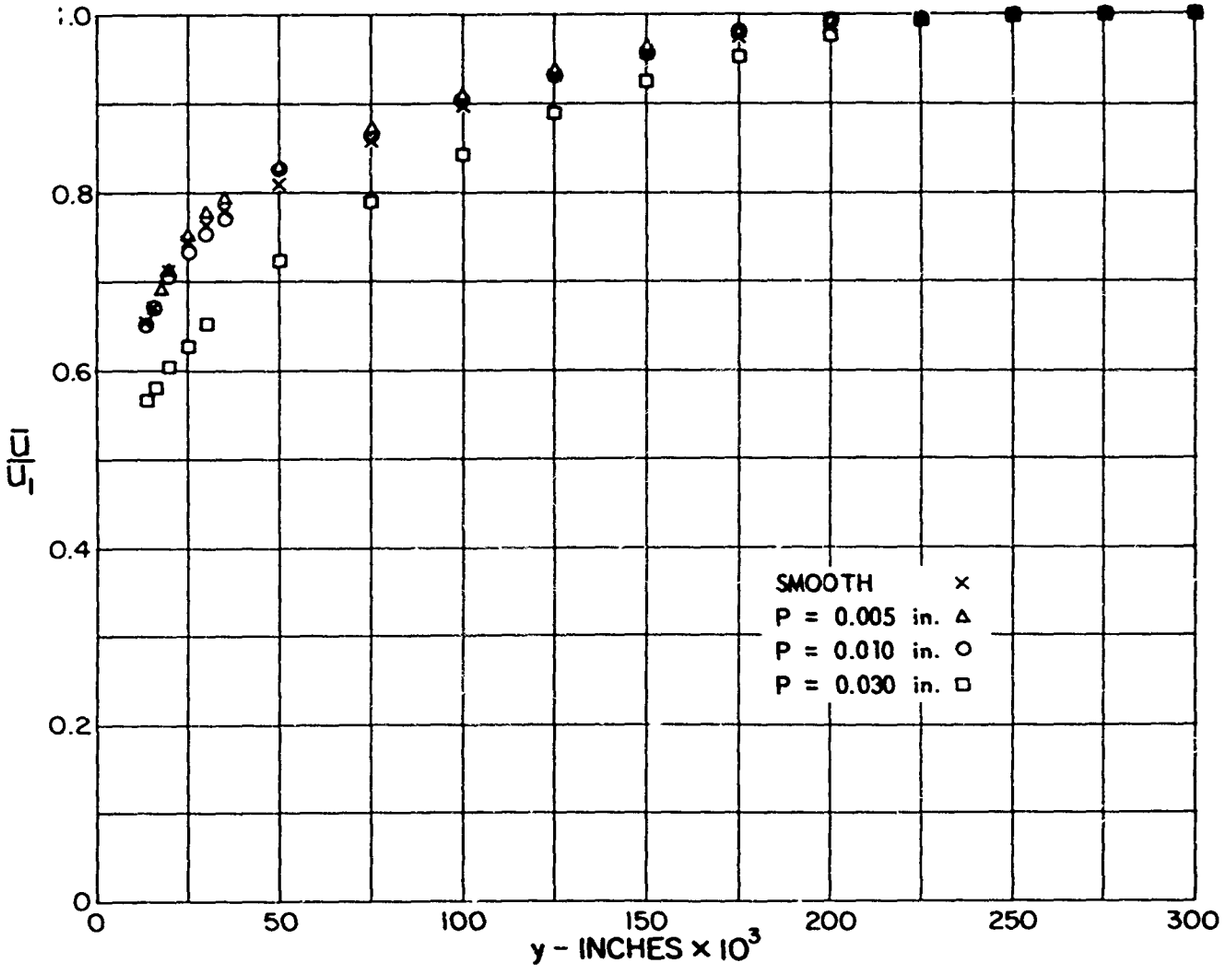

FIGURE 28
VELOCITY RATIO vs DISTANCE FROM THE PLATE SURFACE
FOR VARIOUS DEGREES OF ROUGHNESS
$M_1 = 4.93$, $T_w / T_1 = 2.9$

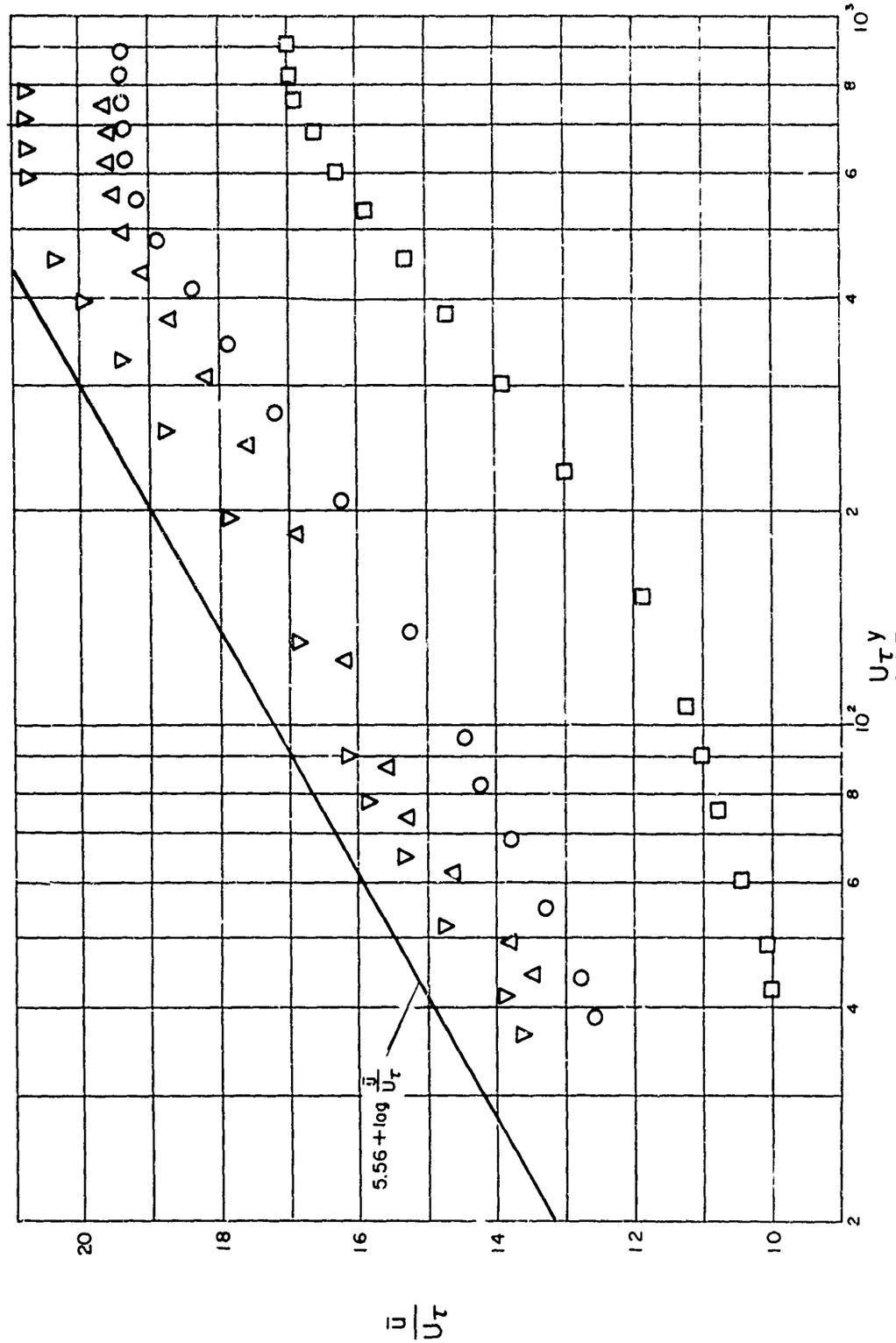

FIGURE 29
EXPERIMENTAL NONDIMENSIONAL VELOCITY DISTRIBUTION
FOR SMOOTH AND ROUGH FLAT PLATES
AT $M_1 = 4.93$ AND $T_w/T_1 = 3.8$

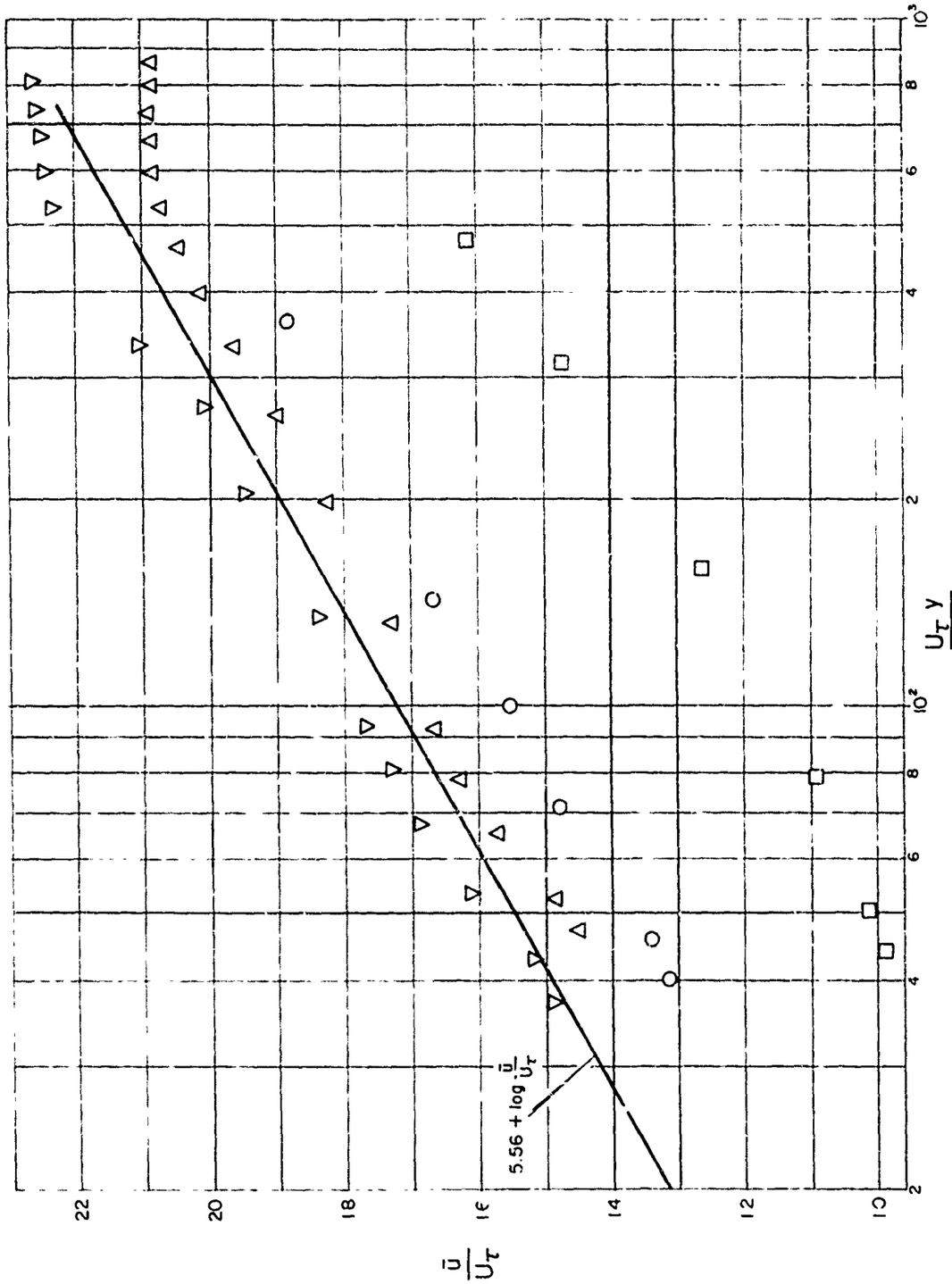

FIGURE 30
EXPERIMENTAL NONDIMENSIONAL VELOCITY DISTRIBUTION
FOR SMOOTH AND ROUGH FLAT PLATES
AT $M_1 = 4.93$ AND $T_w / T_1 = 3.0$

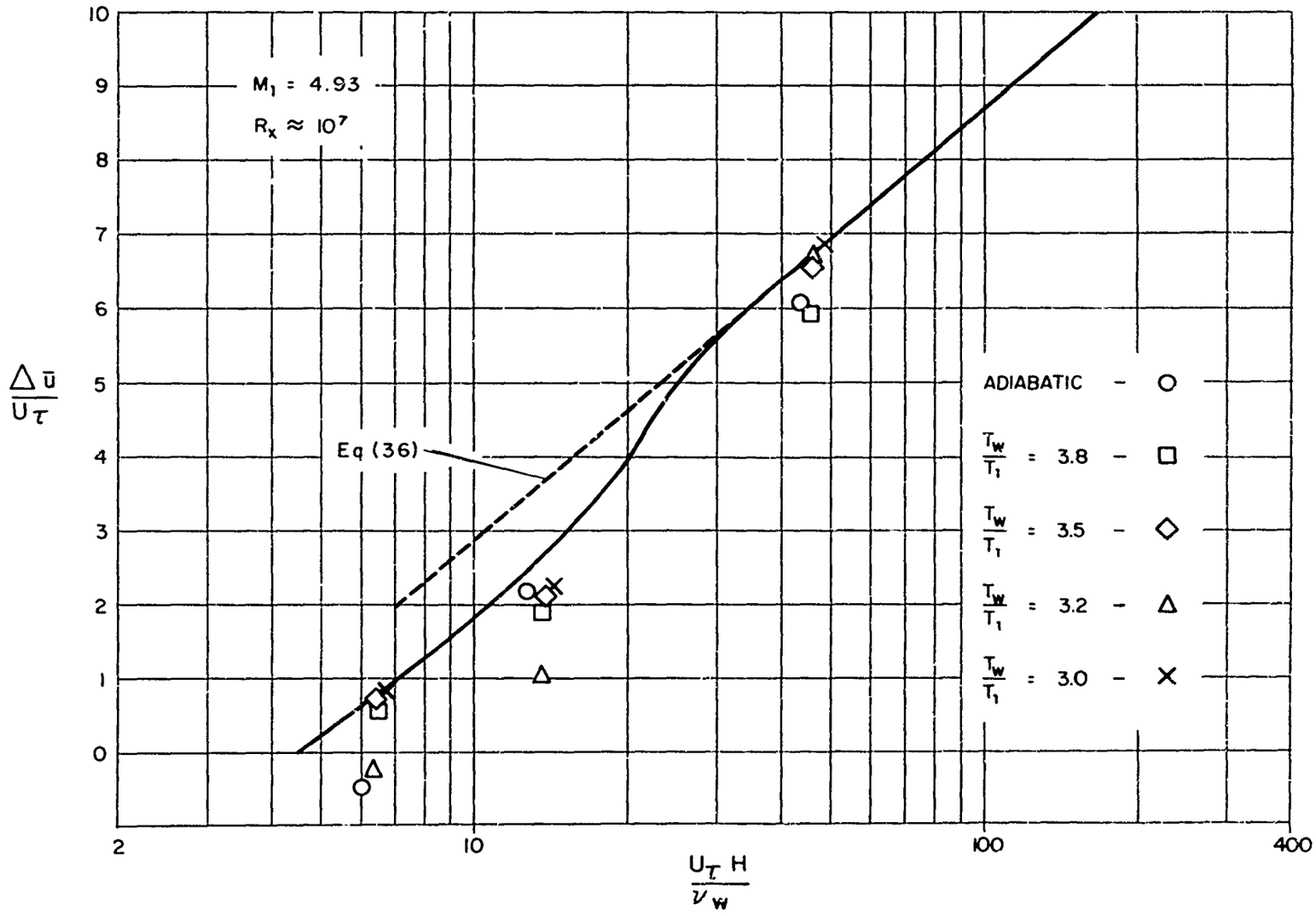

FIGURE 31
THE EFFECT OF NONDIMENSIONAL ROUGHNESS HEIGHT ON THE SHIFT IN NONDIMENSIONAL VELOCITY PROFILE AT $M_1 = 4.93$

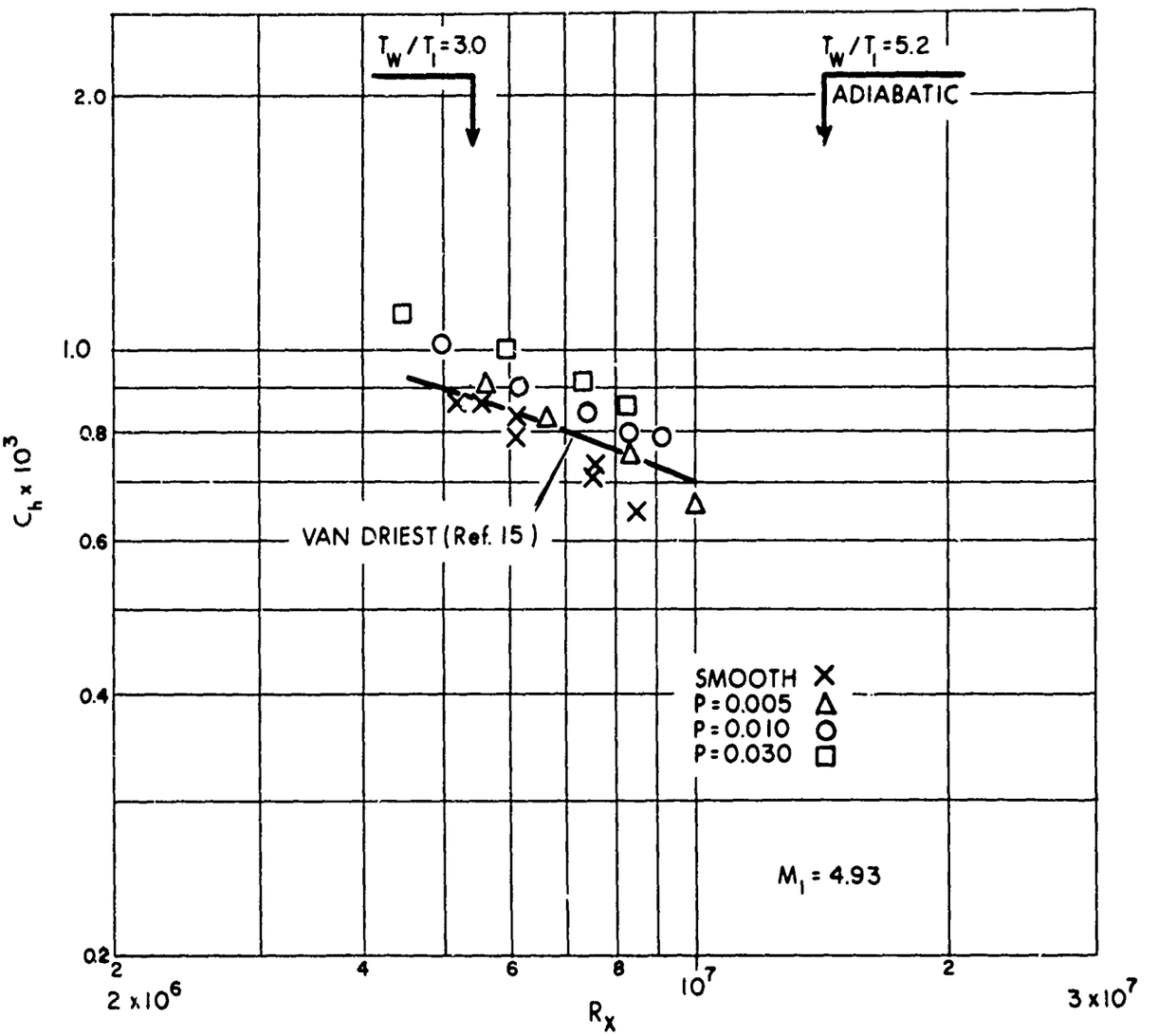

FIGURE 32
EXPERIMENTAL LOCAL STANTON NUMBERS
FOR SMOOTH AND ROUGH PLATES AT $M_1 = 4.93$

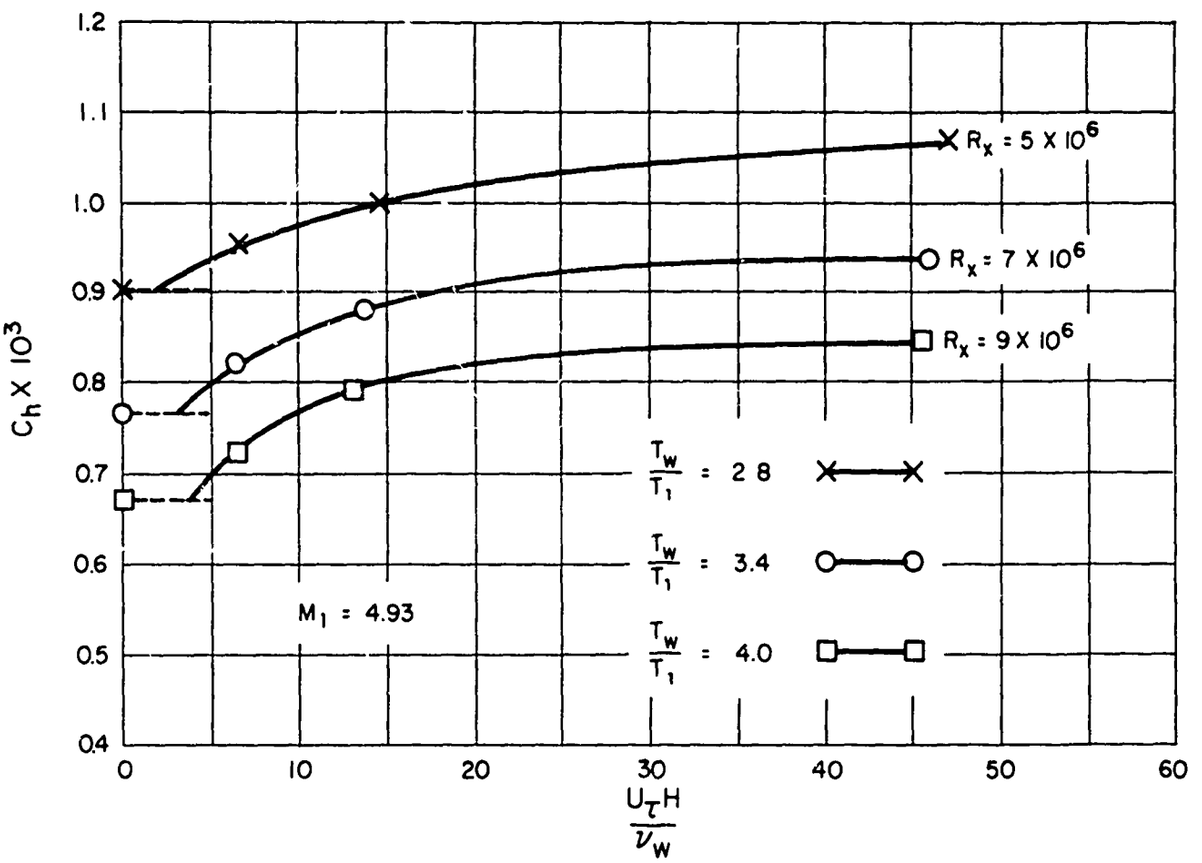

FIGURE 33
VARIATION OF EXPERIMENTAL LOCAL STANTON NUMBER WITH NONDIMENSIONAL ROUGHNESS HEIGHT AT $M_1 = 4.93$

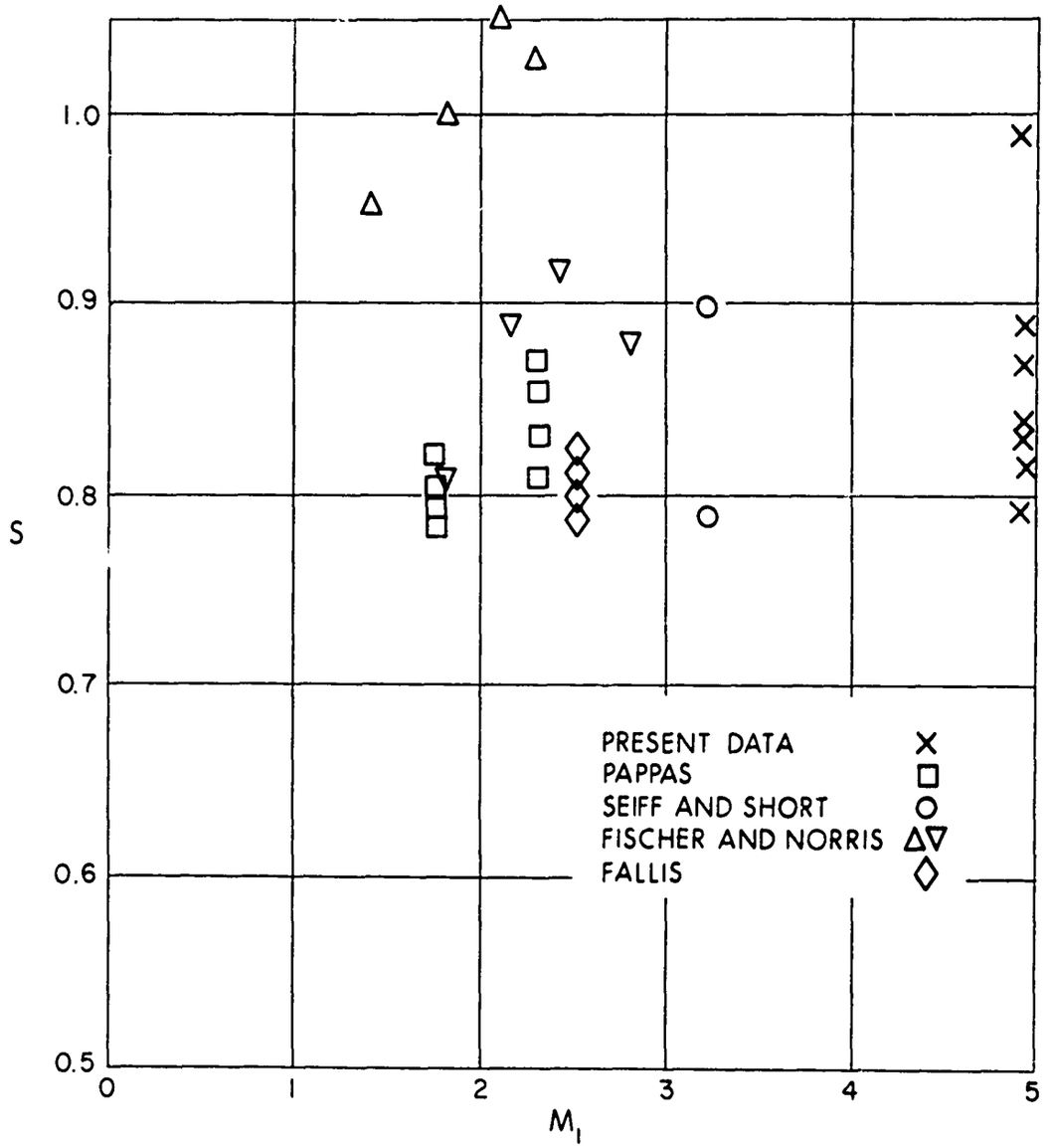

FIGURE 34
VARIATION OF EXPERIMENTALLY DETERMINED REYNOLDS ANALOGY FACTORS WITH MACH NUMBER (SMOOTH SURFACES)

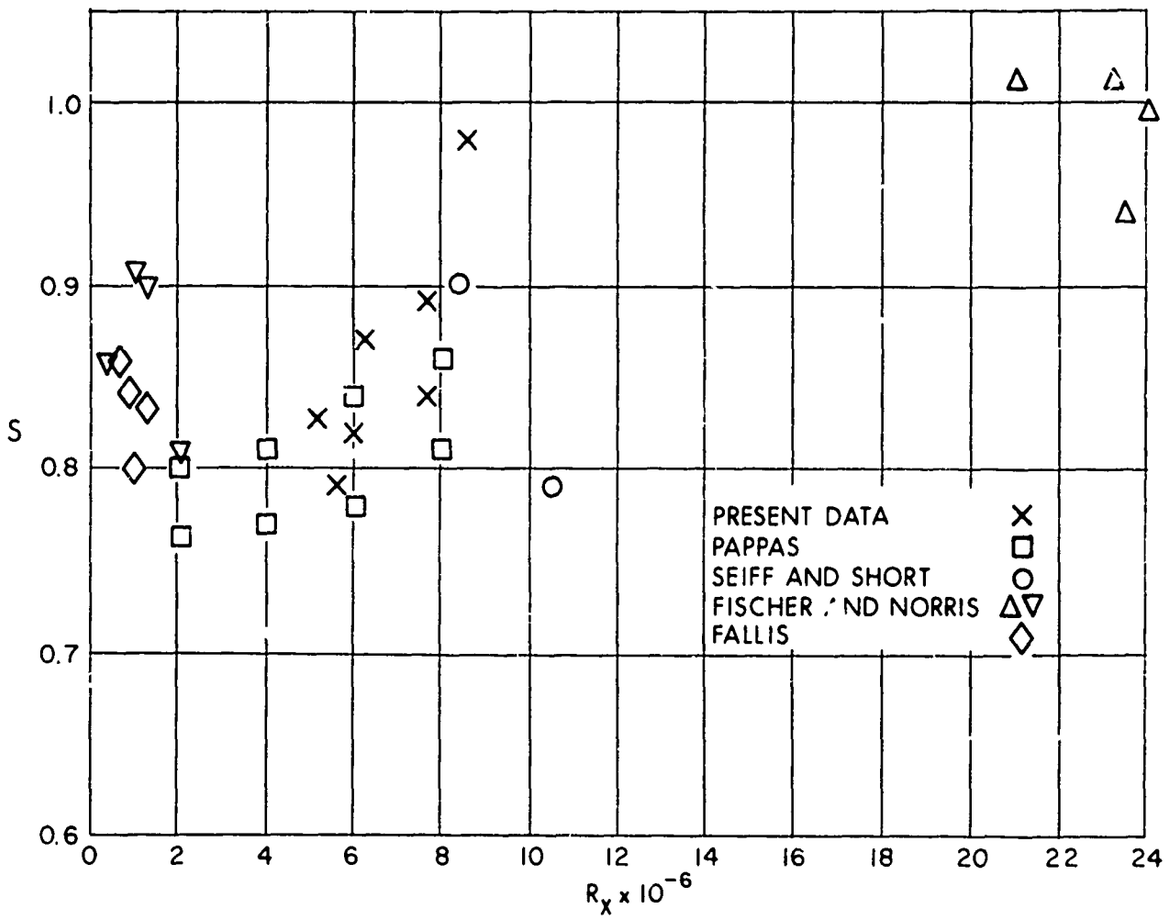

FIGURE 35
VARIATION OF EXPERIMENTALLY DETERMINED REYNOLDS ANALOGY FACTORS WITH REYNOLDS NUMBER (SMOOTH SURFACES)

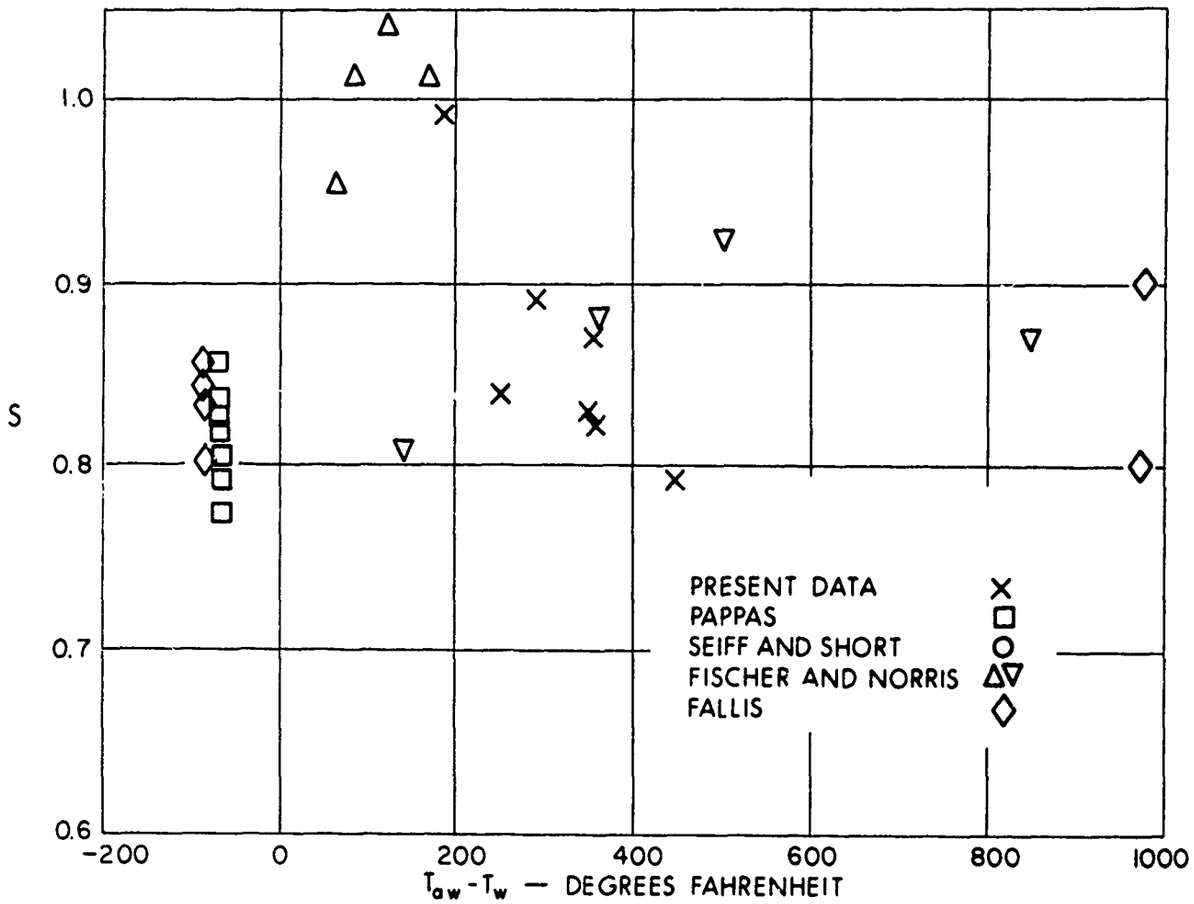

FIGURE 36
VARIATION OF EXPERIMENTALLY DETERMINED REYNOLDS ANALOGY FACTORS WITH THE TEMPERATURE DIFFERENCE ($T_{aw} - T_w$) (SMOOTH SURFACES)

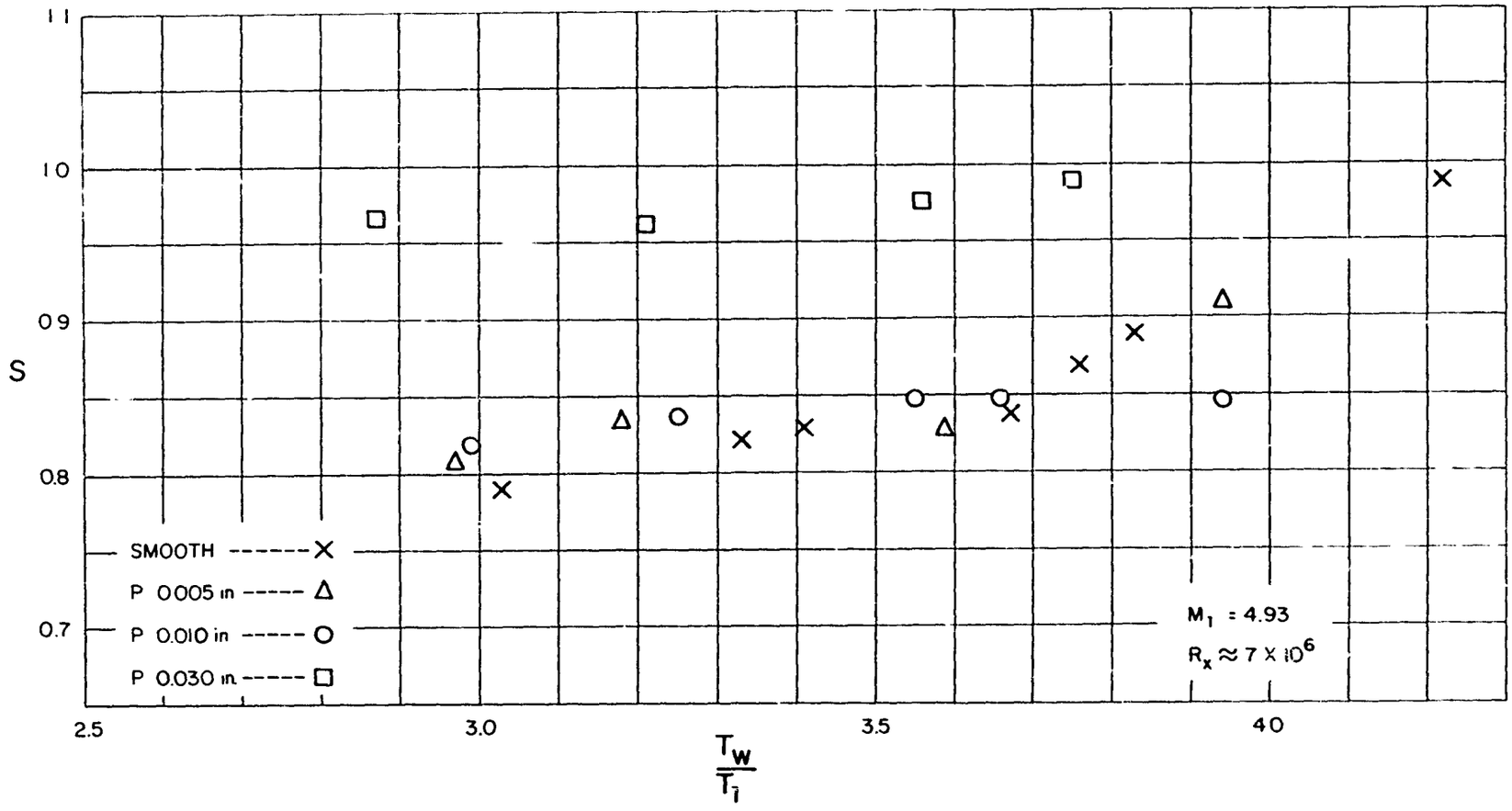

FIGURE 37
EXPERIMENTAL REYNOLDS ANALOGY FACTORS vs TEMPERATURE RATIO
FOR SMOOTH AND ROUGH PLATES AT $M_1 = 4.93$

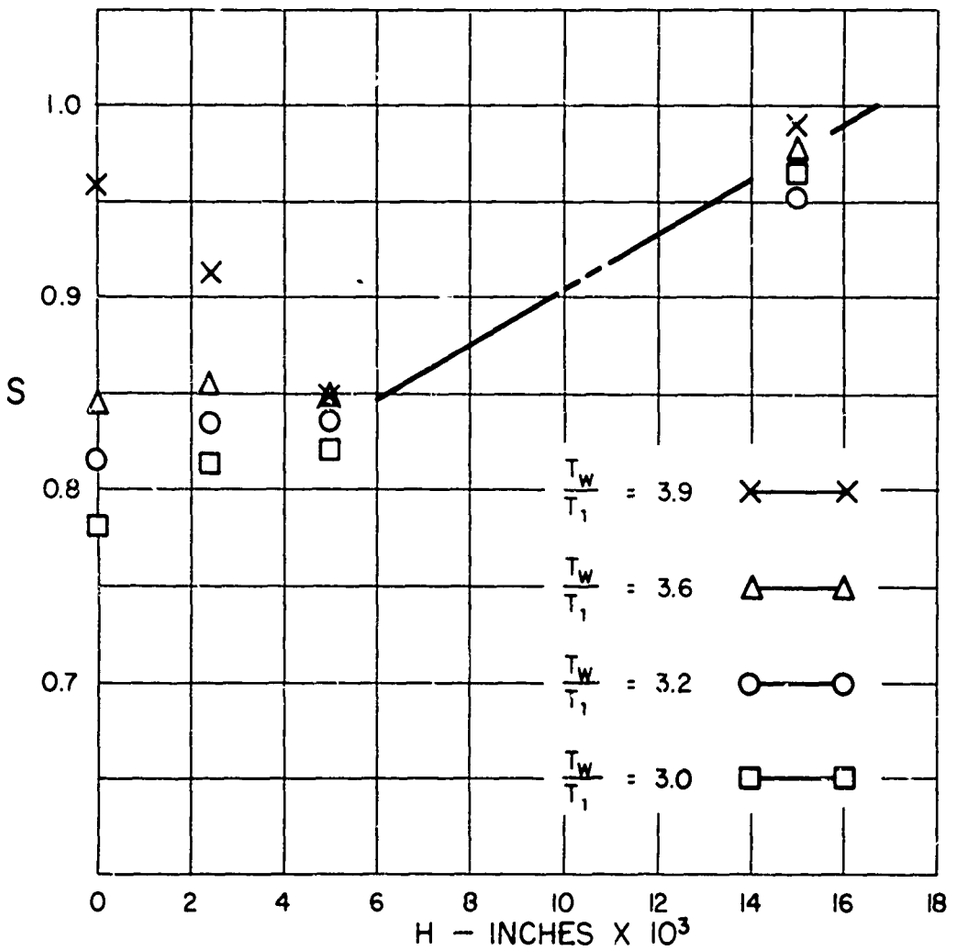

FIGURE 38
THE EFFECT OF ROUGHNESS HEIGHT ON EXPERIMENTAL REYNOLDS ANALOGY FACTORS FOR A FLAT PLATE AT $M_1 = 4.93$

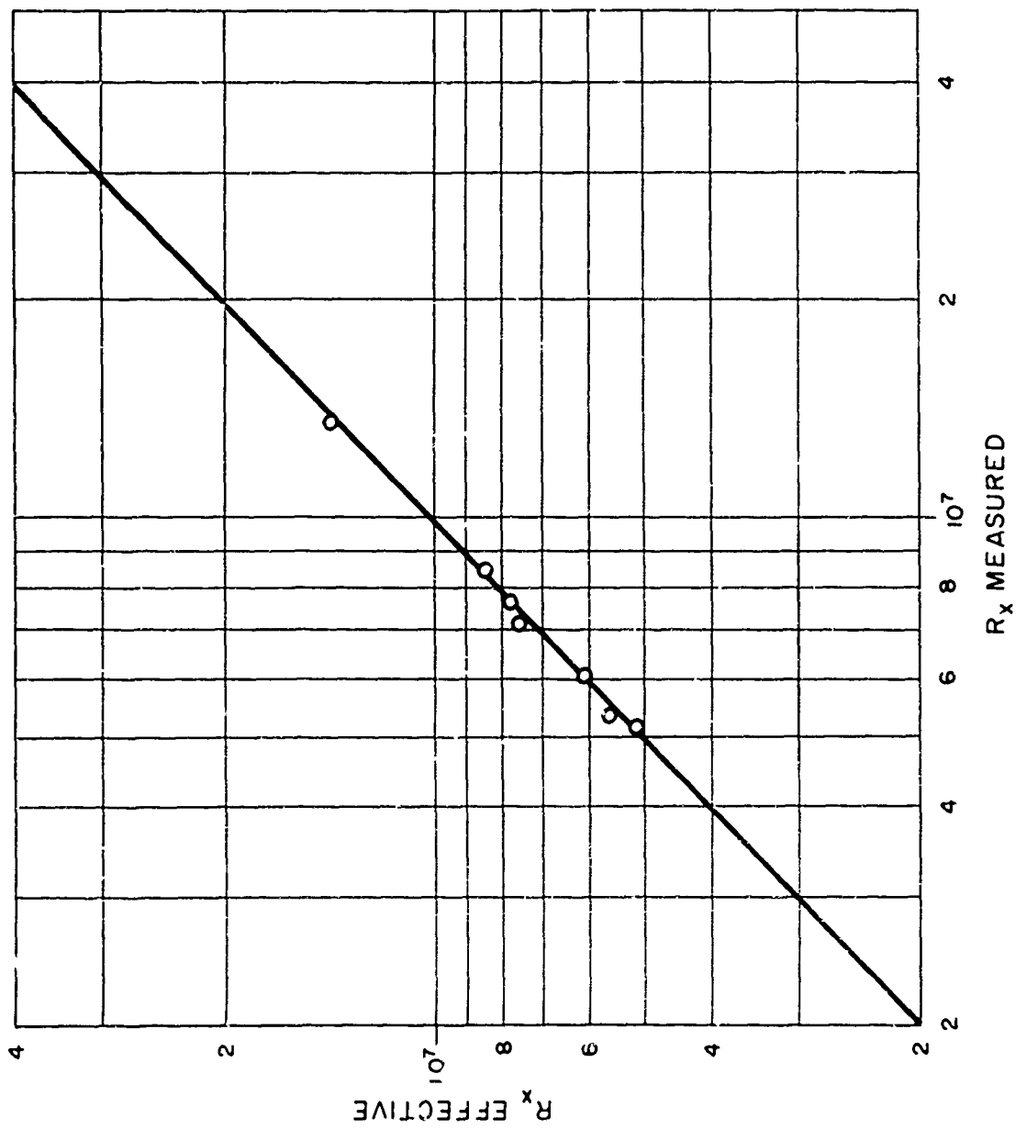

FIGURE 39
EFFECTIVE REYNOLDS NUMBER vs REYNOLDS NUMBER BASED ON MEASURED VALUE OF X (SMOOTH PLATE)

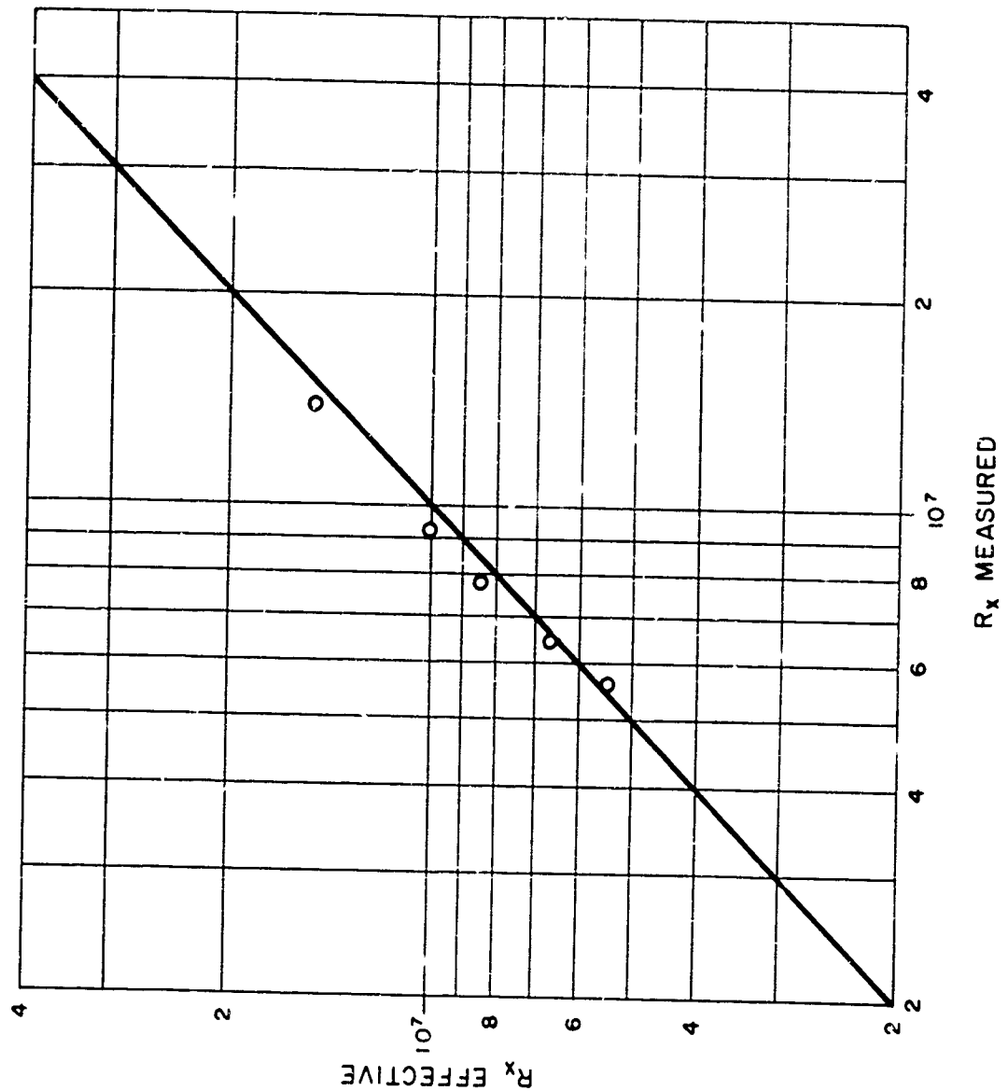

FIGURE 40
EFFECTIVE REYNOLDS NUMBER vs REYNOLDS NUMBER BASED ON MEASURED VALUE OF X (ROUGH PLATE, P = 0.005 in.)

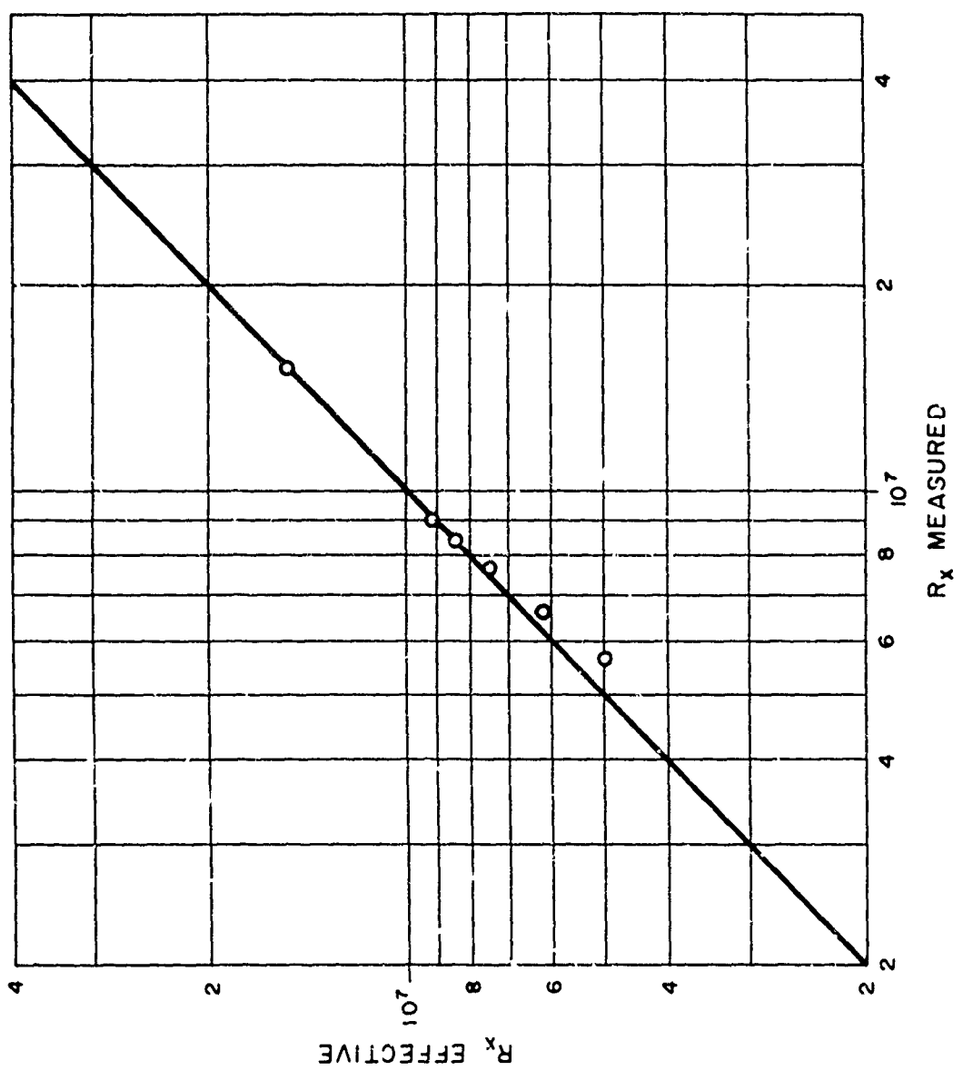

FIGURE 41
EFFECTIVE REYNOLDS NUMBER vs REYNOLDS NUMBER BASED ON MEASURED VALUE OF X (ROUGH PLATE, P = 0.010 in.)

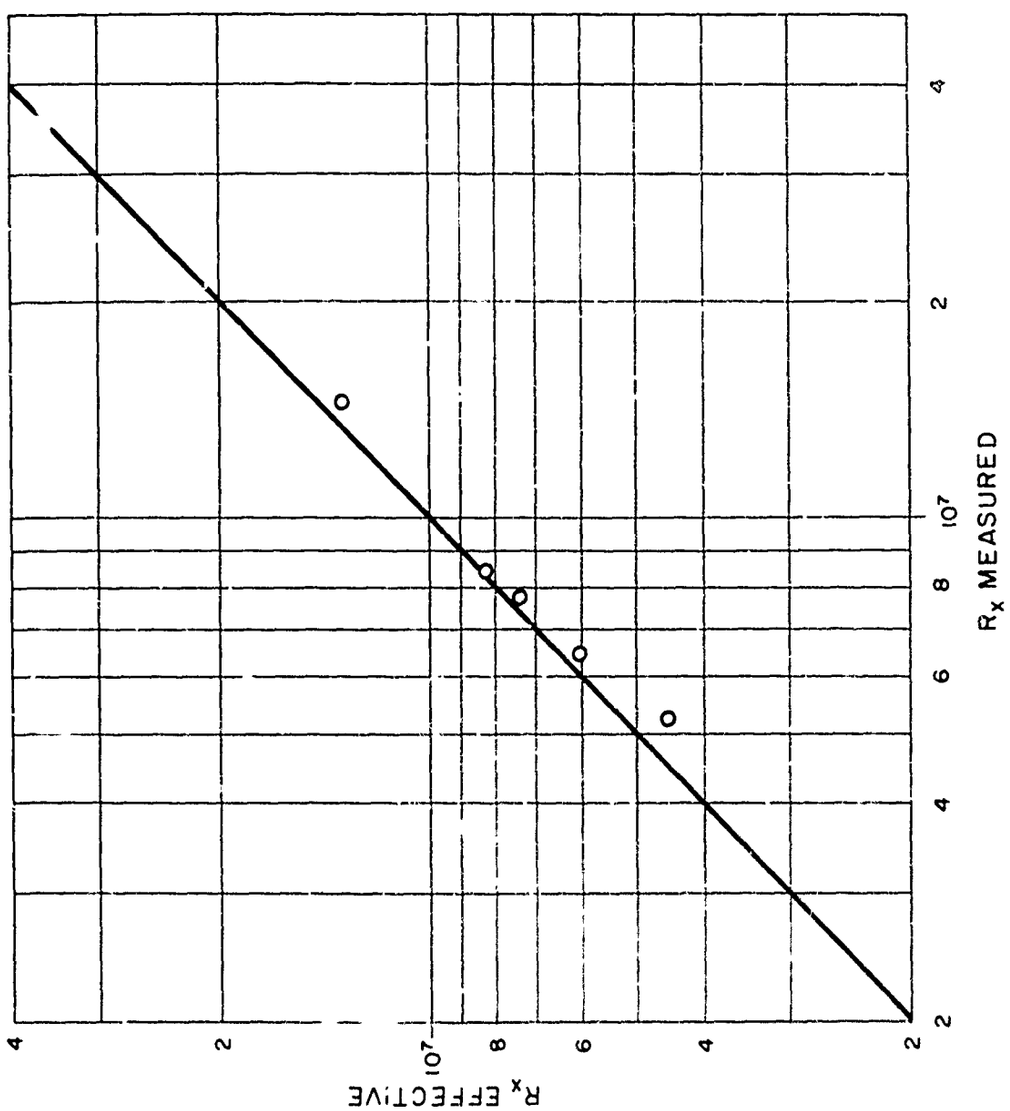

FIGURE 42
EFFECTIVE REYNOLDS NUMBER vs REYNOLDS NUMBER BASED ON MEASURED VALUE OF X (ROUGH PLATE, P = 0.030 in.)